

CONFIDENTIAL



FP7-ICT Future Networks
SPECIFIC TARGETTED RESEARCH PROJECT
Project Deliverable

PHYDYAS Doc. Number	PHYDYAS_ 020
Project Number	ICT - 211887
Project Acronym+Title	PHYDYAS – PHYsical layer for DYnamic AccesS and cognitive radio
Deliverable Nature	Report
Deliverable Number	D8.2
Contractual Delivery Date	January 1, 2010
Actual Delivery Date	February 8, 2010
Title of Deliverable	Space-time spectrum sensing, algorithms and software description
Contributing Workpackage	WP8: Radio scene spectrum analysis and cognitive radio
Project starting date; Duration	01/01/2008; 30 months
Dissemination Level	CO
Author(s)	Markku Renfors, Tero Ihalainen, Ari Viholainen (TUT), Haijian Zhang, Didier Le Ruyet, Daniel Roviras (CNAM), Adnan Al-Adnani, Jonathan Duplicy (AGI), M. A. Rojas, M. A. Lagunas, Carlos Bader (CTTC), Alexandr Kuzminskiy (ALUK – WP8 leader)

Abstract: The deliverable continues investigation of the FBMC PHY as a potential physical layer for CR spectrum sharing networks started in D8.1. Spectrum sensing algorithms have been developed, analyzed and compared with the OFDM case taking into account the increased FBMC frequency selectivity leading to better spectral efficiency of CR networks.

Contents

1	Introduction.....	6
2	Energy Detection Based Spectrum Monitoring in FBMC.....	7
2.1	Spectrum monitoring schemes	7
2.2	Energy detection principle	9
2.3	Analysis of the effect of the spectrum sensing filter	10
2.4	Performance of the sensing subband scheme in FBMC.....	14
2.5	Effects of PA nonlinearities	15
2.6	RF impairments in FBMC spectrum monitoring.....	20
3	Sequential Detection	21
3.1	Main principles.....	21
3.2	Detecting re-appearing PU signal.....	26
3.3	Fading channels and co-operative sensing	31
4	CP Autocorrelation Based Sensing for OFDM PUs.....	34
4.1	FBMC-based frequency-domain implementation.....	34
4.2	Spectrum monitoring concept for PHYDYAS DSA	39
5	Filter Bank based Multiband Spectrum Sensing for Cognitive Radio Networks.....	41
5.1	System model and multiband sensing architecture.....	42
5.1.1	System model	42
5.1.2	Multiband sensing architecture.....	43
5.2	Theoretical sensing performance	44
5.3	Simulations.....	48
5.4	Conclusion	49
6	Candidate Spectral Estimation Based on Filterbank for FBMC Spectrum Sensing in Cognitive Radio	54
6.1	Problem formulation.....	54
6.2	Different approaches on Spectrum sensing based on transmitter detection	54
6.2.1	Filter bank spectral estimation	55
6.2.2	Spectrum sensing using Candidate Spectral Estimation (CASE)	57
6.3	Spectrum sensing having FBMC signal using candidate spectrum estimate	58
6.3.1	Algorithm description	59
6.3.2	Robustness against the SNR increase	59
6.3.3	System capabilities with narrow band interferences to FBMC signal	60

6.3.4	ROC performance (Probability of detection vs. probability of false alarm)	62
6.4	Conclusions	63
7	Complexity Assessment of Analysis Filter Banks.....	64
7.1	Windowed DFT based approach	64
7.1.1	Spectral leakage.....	64
7.1.2	Windowing.....	65
7.1.3	Overlapping and averaging	65
7.2	Filterbanks based analysis.....	66
7.2.1	Architecture	67
7.2.2	Analysis and prototype filter	67
7.3	Comparison	68
7.3.1	Complexity comparison	68
7.3.2	Illustrative examples.....	69
7.4	Conclusions	75
8	Decentralized Dynamic Spectrum Allocation in Uncoordinated Cognitive Radio Networks Based on Adaptive Antenna Array Interference Mitigation Diversity: Finite Amount of Data Spectrum Sensing Effects	76
8.1	System model and problem formulation.....	76
8.2	“Good neighbour” DSA algorithm based on locally estimated second order statistics.....	80
8.3	Spectrum sensing protocol	81
8.4	Markov chain modelling of IM-based DSA with estimated propagation channels and interference statistics.....	82
8.4.1	Probability density function of the SINR estimated over a single interval with T i.i.d. complex Gaussian training samples	82
8.4.2	Markov chain modelling of the IM-based DSA with locally estimated second order statistics	84
8.4.3	Markov chain analysis of the IM-based DSA with locally estimated second order statistics....	88
8.5	Simulation results for higher dimension networks.....	92
8.6	Adaptive averaging for spectrum sensing algorithms in GN IM-based DSA	93
8.6.1	Modified GN algorithm	93
8.6.2	Stationarity test for spectrum sensing with adaptive averaging.....	93
8.6.3	Simulation results	95
8.7	Conclusions	97
9	Summary.....	98
	References	101

List of Acronyms

AA	Adaptive Averaging
ASN	Average Sample Number
AWGN	Additive White Gaussian Noise
BPSK	Binary Phase Shift Keying
BS	Base Station
CASE	Candidate Spectral Estimation
CDF	Cumulative Distribution Function
CP	Cyclic Prefix
CR	Cognitive Radio
CROC	Complementary Receiver Operation Characteristic
DFT	Discrete Fourier Transform
DL	Downlink
DSA	Dynamic Spectrum Access/Allocation
FBMC	Filter Bank based Multicarrier
FC	Fusion Center
FCC	The Federal Communication Commission
FFT	Fast Fourier Transform
FIR	Finite Impulse Response
GN	Good Neighbor
GN-MinSwitch	Good Neighbor algorithm with MinSwitch search
IBO	Input power Back-Off
IFFT	Inverse Fast Fourier Transform
i.i.d	Independent and Identically Distributed
IM	Interference Mitigation
MinSwitch	Minimum Switch Search
MS	Mobile Station
NPR	Nearly Perfect Reconstruction
OFDM	Orthogonal Frequency Division Multiplexing
PA	Power Amplifier
PDF	Probability Distribution Function
PFB	Polyphase Filter Bank
PHY	Physical Layer
PS	Primary System
PSD	Power Spectral Density
PSE	Periodogram Spectrum Estimator
PSW	Prolate Sequence Window
PU	Primary User
QoS	Quality-of-Service
QPSK	Quadrature Phase Shift Keying
RF	Radio Frequency
ROC	Receiver Operation Characteristic
SINR	Signal to Interference plus Noise Ratio
SNR	Signal to Noise Ratio
SPRT	Sequential Probability Ratio Test
SS	Secondary System

STFT	Short-Time Fourier Transform
SU	Secondary User
UL	Uplink
WSS	Wide-Sense Stationary

1 Introduction

The FBMC PHY has been studied and compared with OFDM as a potential physical layer for cognitive radio (CR) spectrum sharing networks in [D8109]. Particularly, spectral efficiency, impact of the RF impairments, and resource allocation techniques have been investigated. It has been shown that FBMC can be considered as a perspective physical layer for future CR networks.

It is well known that spectrum sensing is the core CR/spectrum sharing operation [Hay05] that has been extensively studied in different CR scenarios and applications, e.g., [Cog09]. The state of the art in spectrum sensing has been addressed in Section 2 in [D8109].

This deliverable is devoted to development and analysis of spectrum sensing algorithms for FBMC based networks. Improved selectivity of the FBMC PHY can be exploited for spectrum sensing in different ways. For example, simultaneous spectrum sensing and reception of secondary transmissions using the same device can be considered with FBMC PHY for vertical CR systems with primary (PU) and secondary (SU) spectrum sharing users. Another important example is that low energy leakage between closely spaced frequency bands in FBMC allows spectrally efficient implementation of unsynchronized uncoordinated horizontal CR spectrum sharing networks. In this case spectrum sensing is required for local estimation of signal/interference statistics at each spectrum sharing subsystem.

Energy detection based spectrum monitoring in FBMC is studied in Section 2. Section 3 is devoted to sequential signal detection, where the number of data samples, which are used to make the decision, is not fixed in advance. Taking into account that OFDM is extensively used in current and emerging wireless communications standards, and thus PUs appearing in future cognitive radios will commonly use OFDM waveforms, Section 4 address cyclic prefix (CP) autocorrelation based sensing for OFDM PUs with FBMC-based frequency-domain implementation. Section 5 investigates a multiband detection architecture based on Polyphase Filter Bank (PFB), which aims to reliably sense multiple active bands by exploiting the low leakage property of PFB. In Section 6, the procedure is proposed that is able to detect and label power and central frequency location for any spectral signature (candidate) with noise signal existence, and co-channel interference with different modulation format. Developed implementation in Section 6 complements in a certain way the set of tools developed in Sections 4. Particularly, the work in Section 6 assumes a FBMC system as PU and uses besides of the autocorrelation properties to detect of the signature of desired PUs process to detect it power level. Section 7 presents the investigation on the complexity analysis of FBMC-based spectrum estimation and its comparison with the OFDM case. Section 8 continues investigation of the interference mitigation (IM)-based dynamic spectrum allocation (DSA) algorithms introduced and studied in Section 8 in [D8109]. Particularly, the basic scenario assumes a number of uncoordinated and unsynchronized wireless subsystems sharing spectrum in the same geographical area. It is shown in [D8109] that OFDM is spectrally inefficient PHY in this scenario and FBMC could be much better solution for uncoordinated spectrum sharing and CR networks. A “good neighbour” (GN) approach proposed in [D8109] can be considered as some kind of rule-regulated cooperation between spectrum sharing subsystems without explicit data exchange between them. The IM-based DSA algorithms are studied in [D8109] and the indicated papers by means of the theory of absorbing Markov chains and simulations assuming that local second-order statistics is known at each subsystem. Now, Section 8 introduces spectrum sensing algorithms at each spectrum sharing subsystem to estimate these statistics and studies finite amount of data effects for the GN IM-based DSA. Eventually, Section 9 summarizes the main results of the deliverable.

2 Energy Detection Based Spectrum Monitoring in FBMC

This section focuses on the spectrum monitoring problem, i.e., detecting reappearing primary users during secondary transmissions in cognitive radio systems. The filter bank multicarrier (FBMC) concept is used as the basis as it facilitates simultaneous spectrum sensing and reception of secondary transmissions using the same device. With FBMC, it is possible to support in a spectrally efficient manner narrow, subchannel-wide gaps in the spectrum of the transmitted signal for monitoring purposes. Such scheme allows fast reaction to reappearing primary users and it needs minimum amount of coordination between independent secondary systems operating in the same frequency band. We analyze the effect of the filter bank frequency response on energy detection based spectrum sensing. We also evaluate the impact of spectral regrowth due to transmitter power amplifiers, which is a critical issue in the proposed scheme.

2.1 Spectrum monitoring schemes

The primary goal of the spectrum sensing module of a cognitive radio is to detect the spectrum occupancy in the local area in which the system operates, and identify the spaces which are free of primary users (PUs) and other secondary users (SUs), the so-called spectrum holes. Spectrum holes are also referred to as white spaces and the target is to achieve pre-determined false alarm and missed detection probabilities, P_{FA} and P_{MD} , when identifying white spaces. We will make a distinction between two modes of PU sensing: (1) Spectrum hole acquisition is carried out before local secondary transmission has been started or in other situations where the particular frequency band is not used for secondary transmission. (2) Spectrum monitoring takes place in parallel with secondary transmission and its main target is to detect reappearing PUs in the used frequency channel. Here we focus on the latter functionality.

The main challenge in developing the spectrum monitoring schemes is to reach short reaction time with minimum overhead to the simultaneously on-going secondary transmissions. A common approach for spectrum monitoring is based on quiet blocks in the time-frequency plane [Ste05], e.g., in the form of time-domain gaps between transmission frames or continuous empty bands in frequency domain. Obviously, in the context of multicarrier modulation techniques, there is a lot of flexibility in defining the quiet blocks.

On the other hand, the spectrum sensing scheme has to match the characteristics of the opportunistic, dynamic spectrum access (DSA) scheme which is employed by the secondary systems. One general idea is that the DSA scheme should be able to support independent SU systems operating in the same white space, with minimum coordination between the different systems [Kuz09]. In any case, it is necessary that there exists coarse frequency synchronization between different SUs. However, to reach time synchronous operation of different opportunistic secondary systems would require higher level of coordination between them. This leads to the idea of leaving narrow parts of the spectrum unused in secondary transmission, allowing them to be utilized for spectrum sensing purposes in a continuous manner. In the multicarrier context, the spectrum sensing bands would mean one or a few subbands.

Due to the spectral leakage characteristics, filter bank based multicarrier transmission schemes are much more favourable for this approach than OFDM. In FBMC, one subband is sufficient to isolate a sensing subband from active subcarriers of the adjacent secondary systems. This section focuses on evaluating such a sensing subband scheme taking into account various practical issues, especially the effect of spectral regrowth due to transmitter power amplifier non-linearity, which increases the effective noise level on the sensing subbands.

In multicarrier systems, subband sample -wise energy values can be integrated both in time and frequency directions. This gives the possibility to utilize filter banks with subchannel spacing much smaller than the bandwidth of the signal to be detected. Furthermore, a filter bank with suitable subchannel spacing can be used flexibly in the detection of different types of primary signals and different SNR values by adjusting the integration range [Bel09]. The requirement is that the sensing block contains a sufficient number of independent elements in the time-frequency plane. Here we assume for simplicity that both noise and the possible PU signals have constant power spectral density in the region used for sensing; the extension of this study to frequency selective and fading PU channels is a topic for future studies.

Figure 2.1 shows two basic structures for introducing quiet blocks in multicarrier transmission, either as time-domain quiet periods (i.e., all-zero multicarrier symbols) or as continuous sensing subbands. It is obvious that the latter approach is not feasible in case of OFDM, due to the energy leakage from active subcarriers to the nearby unused ones. However, in FBMC with sufficiently sharp prototype filter frequency response, one guard subband is sufficient to isolate a sensing subband from the active subcarriers. Figure 2.2 shows the subchannel frequency responses in case of the PHYDYAS prototype filter [D5109] [Vih09] with overlapping factor $K = 4$.

Let us now consider the spectrum monitoring schemes of Fig. 2.1 from the secondary system operation point of view. The main idea of opportunistic spectrum use is that the same white space can be used in different, not very distant, locations independently, in an un-coordinated manner. Therefore, co-channel interference between different secondary systems utilizing overlapping frequency channels can always be expected. To reach time-synchronous operation between different SU systems, especially regarding the quiet sensing period, a common stable time-base should be available. Furthermore, the length of the sensing period should be long compared to the signal propagation delays in those signal paths between different SU systems, which are not attenuated well below the targeted PU sensitivity level. In conclusion, it seems to be very difficult to reach sufficiently quiet time-domain sensing blocks in opportunistic spectrum usage scenarios.

On the other hand, some level of coarse frequency synchronization between nearby SU systems must exist, and it is easier to reach than precise time synchronization. The absolute sensing subband locations could be included in the main parameters of an FBMC-based secondary access scheme, and then it would be possible for all the secondary systems to leave the sensing subbands unused at all times.

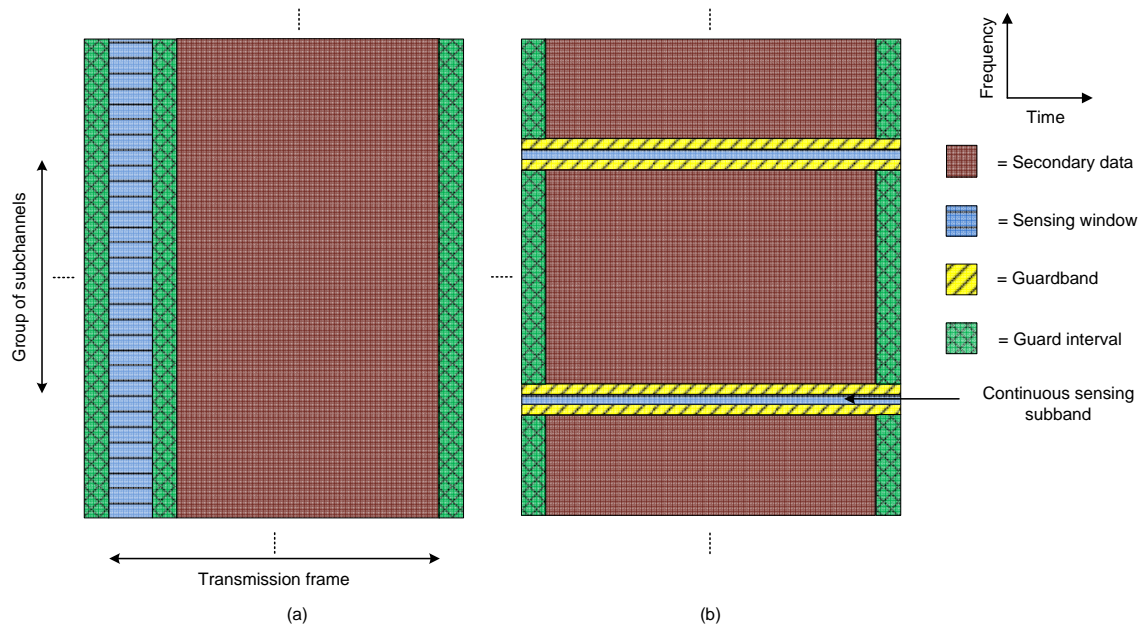


Figure 2.1. Two alternative structures of quiet blocks for spectrum sensing in multicarrier systems.

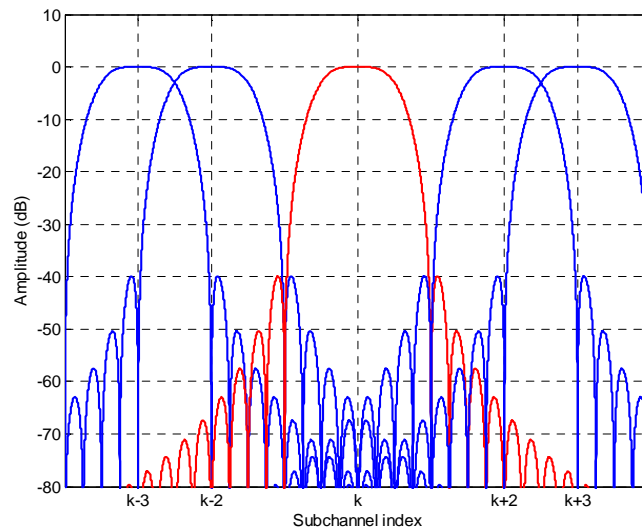


Figure. 2.2. Subchannel frequency responses in FBMC with PHYDYAS filter bank.

The main challenge in the proposed approach is to keep the sensing subband clean enough also with practical analog RF implementations of the transmission chain. Especially, the spectral regrowth due to transmitter power amplifier nonlinearities should be kept at a low-enough level. This issue is considered in Section 2.5. Before that, we will consider the energy detection in FBMC systems in some more details.

2.2 Energy detection principle

We consider spectrum sensing in a multicarrier receiver, where energy detection (radiometer) is carried out at subband level at the output of the analysis bank. In energy detection, the test statistic is obtained as

$$T(\mathbf{Y}) = \frac{1}{N} \sum_{n=0}^{N-1} |Y[n]|^2 \quad (2.1)$$

where $Y[n]$, $n=0,1,\dots,N-1$, are complex independent (uncorrelated) observations. Binary hypothesis testing is carried out based on the test statistic. Using Gaussian approximation, the distributions in the absence (H_0) and presence (H_1) of the PU signal can be written as:

$$\begin{aligned} T(\mathbf{Y})|_{H_0} &\sim \mathcal{N}\left(\sigma^2, \frac{1}{N}\sigma^4\right) \\ T(\mathbf{Y})|_{H_1} &\sim \mathcal{N}\left(P + \sigma^2, \frac{1}{N}(P + \sigma^2)^2\right). \end{aligned} \quad (2.2)$$

Here P and σ^2 are the signal and noise variances, respectively.

We make use of the equations in [Tan08], that relate the sample complexity to the false alarm probability P_{FA} , the misdetection probability P_{MD} , and the operating $SNR = P / \sigma^2$. In case there is no uncertainty and the noise variance is completely known, the required sensing time in samples, N_D , to achieve target P_{FA} and P_{MD} writes:

$$N_D = \frac{\left[\Phi^{-1}(P_{FA}) - \Phi^{-1}(1 - P_{MD})(1 + SNR) \right]^2}{SNR^2}, \quad (2.3)$$

where Φ denotes the standard Gaussian complementary CDF. On the other hand, when the energy detector is assumed to operate under a noise level uncertainty of $x = 10 \log_{10} \rho$ dB, the sample complexity can be approximated [Tan08] according to

$$N_D \approx \frac{\left[\Phi^{-1}(P_{FA}) - \Phi^{-1}(1 - P_{MD}) \right]^2}{\left[SNR - \left(\rho - \frac{1}{\rho} \right) \right]^2}. \quad (2.4)$$

This introduces the so-called SNR wall [Tan08]: For example, with 0.1 dB uncertainty of the noise variance, the sensing time grows without limits when the SNR approaches -13.3 dB.

2.3 Analysis of the effect of the spectrum sensing filter

Figure 2.3 shows the frequency response of the PHYDYAS filter bank prototype filter in relation to the response of an ideal lowpass filter with the same subchannel spacing. This prototype response is the baseband equivalent of all subchannel filters of the FBMC receiver. Since the filter response is far from the ideal one, it is important to examine its effect on the spectrum sensing performance.

In the FBMC receiver, subchannel processing (e.g. fractionally-spaced equalization / frequency domain fine synchronization) is carried out at 2x oversampled rate. In other words complex-valued

subchannel samples are processed instead of the real-valued ones, which are finally sufficient for data reception at the end subchannel processing chain. In the spectrum sensing context, it is interesting to evaluate the possible benefit from using oversampled subband signals instead of critically sampled ones.

In order to handle the frequency dependency of the subchannel filter, we split the subband into even smaller frequency increments of width

$$\Delta f = \frac{f_s}{ML}, \quad (2.5)$$

where f_s is the sampling rate, M is the number of subbands, and L is the number of frequency increments per subband. Let us assume further that the time record length is N/f_s and N is an integer multiple of L . The input to the receiver is either white noise or white noise plus PU signal with flat power spectral density over the spectrum sensing bandwidth.

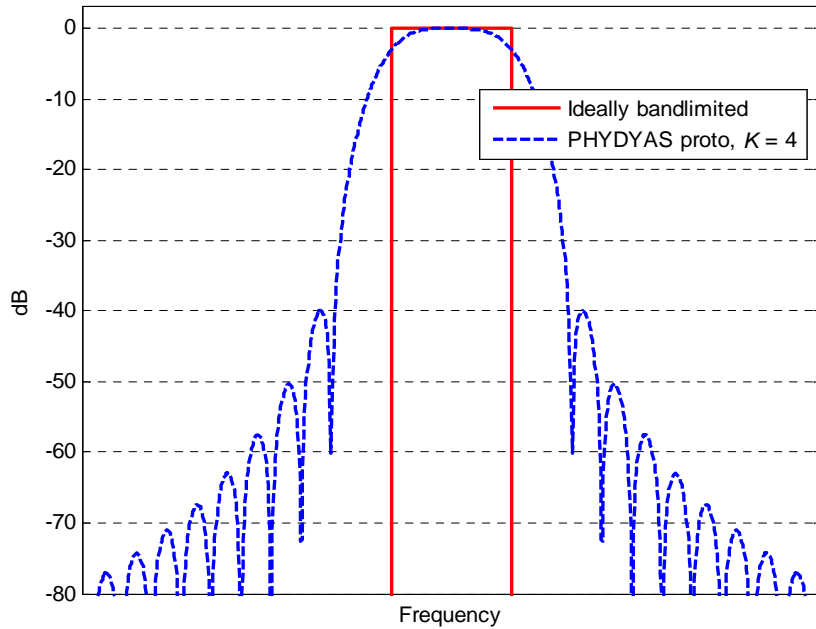


Figure 2.3. Subchannel frequency response of the PHYDYAS filter bank.

Let's start with the case of ideally lowpass filtered and critically sampled subband signals. In this case we obtain N independent uncorrelated observations per subband. Alternatively, e.g., by taking L -point DFT's of the subband signal, we obtain N/L independent observations from each of the L frequency increments. Due to the flat input spectrum and orthogonality of the DFT, also in this case we obtain N independent and identically distributed samples, so the decision statistic for energy detection is essentially the same in both cases.

Let's consider next the case of practical subchannel filter response with *critically* sampled subband signal. The subband signal has again flat spectrum under both hypotheses due to aliasing and square-root Nyquist response of the subchannel filter. Thus the discussion of the previous case is valid also here.

Let us then consider the case of practical subchannel filter response with 2x *oversampled* subband signal. In this case there is practically no aliasing since the subband signal is contained within the frequency band $[-f_s/M, f_s/M]$. Now $2L$ frequency increments of Δf are needed to cover the overall subband. The subchannel frequency response is assumed to be flat within each frequency increment with F_l , $l = -L, \dots, L$, and it satisfies

$$\sum_{l=-L}^L |F_l|^2 = L. \quad (2.6)$$

It follows from Parseval's theorem that the basic subband sample -wise test statistic is equivalent to the test statistic obtained by taking the mean of the frequency increment -wise test statistics. Now the signal within each frequency increment has Gaussian distribution with zero mean and variance $|F_l|^2 \sigma^2$ under H_0 and $|F_l|^2 (P + \sigma^2)$ under H_1 . Thus the frequency increment -wise test statistics have the distributions $\mathcal{N}\left(|F_l|^2 \sigma^2, \frac{L}{N} |F_l|^4 \sigma^4\right)$ and $\mathcal{N}\left(|F_l|^2 (P + \sigma^2), \frac{L}{N} |F_l|^4 (P + \sigma^2)^2\right)$ under H_0 and H_1 , respectively. The overall test statistic is obtained as the sum of the frequency increment -wise test statistics weighted by $1/L$. Using Gaussian approximation, this is a sum of L independent Gaussian variables and it has mean

$$\frac{1}{L} \sum_{l=-L}^L |F_l|^2 (P + \sigma^2) = (P + \sigma^2) \quad (2.7)$$

and variance

$$\frac{1}{L^2} \sum_{l=-L}^L \frac{L}{N} |F_l|^4 (P + \sigma^2)^2 = \frac{1}{N} (P + \sigma^2)^2 \cdot \sum_{l=-L}^L \frac{|F_l|^4}{L} = \frac{1}{N} (P + \sigma^2)^2 \cdot \beta \quad (2.8)$$

With the PHYDYAS prototype filter design [D5109],

$$\beta = \sum_{l=-L}^L \frac{|F_l|^4}{L} = 0.8228. \quad (2.9)$$

The variance of the test statistic is reduced by this factor, under both hypotheses, and consequently the needed sample complexity is reduced by the same factor in subband-wise sensing. In summary, N samples at subcarrier symbol rate and $2\beta N = 1.65N$ samples at 2x oversampled rate result in the same P_{FA} and P_{MD} . The needed time record length is reduced by the factor of 0.8228 in the latter case.

It should be emphasized that the gain from using fractionally-spaced samples is fully obtained only in the scheme of Fig. 2.1 (b), i.e., when using just one subband for sensing. If several adjacent subbands are used, the additional samples (beyond critical sampling) in the inner subbands would be fully correlated with the other observations, and the benefit comes from the two edge subbands only.

This analytical model of the effects of the sensing filter is tested in Fig. 2.4 in terms of complementary receiver operation characteristic (CROC) plots, which represent P_{MD} as a function

of P_{FA} . We can see that the experimental data, obtained from an FBMC test-bed (with PHYDYAS prototype filter) exploiting sensing subband based energy detection, matches quite well with the analytical model ($\beta = 0.8228$), much better than with the simplistic basic model with $\beta = 1$.

The analytic results are based on the expressions

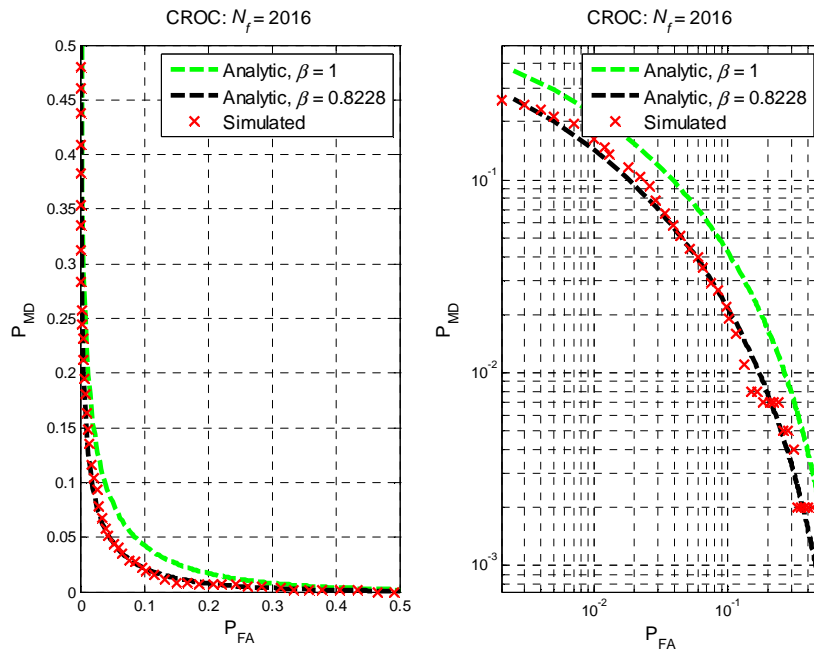
$$P_{FA} = Q\left(\frac{\gamma - \sigma^2}{\sqrt{\beta/N}\sigma^2}\right) \quad (2.10)$$

and

$$P_{MD} = 1 - Q\left(\frac{\gamma - (P + \sigma^2)}{\sqrt{\beta/N}(P + \sigma^2)}\right), \quad (2.11)$$

where γ denotes the decision threshold.

It should also be noted that the above analysis is quite general and applies to any spectrum sensing filter frequency response and it can be applied also in other scenarios. However, the simplifications due to (2.6) are valid only when a square-root Nyquist filter is used.



(a)

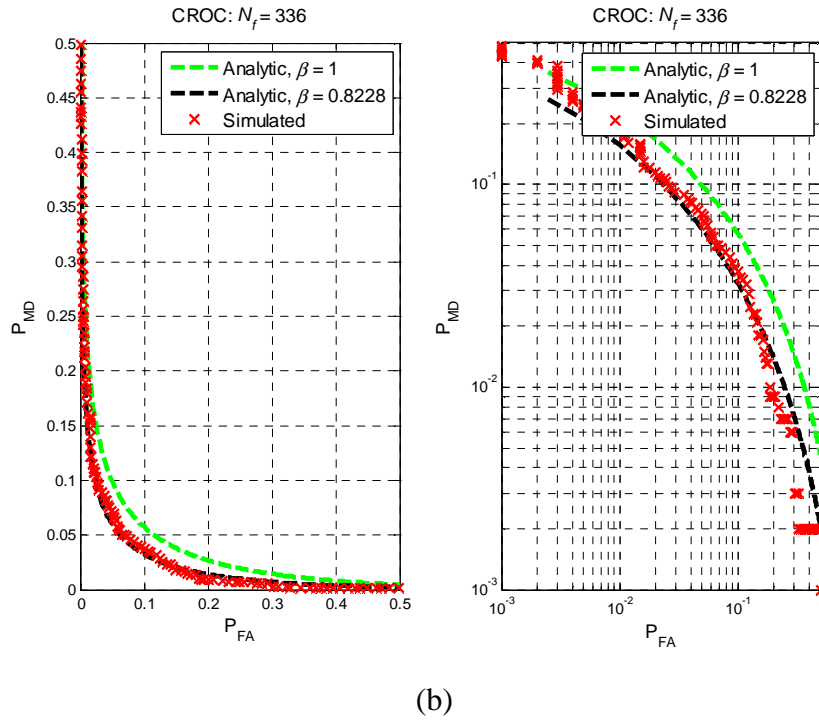


Figure 2.4. Verification of the analytical model of sensing filter effects using CROC plots. Number of fractionally-spaced observations $N_f = 2N$. (a) PU SNR $|_{H_1} = -10$ dB, (b) PU SNR $|_{H_1} = -6$ dB.

2.4 Performance of the sensing subband scheme in FBMC

We consider an FBMC system where the subcarriers are allocated in groups of 18. The subcarrier spacing is 10 kHz. In the sensing subband scheme, 3 all-zero subbands are inserted between such groups. In the time-domain quiet period scheme, just one all-zero subcarrier is used as a guard between adjacent groups. In the filter bank design, overlapping factor of $K = 4$ is assumed, so the length of time-domain guards is 4 subcarrier samples. In the quiet period scheme, the length of the quiet period is chosen in such a way that the total overheads due to quiet periods and guards are the same in the two schemes. Then we can calculate the effective size (including the effect of β of (2.8)) of the decision statistics for both schemes, as a function of the sensing interval. From this information, the sensitivity of spectrum sensing can be plotted, as shown in Fig. 2.5. Here perfect knowledge of the noise level is assumed. The ‘best case’ and the ‘worst case’ refer to the PU center frequency in relation to the sensing subband grid, which has an effect on the number of sensing subbands hitting the PU band. It can be seen that the sensing subband scheme is actually more effective with short sensing intervals. With longer sensing intervals, the quiet period scheme achieves approximately 1 dB better sensitivity, however, with reduced time resolution in sensing.

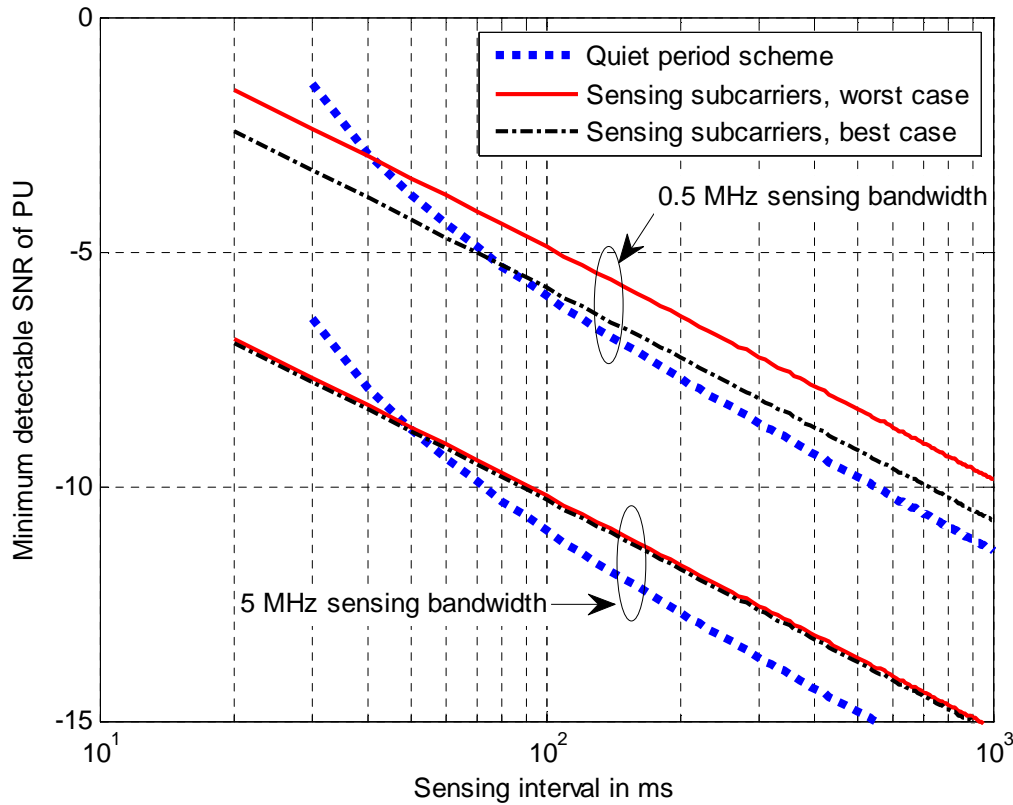


Figure 2.5. Sensitivity as a function of sensing interval with quiet period scheme and sensing subcarrier scheme. Groups of 18 subcarriers, the same overheads due to guards in both schemes.

2.5 Effects of PA nonlinearities

Figure 2.6 shows a subchannel-level signal model for an FBMC secondary device performing sensing subband based spectrum monitoring. The depicted exemplary case shows the dedicated sensing subband isolated by single-subchannel guard bands from the surrounding active secondary signal multiplexes SU X and SU Y. The secondary user signal-to-noise ratio (SU SNR) defines the received SU signal power relative to the effective noise floor in the secondary receiver. Similarly, the primary user signal-to-noise ratio (PU SNR) characterizes the level of the received primary user signal power (under hypothesis H_1) in comparison to the noise floor. The PU SNR and SU SNR(s) jointly with SU transmitter power amplifier characteristics set the requirements for the energy detector.

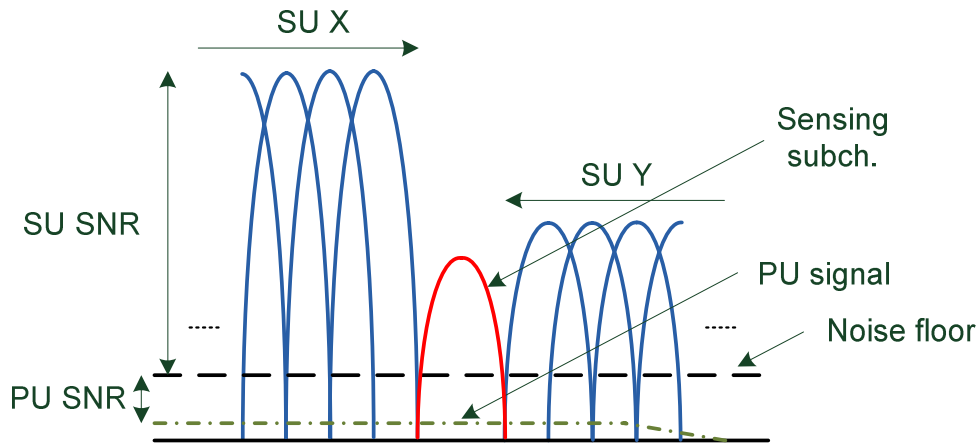


Figure 2.6. A signal model for the sensing subband based spectrum monitoring analysis.

The performance of the continuous sensing subband based monitoring scheme has been tested through simulations. Specifically, the proposed spectrum monitoring scheme was analyzed by running energy detection at a dedicated sensing subband in an FBMC secondary receiver during active secondary multiplexing, according to the signal model of Fig. 2.6. The secondary data transmission was modeled using following system parameters:

<i>Sampling frequency:</i>	1.4 MHz
<i>Transform size, M:</i>	128
<i>Overlapping factor, K:</i>	4
<i>Prototype filter design:</i>	NPR, frequency-sampling based design
<i>Transmission mode:</i>	Resource allocation in groups of 18 subcarriers (like UL-AMC23)
<i>Power amplifier model:</i>	PHYDYAS PA (see [D8109] for details)
<i>Channel model:</i>	AWGN.

The PU signal under hypothesis H_1 was modelled as a wideband (with respect to the bandwidth of the sensing subband) single-carrier signal with raised cosine pulse shaping. Moreover, in all the experiments considered the sensing subband was located within the bandwidth occupied by the active primary signal.

One essential practical aspect influencing the performance of the sensing subband scheme is the SU transmitter power amplifier (PA). Running the PA in its nonlinear operation region results in out-of-band spectral power leakage, which in turn will increase the effective level of the noise experienced by the energy detector in the spectrum monitoring subcarriers at the SU receiver. In the following analysis, we consider a PA model, which is specified in details in [D8109] and for which the relative power level of the spectral regrowth component corresponding to different PA input back-off (IBO) values are tabulated in Table 2.1.

Table 2.1. Spectral regrowth characteristics of the PHYDYAS PA model. Top row: input back-off. Bottom row: relative power level two subcarrier spacings from the active band edge subcarrier.

5.5 dB	6.0 dB	7.5 dB	8.0 dB	11.0 dB	12.0 dB	18.0 dB	No PA
-25.0 dB	-26.7 dB	-31.0 dB	-35.5 dB	-42.0 dB	-45.1 dB	-56.9 dB	-61.5 dB

The effective PU signal-to-noise ratio (under H_1) can be expressed as $P / \bar{\sigma}^2$, where

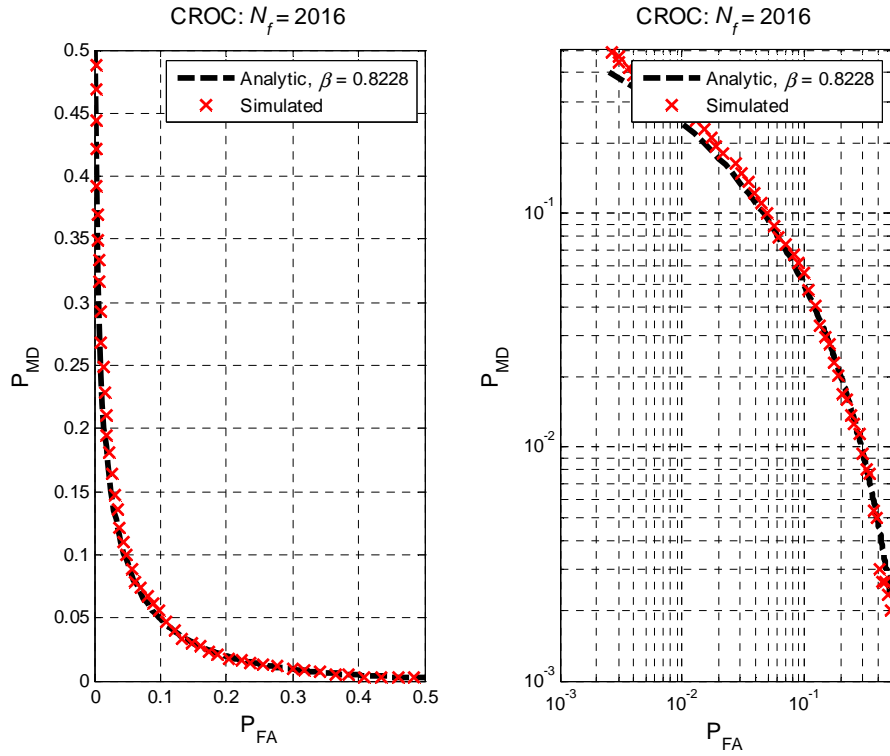
$$\bar{\sigma}^2 = \sigma^2 + \sum_{j=1}^2 \cdot 10^{SNR_{dB}^j/10} \cdot \sigma^2 \cdot 10^{\alpha_{dB}^j/10}. \quad (2.12)$$

SNR_{dB}^j and α_{dB}^j denote the power of the SU j (located next to the monitoring subcarrier in frequency) w.r.t. the noise floor and the PA back-off –dependent relative (w.r.t. to the SU signal power) level of the spectral regrowth component, respectively. Some example cases of $P / \bar{\sigma}^2$ are listed in Table 2.2.

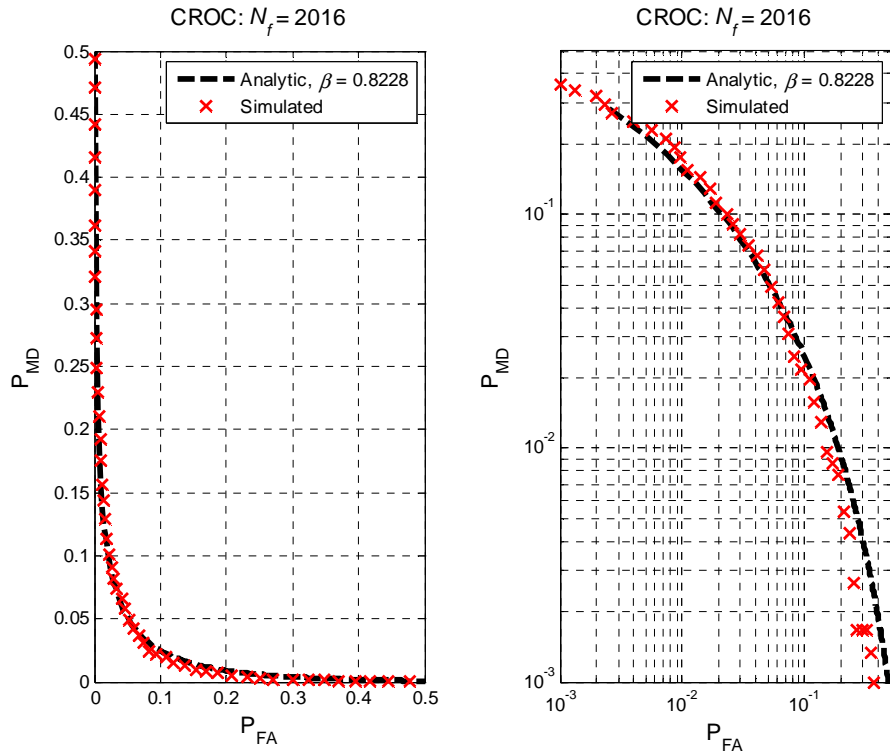
Table 2.2. Effect of spectral regrowth on effective PU SNR. Nominal PU SNR $|_{H_1} = -10$ dB .

SU SNRs	IBO					No PA
	6.0 dB	7.5 dB	8.0 dB	12.0 dB	18.0 dB	
15 dB	-10.55	-10.21	-10.08	-10.01	-10.00	-10.00
25 dB	-13.71	-11.77	-10.71	-10.08	-10.01	-10.00
35 dB	-21.62	-17.80	-14.44	-10.76	-10.06	-10.02
45 dB	-31.34	-27.10	-22.75	-14.70	-10.53	-10.19
55 dB	-40.31	-37.02	-32.53	-23.13	-13.60	-11.61

An analytical model for the test statistic in the monitoring subcarriers can be obtained by substituting $\bar{\sigma}^2$ for σ^2 in the expressions in (2.2) and including the factor $\beta = 0.8228$. The CROC curve derived based on the experimental data is compared to that of the analytical model in Fig. 2.7, showing fairly accurate match.



(a)



(b)

Figure 2.7. Verification of the effective PU SNR analysis through CROC plots. Number of fractionally-spaced observations $N_f = 2N$. PU SNR $|_{H_1} = -10$ dB, SU SNRs = 15 dB (a) SU IBOs = 6 dB, (b) SU IBOs = 9 dB.

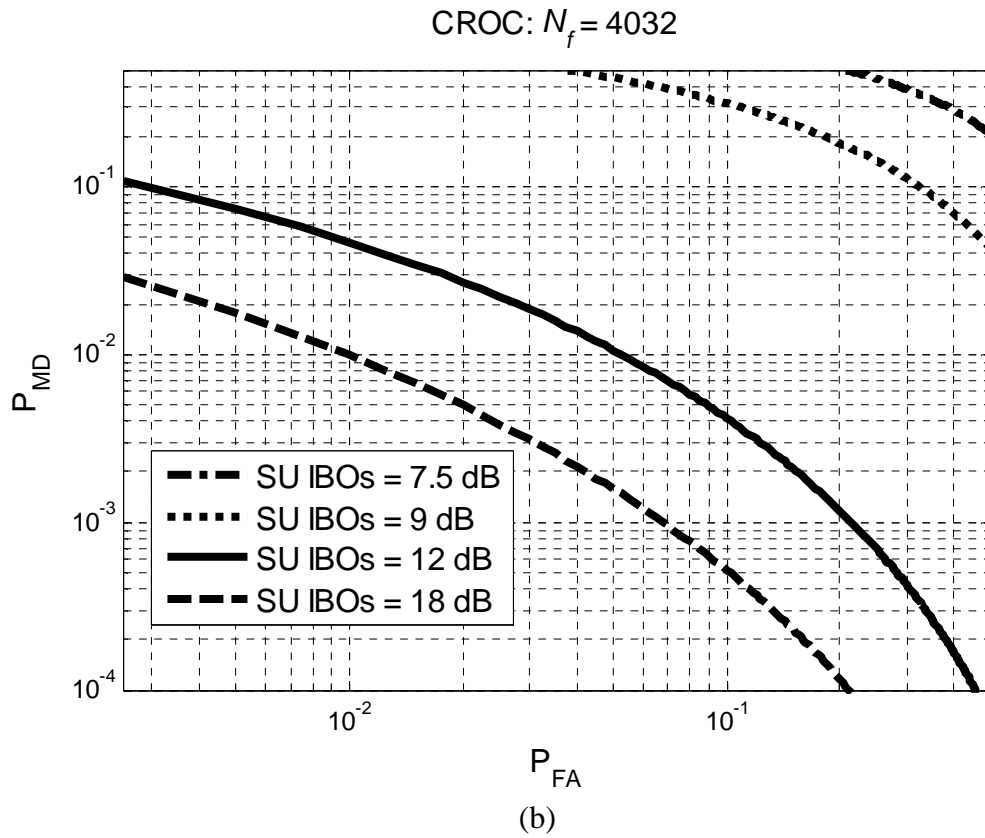
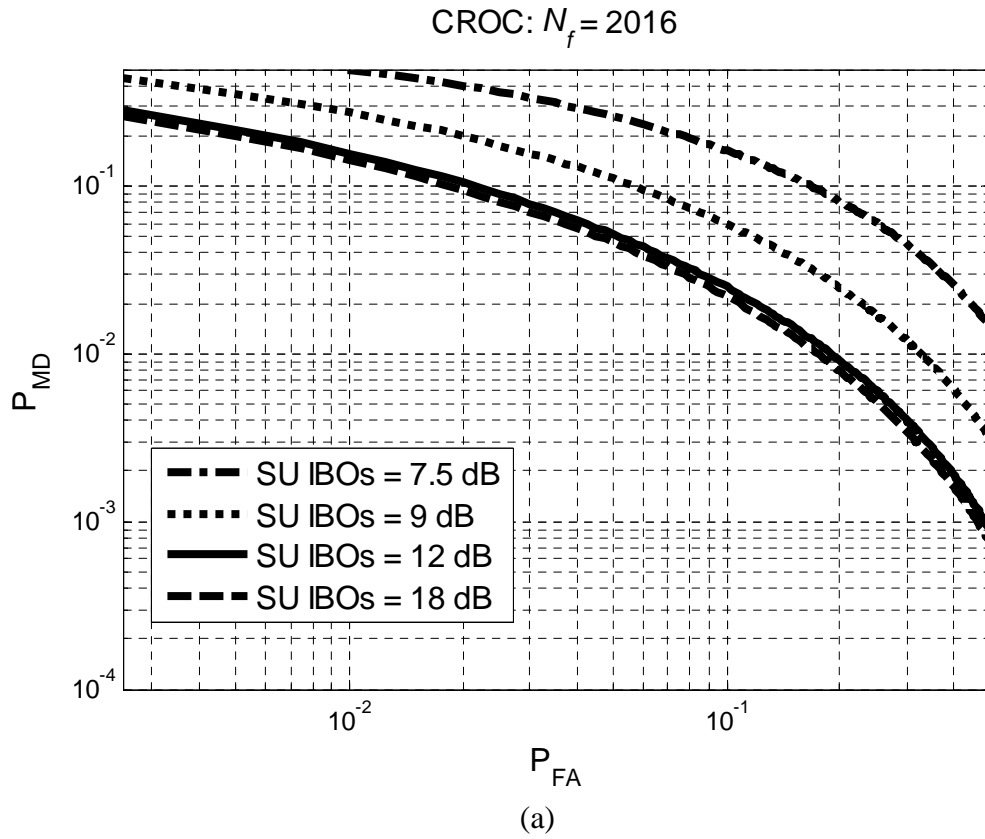


Figure 2.8. Analytic performance results with spectral regrowth effects and different SU signal-to-noise ratios. Number of fractionally-spaced observations $N_f = 2N$. PU SNR $|_{H_1} = -10$ dB (a) SU SNRs = 25 dB, (b) SU SNRs = 35 dB.

2.6 RF impairments in FBMC spectrum monitoring

The main challenge of the proposed sensing subcarrier scheme is due to the spectral regrowth effects. As demonstrated in Table 2.2, if the power levels of different secondary users are well under control (e.g., 25 dB SU-SNR, 10 dB back-off), the spectral regrowth effect is comparable to the noise uncertainty always experienced in energy detection based spectrum sensing. When the dynamic range of secondary users grows (e.g., 40 dB SU-SNR, 10 dB back-off), the spectral regrowth effects become comparable to the channel noise level. The increased effective noise level can be compensated by larger integration range. However, in this case the estimation of the level of spectral regrowth (or effective noise level) becomes a challenging problem. In order to expand the feasible SU dynamic range further, effective PAPR mitigation and power amplifier linearization methods are of crucial importance.

In general, the spectral regrowth characteristics of the transmitter depend heavily on the power amplifier design, transmitted power level, etc. Then, it is not easy to estimate the effective noise level in a sensing subcarrier, if there is uncertainty about the existence of a possible underlying PU signal. The following approaches can be conceived for solving this problem:

- Estimating spectral regrowth level from the level of nearby active subcarriers and knowledge of PA characteristics. This could be facilitated by transmission parameter signalling providing information about each SU's spectral characteristics.
- Statistical signal processing methods for detecting the part of noise in the sensing subband which is correlated with the nearby active subcarriers (e.g., based on ideas of [Val06]).
- Using spectrum sensing methods which are not sensitive to noise uncertainty.

The transmitter PA nonlinearity is clearly the most critical RF imperfection in this context. Still also the intermodulation distortion introduced by nonlinearities in the receiver has similar effects. In some of the mentioned techniques, the transmitter and receiver nonlinearities could be handled jointly.

3 Sequential Detection

Minimal monitoring time is an essential feature because a CR should be able to vacate the frequency band very quickly when a PU reappears. Classical detection methods, such as energy detection, can be categorized as *fixed sample size tests*, because the number of required data samples (integration time) is fixed in advance. This means that a reliable monitoring decision can be made only after all the data is processed. The needed amount of data can be pre-calculated based on the SNR level and desirable false-alarm probability. High sensitivity, i.e., low target SNR levels require large amount of data and it results in long monitoring time. In the following subsections we consider potential methods to decrease the detection time.

3.1 Main principles

In sequential detection, the number of data samples, which are used to make the decision, is not fixed in advance. The basic idea is that data samples (observations) are tested as individual sample or a small group of samples are available and the decision is made as soon as a sufficient amount of information is collected. In this manner, the reliable decision could be made much faster than when using those classical detection methods.

Sequential detection using hypothesis testing

A typical sequential detection method is based on statistical hypothesis testing or more specifically on the sequential probability ratio test (SPRT) proposed already in [Wal45]. Recently, sequential spectrum sensing schemes for cognitive radio have been proposed for example in [Kun07], [Cha08], [She08], [Cha09], [Xin09]. The objective is to distinguish whether data samples belong to H_0 (noise) or H_1 (PU signal + noise) hypothesis. A sequential detection test can be described to be a procedure, where the detector either selects one of the two hypotheses or waits and collects more observations. The mathematical description of this procedure is as follows:

$$\begin{cases} \text{If } T_n < A \Rightarrow \text{select } H_0 \\ \text{If } T_n > B \Rightarrow \text{select } H_1 \\ \text{Otherwise} \Rightarrow \text{continue testing (i.e., } n+1). \end{cases} \quad (3.1)$$

Here T_n is a selected test statistic for n samples and A and B are pre-calculated thresholds that typically depend on the desired performance. An example procedure of sequential detection is illustrated in Fig. 3.1.

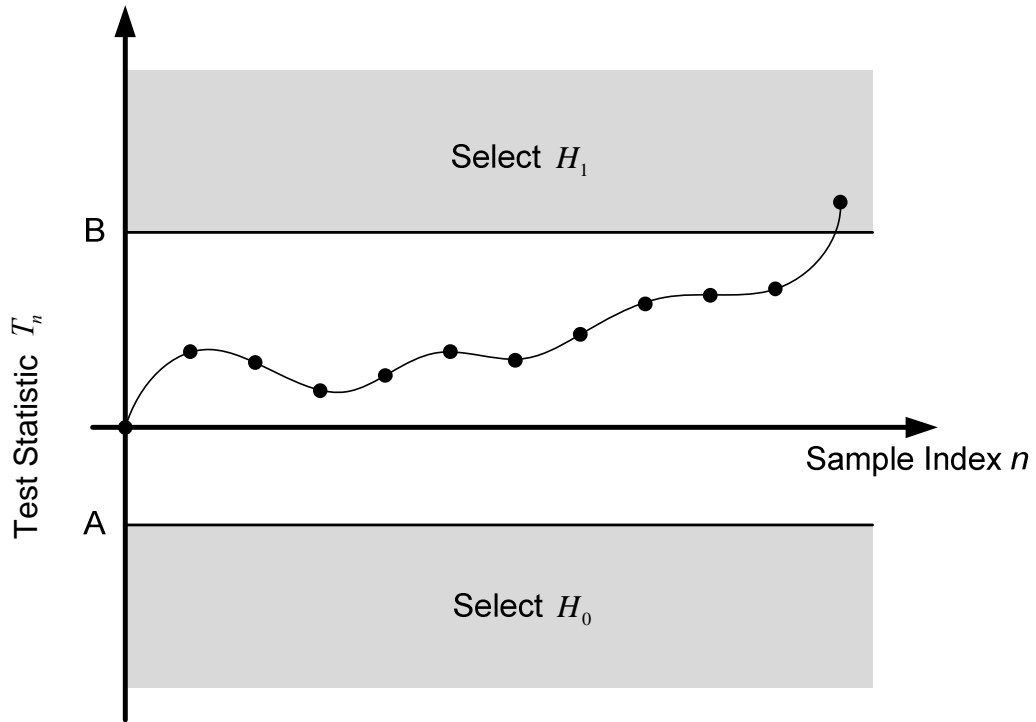


Figure 3.1. An example procedure of sequential detection.

In this section, we only concentrate on the energy based detection method and the main interest is its test statistic. As already mentioned, in the classical fixed sample size case the test statistic is defined as follows

$$T_N^{ED} = \frac{1}{N} \sum_{i=1}^N |Y[i]|^2, \quad (3.2)$$

where the available data samples are denoted as $Y[1], Y[2], \dots, Y[N]$. For sequential detection, the used test statistic is typically a probability (likelihood) ratio or log-likelihood ratio. At the n th sample instance, these ratios can be written as

$$T_n = \prod_{i=1}^n \frac{f_1(r_i)}{f_0(r_i)} = \prod_{i=1}^n \Lambda_i \quad (3.3)$$

or

$$T_n = \sum_{i=1}^n \log \left(\frac{f_1(r_i)}{f_0(r_i)} \right) = \sum_{i=1}^n \log \Lambda_i, \quad (3.4)$$

where f_0 and f_1 are probability density functions (PDFs). The exact form of these PDFs depends on the distribution of the random variable r_i . Here, we want to distinguish two different approaches. In the first one, the test statistic is calculated after each data sample, i.e., $r_i = |Y[i]|^2$ (for $i = 1, 2, \dots$). This kind of approach is considered for example in [Kun07][She08]. It is mentioned that r_i follow a

central chi-square distribution under H_0 and a non-central chi-square distribution with two degrees of freedom and a non-centrality parameter λ (received SNR) under H_1 . The calculation of the test static consists of the zero-th order modified Bessel function of the first kind and this can increase the complexity.

Here, we propose a novel idea that is based on the use of block of samples, i.e., $r_{b_s,i} = \frac{1}{b_s} \sum_{n=(i-1)b_s+1}^{ib_s} |Y[n]|^2$ (for $i = 1, 2, \dots$). Now $r_{b_s,i}$ can be approximated using the Gaussian distribution as follows

$$r_{b_s,i} \sim \begin{cases} \mathcal{N}\left(\sigma^2, \frac{1}{b_s} \sigma^4\right), & \text{under } H_0 \\ \mathcal{N}\left(P + \sigma^2, \frac{1}{b_s} (P + \sigma^2)^2\right), & \text{under } H_1, \end{cases} \quad (3.5)$$

where σ^2 is the noise variance, P is the signal variance, and b_s is the block size. By using this observation, we are ready to write the corresponding PDFs for the proposed approach

$$\begin{cases} f_0(r_{b_s,i}) = \frac{1}{\sqrt{2\pi\sigma_0^2}} e^{-\frac{(r_{b_s,i}-\mu_0)^2}{2\sigma_0^2}} \\ f_1(r_{b_s,i}) = \frac{1}{\sqrt{2\pi\sigma_1^2}} e^{-\frac{(r_{b_s,i}-\mu_1)^2}{2\sigma_1^2}}. \end{cases} \quad (3.6)$$

The corresponding mean (μ_0, μ_1) and variance (σ_0, σ_1) values are given in (3.5).

Typically, the thresholds for the sequential hypothesis test are functions of the required performance. More specifically, they are determined by the false-alarm P_{FA} and detection P_D probabilities. The upper and lower thresholds can be written as [Wal45]

$$B = \frac{P_D}{P_{FA}} \quad \text{and} \quad A = \frac{1 - P_D}{1 - P_{FA}}. \quad (3.7)$$

In order to obtain the desirable overall performance, it is even possible that these thresholds have to be subsequently adjusted during the test procedure [Xin09].

Basically, there is no automatic guarantee that the described sequential test process is every time faster than the fixed sample size test. Therefore, a *truncated sequential test* can be used for a practical implementation. The truncation means that when a maximum allowable number of samples is reached, the test is forced to take a decision by using a certain criteria. A truncated sequential test can be formulated as follows:

$$\begin{cases} \text{If } T_n < A \text{ and } n < N \text{ or } T_N \leq \gamma \Rightarrow \text{select } H_0 \\ \text{If } T_n > B \text{ and } n < N \text{ or } T_N > \gamma \Rightarrow \text{select } H_1 \\ \text{Otherwise} \Rightarrow \text{continue testing (i.e., } n+1). \end{cases} \quad (3.8)$$

Here γ is the predetermined threshold and N denotes the maximum number of data samples that can be waited until decision has to be made. This can be interpreted in such a manner that the result of fixed sample size test is used if the sequential test has not earlier reached the decision.

Sequential change-point detection

In the literature, hypothesis based testing is not the only option. An alternative approach is called as *change-point detection* or *quickest detection* [Lai08], [Li08], [Kim09-1]. In this method, the objective is to detect changes in the distribution of the observations as quickly as possible. Initially, data samples $Y[1], Y[2], \dots, Y[q]$ follow a distribution F_0 (with the corresponding density function f_0), but after a change-point at the sample index q the distribution of samples $Y[q+1], Y[q+2], \dots$ changes to F_1 (with the corresponding density function f_1) due to the activity of a PU. Once the distribution change is detected, the SU should start or end its transmission. The required action depends on the direction of the distribution change ($F_0 \rightarrow F_1$ or $F_1 \rightarrow F_0$). Clearly, the same framework can be used to detect both the empty frequency band and the reappearing of a PU. In the case of change-point detection, the basis of the decision making is the log-likelihood ratio. However, the overall procedure is not so straightforward because probability density functions are not necessarily fully specified. There exist different tests and algorithms that can be used depending on the knowledge of noise variance σ^2 and received PU signal variance P [Lai08].

Performance analysis of sequential detection

In this following analysis, we only concentrate on the hypothesis based sequential detection. Moreover, the test statistic is calculated based on a block of samples, i.e., $r_i = r_{b_s, i}$. We assume that the noise is additive white Gaussian with mean 0 and variance 1, whereas the PU signal is modelled as a noise with mean 0 and variance P . The design probabilities are $P_{FA} = 0.1$ and $P_{MD} = 0.01$. The transmission channel is assumed to be ideal, so the only changing parameters are PU's SNR and the used block size b_s . The performance is tested through 5000 simulations (PU is either active or absent during the whole detection time) per each SNR value and block size. The performance metrics are the average sample number (ASN) and the realized false-alarm P'_{FA} and misdetection P'_{MD} probabilities. The results are shown in Figs. 3.2 and 3.3.

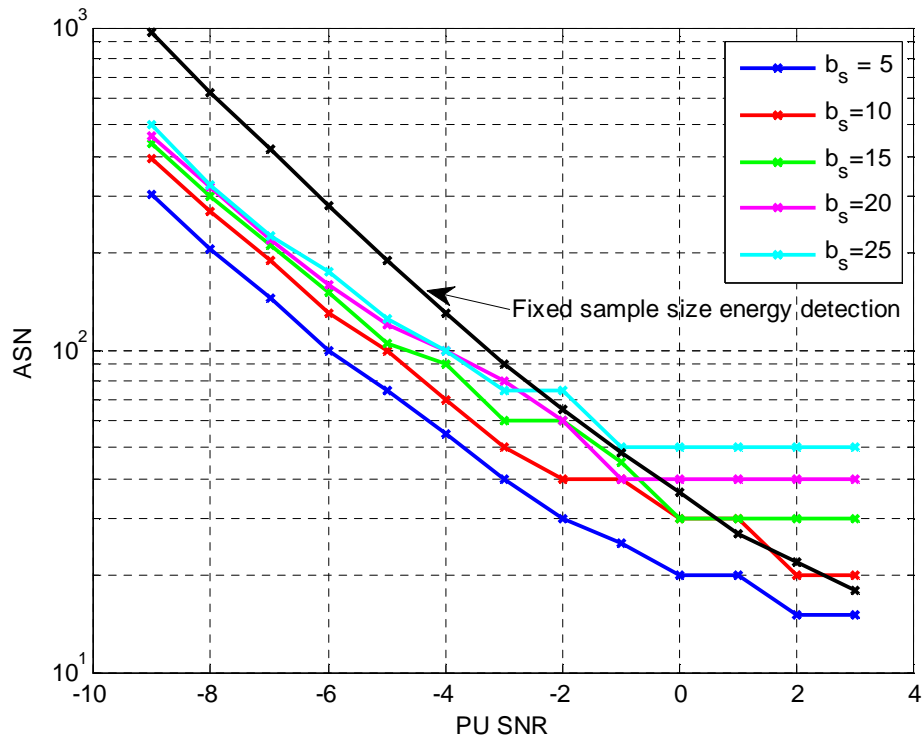


Figure 3.2. Average sample number as a function of SNR using different block sizes.

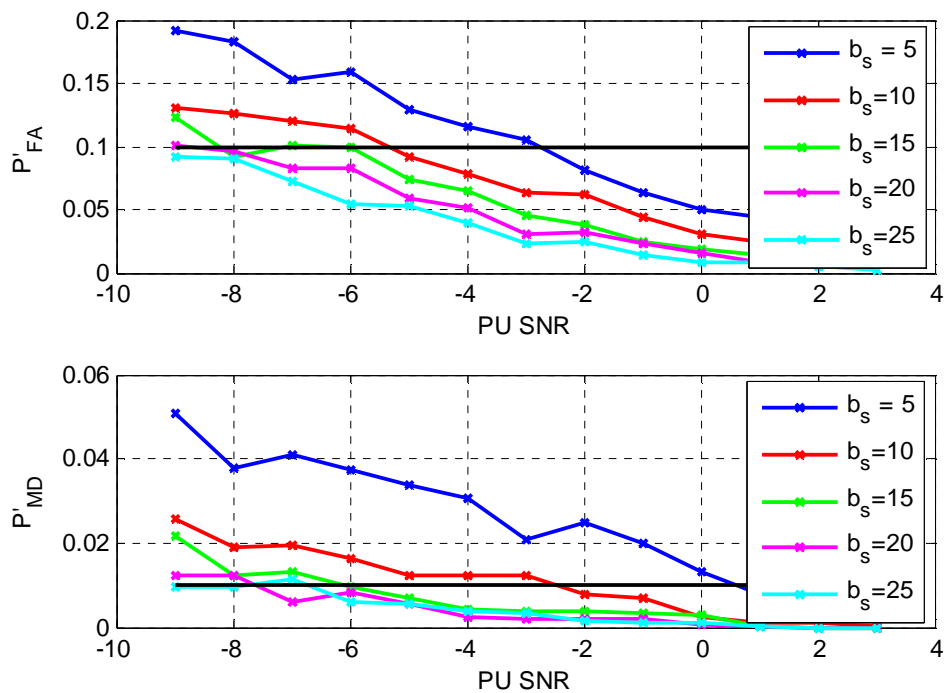


Figure 3.3. Realized false-alarm and misdetection probabilities as a function of SNR using different block sizes.

Figure 3.2 shows that the sequential detection is able to reduce ASN when compared to the classical energy detection. Clearly, the smaller is the block size the larger is the improvement. Logically, positive SNR values are slightly exceptional because in those cases the block size can be already

higher than the amount of samples required in classical energy detector. The realized false-alarm and misdetection probabilities appear to be contradictory with the design values for small block sizes. A probable reason is that the distribution of r_i 's does not yet follow the Gaussian distribution well enough. The approximation will get better when the block size is larger than 15 samples. A possible solution for smaller block sizes is to adjust decision thresholds during the test procedure as mentioned in [Xin09]. One important point to notice is that if a basic energy detector is designed for a low target PU SNR, it takes the same time to detect a much stronger PU signal. On the other hand, a sequential detector is able to detect a strong PU signal in a very short time.

3.2 Detecting re-appearing PU signal

General analysis

In the analysis considered so far, it is assumed that the PU is either absent or active during the whole sensing interval of N observations, which are used to construct the test statistic,

$T(\mathbf{Y}) = \frac{1}{N} \sum_{n=0}^{N-1} |Y[n]|^2$. In practice, it may happen that the PU becomes active (reappearing PU) during the measurement period. In such cases only some fraction of samples within the sensing window, say $0 \leq N_1 \leq N$ samples, are measured after PU becomes active. Such a transient phase and the related test statistic distributions are illustrated in Fig. 3.4.

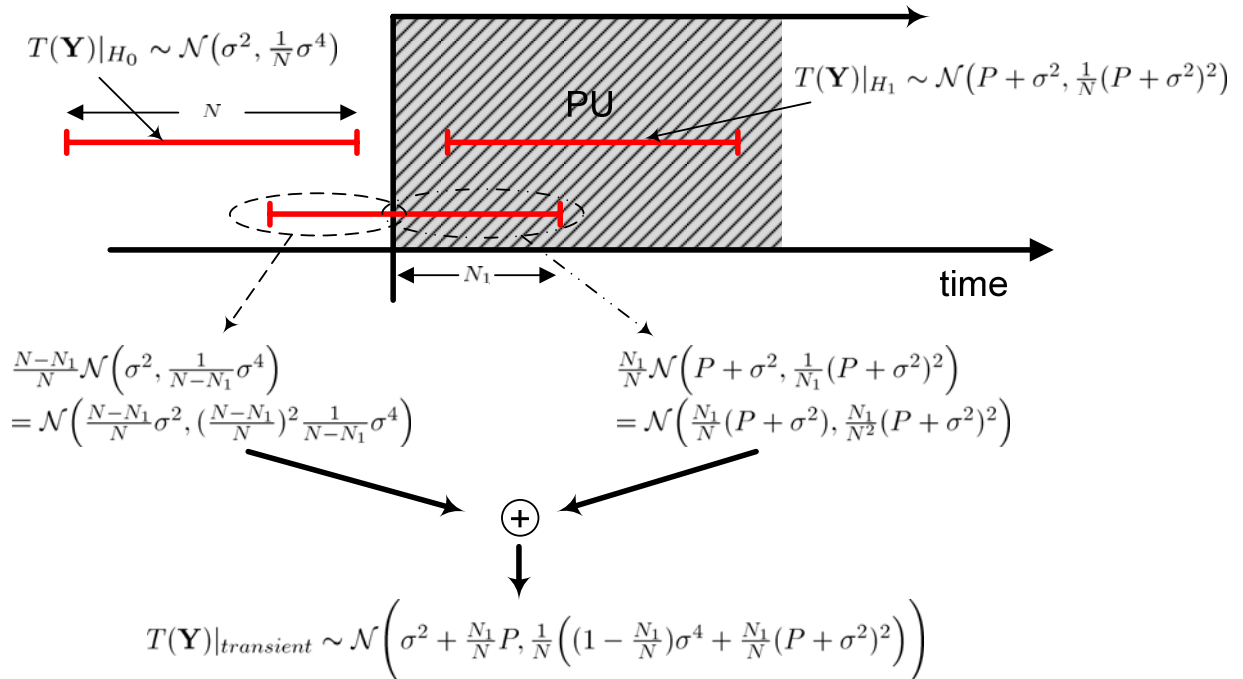


Figure 3.4. Analytic model for the distribution of the test statistic during a transient phase, when a PU reappearance falls within the sensing interval.

The distribution of the test statistic during the transient phase, $T(\mathbf{Y})|_{transient}$, can be derived as follows. The sensing window can be split into two distinct sub-windows such that one of them contains only those observation samples before the PU becomes active ($N - N_1$ samples; see Fig.

3.4 for clarification) while the other contains the remaining N_1 samples. The distributions of the test statistic corresponding to the observation samples within these sub-windows are $\mathcal{N}\left(\sigma^2, \frac{1}{N-N_1}\sigma^4\right)$ and $\mathcal{N}\left(P+\sigma^2, \frac{1}{N_1}(P+\sigma^2)\right)$, respectively. The overall sequence of N samples can be interpreted as a linear combination of these independent normal random variables using relative weights of $\frac{N-N_1}{N}$ and $\frac{N_1}{N}$, respectively. Now, by making use of the following property of independent normal distributions

$$\begin{cases} X_1 \sim \mathcal{N}(\mu_1, \sigma_1^2) \\ X_2 \sim \mathcal{N}(\mu_2, \sigma_2^2) \end{cases} \Rightarrow aX_1 + bX_2 \sim \mathcal{N}(a\mu_1 + b\mu_2, a^2\sigma_1^2 + b^2\sigma_2^2) \quad (3.9)$$

we obtain an expression for the mixture-distribution

$$T(\mathbf{Y})|_{transient} \sim \mathcal{N}\left(\sigma^2 + \frac{N_1}{N}P, \frac{1}{N}\left(\left(1 - \frac{N_1}{N}\right)\sigma^4 + \frac{N_1}{N}(P + \sigma^2)^2\right)\right). \quad (3.10)$$

The weighting between H_0 and H_1 distributions depends on, N_1 , a parameter defining the relative amount of observation samples collected before and after the reappearance of the PU signal.

The probability of detecting the presence of PU signal during transient phase, $P_{D,tr}$, can be defined as the *towards* $+\infty$ tail probability of the distribution in (3.10), with respect to a given decision threshold, when $0 < N_1 < N$. $P_{D,tr}$ can be interpreted to gradually increase within the lower and upper limits of $P(T(\mathbf{Y}) > \gamma|_{H_0}) = P_{FA}$ and $P(T(\mathbf{Y}) > \gamma|_{H_1}) = P_D$, respectively.

Figures 3.5 (a) and (b) illustrate the behaviour of the detection probability during the transient phase with two alternative representations. A fixed sized sensing window with $N = 300$ samples is used for detecting the PU at different operating SNRs. Performance is shown for a number of alternative cases corresponding to different PU reappearance times in relation to the sensing window position. The decision threshold is designed to achieve false alarm probability of 0.1 with $N_1 = 0$. The noise variance is assumed to be perfectly known. Results of the experimental data (based on 5000 tests) can be observed to closely match with those of the analytical distribution model in (3.10).

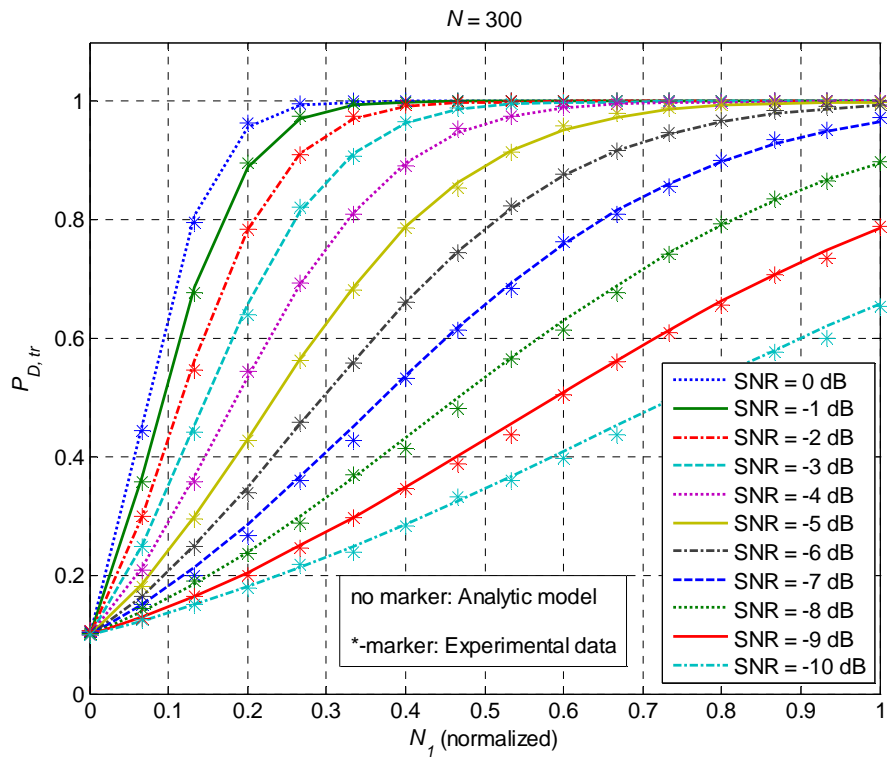
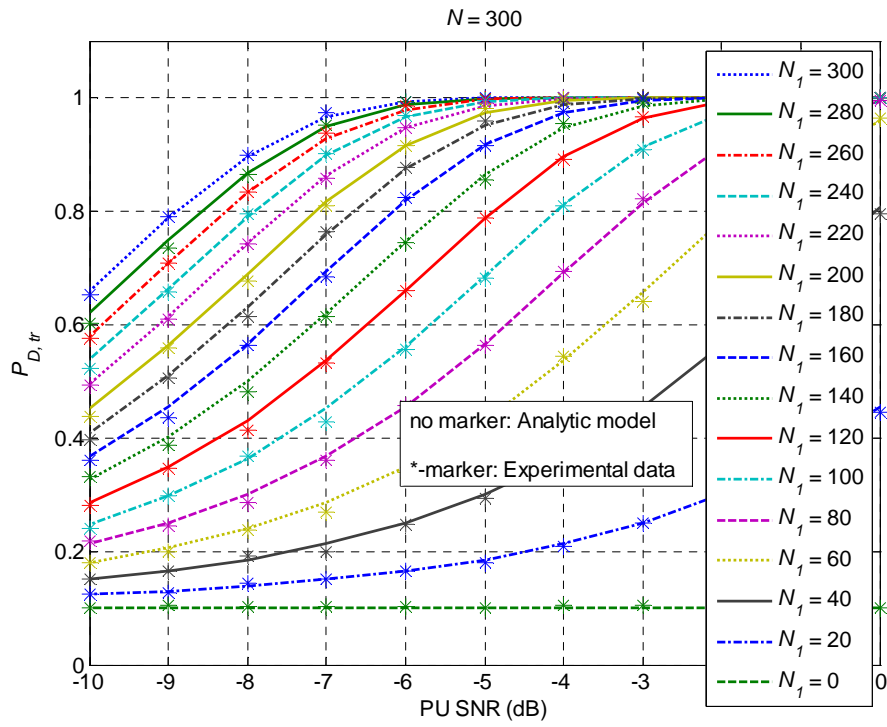


Figure 3.5. Probability of detection as a function of (a) PU SNR and (b) normalized N_1 parameter (N_1 / N) when PU reappearance falls within energy detector sensing window. Lines without markers represent the performance based on the analytical model, whereas *-markers show the experimental results based on 5000 tests.

Sequential detection point of view

Logically, the reappearance of the PU signal could be modelled as a change-point problem but we will show that the hypothesis based sequential detection is also a practical tool for this scenario. The main idea is to use independent sequential detection processes with different starting times as illustrated in Fig. 3.6. The period between two successive processes can be freely chosen. For example, a new process can be started as soon as the previous one has made the decision or several consecutive processes can be partly overlapping. It is also possible to use short idle periods if needed. An advantage of this approach is that the overall decision making procedure is very straightforward and parallel detection processes can be implemented easily. The process can be based on block-wise decision statistics. Then, what is needed is a set of accumulators, one for each of the parallel decision processes.

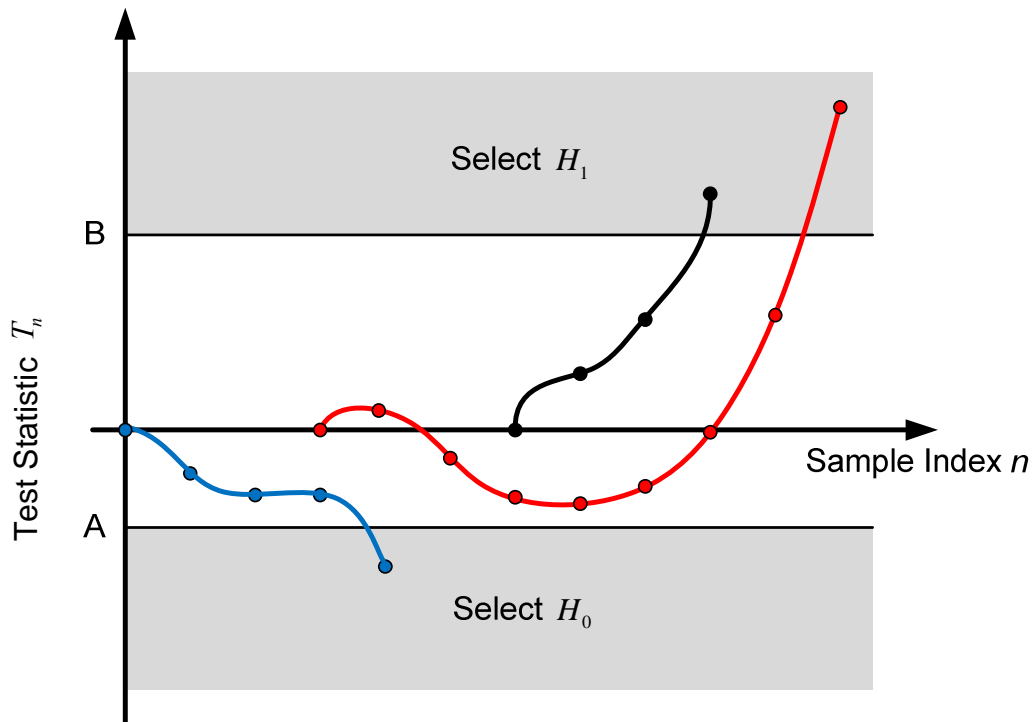


Figure 3.6. The detection of reappearing of PU signal using parallel sequential detection processes with different starting times.

The performance of the hypothesis based continuous sequential detection in the case of reappearing of a PU signal has been evaluated using simulations with ideal transmission channel. Again, it is assumed that the noise is additive white Gaussian with mean 0 and variance 1, whereas the PU signal is modelled as a noise with mean 0 and variance $P=0.2512$ (equivalent to PU SNR = -6 dB). The decision thresholds are defined using probabilities $P_{FA}=0.1$ and $P_{MD}=0.01$. The block size of 15 is used for the calculation of r_i . The PU signal reappears at the sample index 300 and the starting time indexes for 5 different detection processes are chosen to be [1,101,153,254,305].

By observing the results, which are obtained from an example simulation, shown in Fig. 3.7, we can identify different performance patterns:

- All samples during the process belong to a noise-only part and the decision is hypothesis H_0 . Naturally, there is always the possibility of false-alarm by making the wrong decision.
- At the beginning, a certain amount of samples belong to a noise-only part and the rest of the samples include a PU signal. The value of the test statistic approaches the lower threshold but the process recovers and makes a correct decision.
- At the beginning, a certain amount of samples belong to a noise-only part and the remaining samples belong to a PU signal. In spite of the PU signal samples, the value of the test statistic crosses the lower threshold resulting in a wrong decision.
- Most of the samples or all samples belong to a PU signal, the decision is reached quite quickly. However, there is always the possibility of misdetection.

Evidently, the speed of the decision making depends on several different variables such as the PU signal SNR, the block size, the starting times of the processes, and even the properties of the data samples. However, the proposed approach is very flexible and the overall performance looks promising.

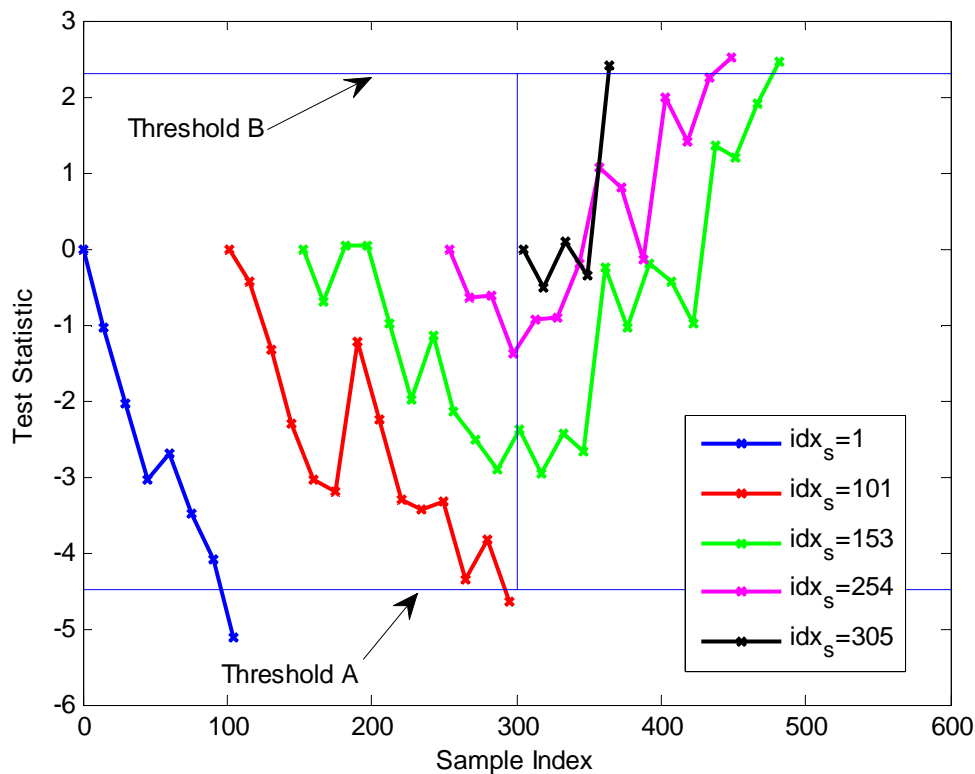


Figure 3.7. An example case of simulated performance of continuous sequential detection in the context of a reappearing PU signal.

3.3 Fading channels and co-operative sensing

Frequency selectivity

Most of the spectrum sensing publications, and also this report so far, have focused on the AWGN channel case. However, in most cognitive radio scenarios, the channel is frequency selective and fading. Next we discuss briefly about these issues.

The analysis of Section 2.3 leading to (2.7) and (2.8) can be applied also to analyze the effects of channel frequency selectivity by replacing the prototype filter frequency response with the channel frequency response and ignoring the oversampling related discussions. In order to test this model, we have considered a wideband Vehicular A channel model using 1000 independent quasi-static channel instances and sample complexity of $N=1000$ samples. The channel impulse response is scaled for unit power gain in order to analyze the effect of frequency selectivity only. Then the test statistic distribution can be modelled as Gaussian:

$$\begin{aligned} T(\mathbf{Y})|_{H_0} &\sim \mathcal{N}\left(\sigma^2, \frac{\beta}{N}\sigma^4\right) \\ T(\mathbf{Y})|_{H_1} &\sim \mathcal{N}\left(P + \sigma^2, \frac{\beta}{N}(P + \sigma^2)^2\right) \end{aligned} \quad (3.11)$$

with

$$\beta = \sum_{l=1}^L \frac{|F_{ch}|^4}{L} \quad (3.12)$$

where F_{ch} is the FFT of the channel impulse response.

Experimentally, the analytical results (i.e., calculating β using (3.12) from known channel responses) match fairly well with simulations (calculating β from experimental variance according to (3.11). Specifically, over a set of 1000 independent channel instances, the maximum value of coefficient β is 2.1 and its mean value is 1.5, both in simulations and in the analytical model. Further, in 90 percent of the cases, $\beta < 1.68$ in the analytical model and $\beta < 1.68$ in simulations. Thus using a β value in the range 1.7...2 seems to give a good conservative basis for modelling the effect of a wideband frequency-selective channel in energy detection. Obviously, narrowband cases become critical for sensing performance. Detailed evaluation of different channel models remains a topic for future studies.

Fading channels

In general, channel fading has severe effects on energy detection based spectrum sensing because it effects also on the mean of the decision statistic. The effect of flat fading on energy detection performance has been analyzed in the literature, see [Dig03] and various later contributions. Antenna diversity is an effective approach to overcome the effects of small-scale fading, whereas co-operative spectrum sensing is effective against both small-scale and large-scale fading (shadow fading). Both techniques have been widely analyzed in the literature and analytic formulas are available for various scenarios, however, mostly for the flat-fading case.

Based on the above discussion, it seems natural to model the overall frequency selective fading process in energy detection in two parts:

- Taking the frequency selectivity into account through a proper choice of the β - coefficient.
- Using the flat-fading models from the literature for the selected antenna diversity or co-operative sensing scheme.

Detailed elaboration and verification of this approach remains a topic for future studies.

Sequential detection has been identified in the literature as an effective tool in co-operative sensing for combining the sensing information in the fusion centre from different sensing devices [Cha08], [Cha09]. This will be discussed briefly below. Sequential detection is useful also in the context of antenna diversity. For example, an effective way to implement selection combining in spectrum monitoring could be as follows: Use the method of Section 3.2 independently for each of the antennas. Once any of the sequential detection processes declares that a PU is present, then this is accepted as a decision for the overall detection process. Alternatively, the soft decision combining process described below could be used for combining the sensing information from different antennas.

Sequential co-operative detection

In principle, every SU may carry out sequential detection independently of the other SUs and make its own decisions based on the test statistic it has collected. On the other hand, sequential detection can also be applied in a distributed co-operative manner [Cha09]. In this case, a so-called fusion center (FC) makes the final decisions based on the information sent by SUs. This FC can be a specific central node or one of the SUs.

In general distributed co-operative sequential detection has several advantages when compared with non-cooperative detection [Cha09]. For example, it can

- improve the detector performance
- facilitate the use of simpler detectors
- decrease detection time
- increase the coverage
- allow the mitigation of the effects of shadowing and fading.

In the sequential co-operative detection, there are two different approaches available: *soft decision combining* and *hard decision combining*. In the soft combining, every SU transmits its decision statistic (possibly complemented with the measured SNR) to the FC as soon as it exceeds the local threshold. After receiving a SU statistic, the FC performs a hypothesis test to decide whether test statistics belong to H_0 or H_1 hypothesis. If information is not sufficient for making a decision at a specified reliability level, the FC acquires an additional test statistic from another SU and repeats the procedure. Clearly, this kind of double sequential testing is not necessarily the best solution with respect to detection time and computational complexity. Consequently, the hard decision could be more appropriate for co-operative detection because now every SU sends just its binary decision to the FC. In this case, the FC can test different SU decisions sequentially by using simple OR, majority, or AND rule [Kun07]. The meaning of these rules is that the H_1 hypothesis is accepted if at least one of the SU, a specific number of SUs, or all SUs have detected the PU, otherwise the H_0 hypothesis is selected.

Boosting Protocol

In co-operative detection, after detecting a PU signal, the fusion center uses signalling channels to inform all the elements of the SU system to stop transmissions in the affected frequency band, and starts a process to move the transmission to another white space. Another scheme is the boosting protocol proposed in [Wei03]. In this scheme, any element of the SU system, after detecting the presence of a PU, sends a short special pilot-like signal at high power level, which informs the base station quickly about the reappearance of a PU. This can be regarded as OR-type co-operative sensing with special signalling channel.

4 CP Autocorrelation Based Sensing for OFDM PUs

OFDM is extensively used in current and emerging wireless communications standards, and thus PUs appearing in future cognitive radios will commonly use OFDM waveforms. Therefore, it is interesting to consider exploiting the specific features of OFDM in spectrum sensing. A common feature of almost all OFDM based systems is the presence of cyclic prefix (CP), which introduces peaks in the autocorrelation in the received waveform at lags corresponding to the length of the useful symbol period. This characteristic has been used, e.g., for synchronization purposes, and also for spectrum sensing [IEE06], [Cha08], [Cha09], [Han08], [Che08]. Based on these studies, CP-autocorrelation approach appears as an effective, low-complexity spectrum sensing method, which overcomes the noise uncertainty problem of energy detection.

4.1 FBMC-based frequency-domain implementation

The autocorrelation of the received waveform is basically a time-domain operation. Usually, it is assumed that the spectrum sensing bandwidth matches the full bandwidth of the PU signal, and contains either noise only or noise plus PU signal. Considering spectrum monitoring, this situation could be reached only using quiet periods, and further, the quiet periods should be synchronized between different locally operating secondary systems. In case of uncoordinated secondary systems, the situation could be as illustrated in Fig. 4.1.

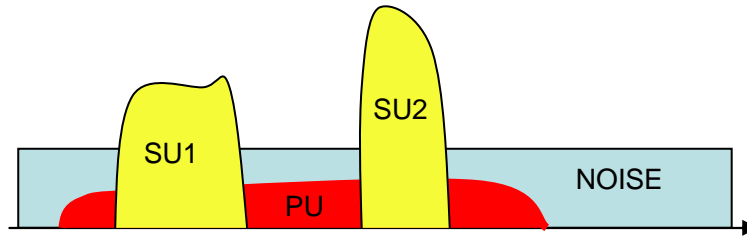


Figure 4.1. A typical spectrum monitoring scenario with uncoordinated secondary systems.

Of course, it is possible to do the autocorrelation for the clean part(s) of the PU signal band only, but this would require additional highly configurable filtering in the receiver. This raises interest to consider possibilities to do the autocorrelation utilizing subband signals which are clean from secondary user signals. Actually, in an FBMC receiver, the autocorrelation for a specific time lag τ , normalized to the FBMC subcarrier sample interval, can be implemented in frequency domain as:

$$\begin{aligned}
 C_X(\tau) &= \frac{1}{N} \sum_{n=1}^N \sum_{k \in \Omega} y_{k,n}^* \cdot y_{k,n+n_\Delta} e^{-j2\pi\tau k} \\
 &= \frac{1}{N} \sum_{k \in \Omega} \left(\sum_{n=1}^N y_{k,n}^* \cdot y_{k,n+n_\Delta} \right) e^{-j2\pi\tau k}
 \end{aligned} \tag{4.1}$$

where $y_{k,n}$, $k = 0, \dots, M-1$, are the subband output samples from the analysis bank, Ω is the set of used subcarriers, and N is the integration length in FBMC subband samples. The latter form of (4.1) is computationally efficient. Equation (4.1) indicates the possibility of using different subcarrier samples in the basic autocorrelation calculation, with spacing of n_Δ . This helps to maximize the

correlation observation for different combinations of the PU OFDM symbol duration and FBMC subband sample interval.

Let us consider the following example case:

- OFDM: useful symbol length is $T_U = 512$ samples, CP length $T_{CP} = 128$ samples, 300 active subcarriers, QPSK modulation
- FBMC: 768 subbands utilizing the PHYDYAS filter bank with $K = 4$.
- Three choices of sensing subbands
 1. Full-band sensing: 450 FBMC subbands covering the 300 OFDM subcarriers
 2. Partial band sensing: 22 contiguous subbands
 3. Distributed sensing subbands: 22 subbands with spacing of 21

With these parameters, the subband sample interval corresponds to 384 high-rate samples and the lag of 512 samples corresponds to 1.33 subband sample intervals. Experimentally it can be verified that with $n_\Delta = 0$ the correlation is weak, but with $n_\Delta = \pm 1$ and $n_\Delta = \pm 2$ strong correlation exists. With $n_\Delta = \pm 1$ there is strong additional correlation with zero lag due to oversampled subband sequences, so we favor the choice $n_\Delta = \pm 2$. Figure 4.2 illustrates an example of the corresponding autocorrelation for lags $0, 1, \dots, M-1$ (in high rate samples). Notice that these autocorrelation sequences can be calculated easily using DFT. Figure 4.3 illustrates the distributed subband sensing case in a similar way. We notice that the autocorrelation sequence becomes repetitive in such a way that one of the main peaks is at the expected location.

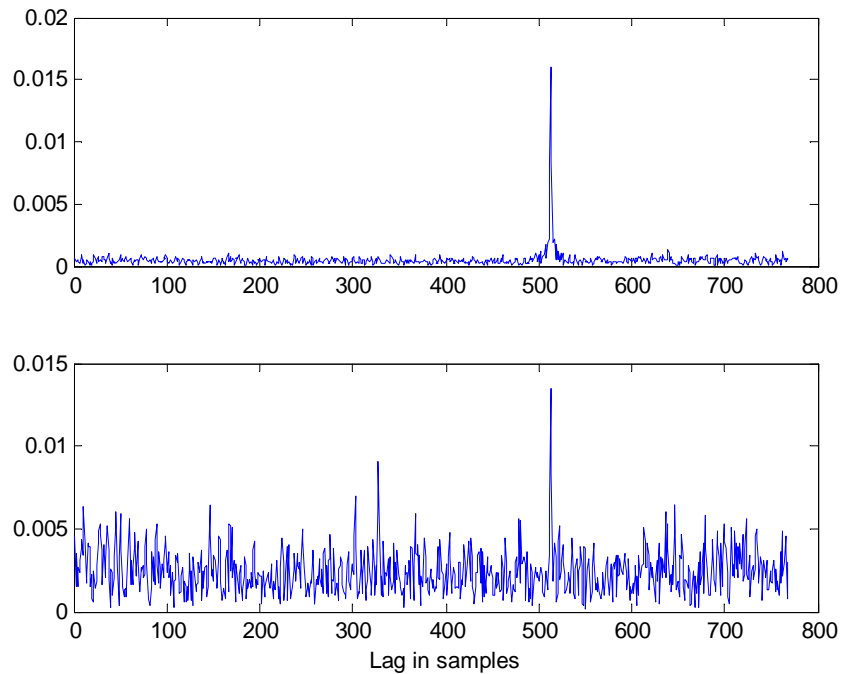


Figure 4.2. Example of autocorrelation magnitudes obtained through FBMC subband processing. Full-band sensing case with integration over 200 subband samples, AWGN channel. (a) Noise free case. (b) $\text{SNR} = -6$ dB.

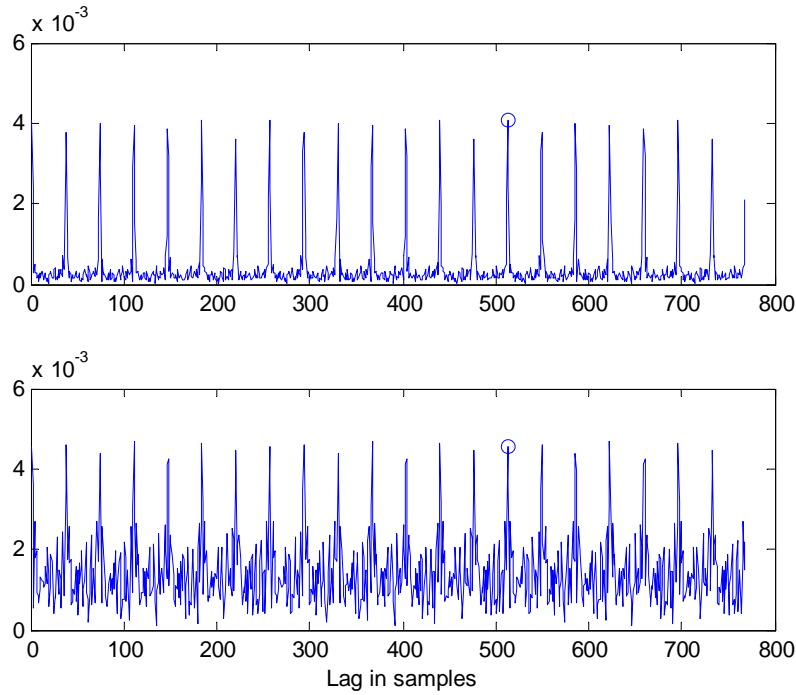


Figure 4.3. Example of autocorrelation magnitudes obtained through FBMC subband processing. Distributed subband sensing case with integration over 1000 subband samples, AWGN channel.

(a) Noise free case. (b) SNR = -6 dB.

It is shown in [Cha08] that the noise in the autocorrelation-based decision statistic can be well-modelled as Gaussian distributed. The autocorrelation coefficient is

$$\rho = \frac{E(r_n r_{n+M_{OFDM}}^*)}{E(r_n r_n^*)} = \begin{cases} 0 & \text{under } H_0 \\ \frac{T_{CP}}{T_U + T_{CP}} \frac{SNR}{1 + SNR} & \text{under } H_1. \end{cases} \quad (4.2)$$

In time domain implementation, it is enough to do the autocorrelation calculation over the CP length only, if the spectrum sensing device is synchronized to the PU. This would reduce noise in the decision statistic, but such assumption is not realistic in practical spectrum sensing scenarios. In the FBMC-based frequency domain implementation, the decision statistic is affected by the analysis filter bank effects and the choice of n_Δ . The Gaussian model seems to be valid, but further work is needed to get analytic expressions for the variance and mean.

Ideally, the autocorrelation coefficient is real, and the sensing decision can be based on the real part of the calculated autocorrelation value. However, this is valid only if the sensing receiver is frequency-synchronized to the PU signal. A carrier frequency offset of ε (normalized to subcarrier spacing) would cause a phase rotation of $2\pi\varepsilon$ to the observation. If frequency synchronization cannot be assumed, the decision should be based on (squared) magnitude of the observed autocorrelation value.

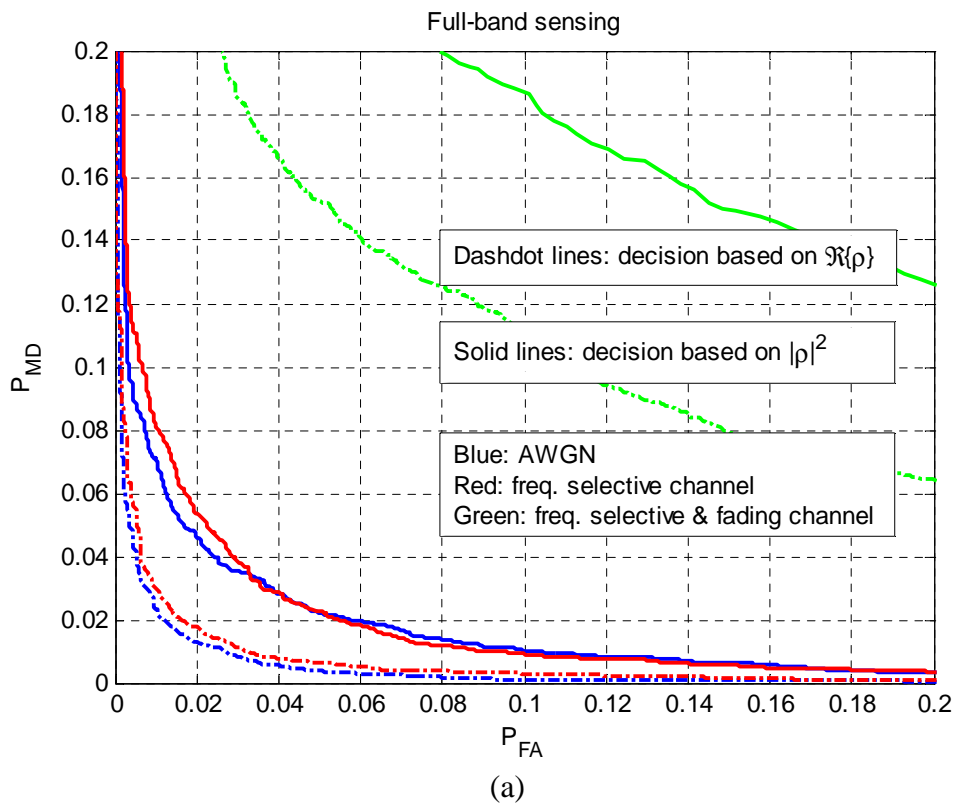
Figure 4.4 shows the sensing performance, in terms of CROC curves, in the example case for all three choices of the sensing subbands, and for both real part and squared magnitude based criteria. The results are shown for three cases of the PU channel model:

- AWGN channel
- Frequency selective channel utilizing the Vehicular A power delay profile; channel power gain is normalized to 1 for each channel instance.
- Vehicular A channel with independently Rayleigh-fading multipath components.

The channel is assumed to be stationary during each sensing interval. The results are for 5000 independent OFDM symbol, noise and channel instances.

We can observe that both in full-band sensing and with distributed sensing subbands, the channel frequency selectivity has minor effect on the performance, whereas fading degrades the sensing performance significantly. In the partial band sensing case, the effects of frequency selectivity are significant. All in all, these results give an experimental verification that the CP autocorrelation based spectrum monitoring, implemented through FBMC subband processing, is a promising approach for OFDM PUs.

It is important to notice that sequential detection methods, discussed in Section 3, can easily be combined with frequency-domain CP autocorrelation method, in the same way as time-domain methods are used in [Cha09].



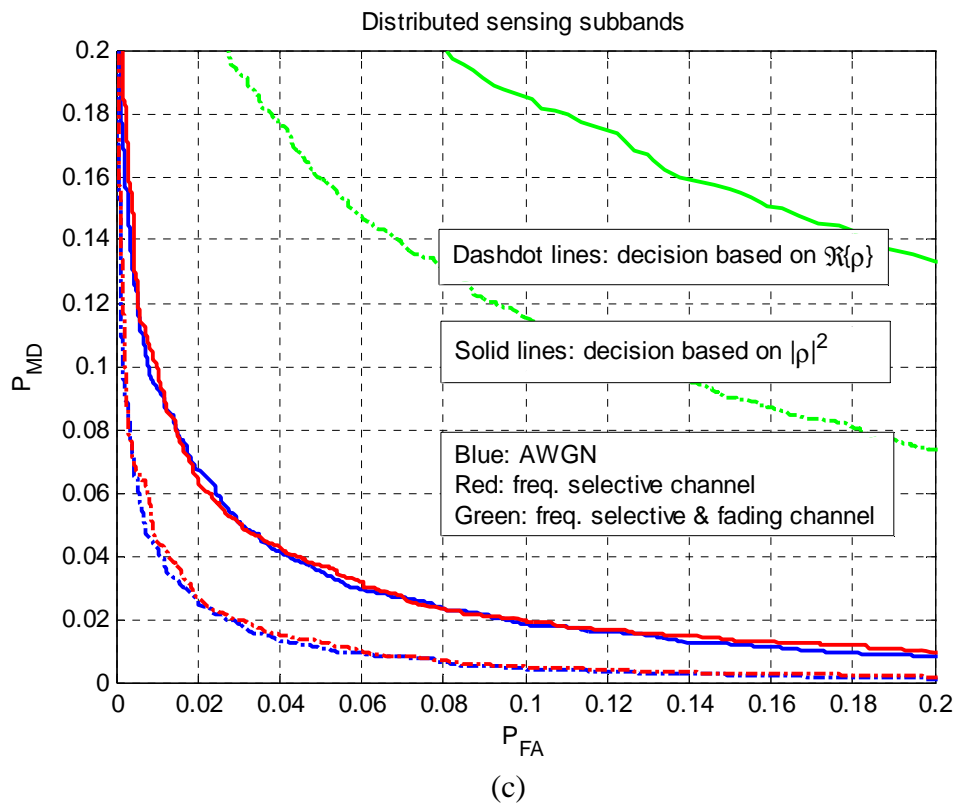
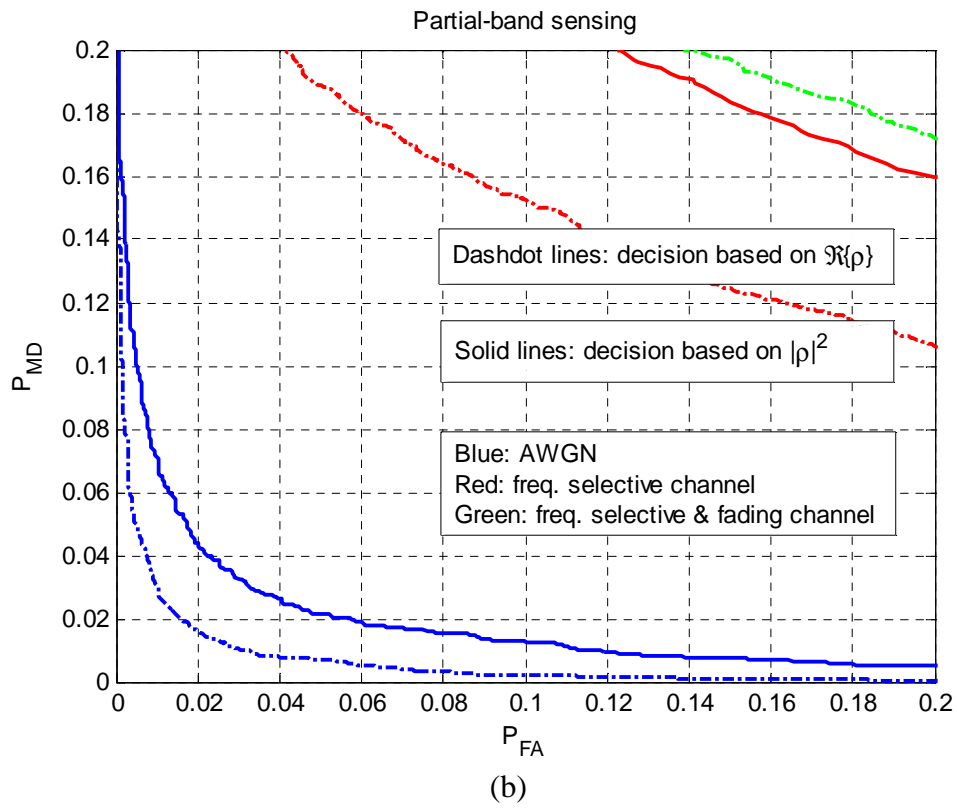


Figure 4.4. Complementary ROC performance curves for different sensing subband configurations: a) full-band sensing scheme, b) partial sensing scheme, and c) scheme based on distributed sensing subbands. Different decision criteria and different channel models.

4.2 Spectrum monitoring concept for PHYDYAS DSA

In this subsection we formulate a possible spectrum monitoring concept which is consistent with the dynamic spectrum access (DSA) scheme developed in the PHYDYAS project. It utilizes techniques developed above in Sections 2-4 of this document, many of which are novel to the best of our knowledge. The proposed spectrum monitoring scheme includes the following elements:

- Sensing subband model with energy detection or frequency-domain CP autocorrelation based method for OFDM PUs.

Sensing subband model is selected because it allows spectrum monitoring in scenarios where several independent SU systems utilize the same white space with minimum amount of coordination. This model offers also sufficient frequency diversity, i.e., it doesn't compromise the sensing performance with frequency selective channels.

- Co-operative spectrum sensing, possibly together with antenna diversity in some of the SU elements.
- Using sequential detection at all levels (basic sensing, antenna combining, sensor fusion). Sequential detection is tuned for rapid detection of reappearing PUs through multiple parallel sensing processes.
- Using the base station as the fusion center to achieve high sensitivity in co-operative detection.
- In addition, the boosting protocol is used to reach rapid action in case of reappearing strong PUs. In this context, the sensing subcarriers within the frequency band of the detected PU are used for sending signalling information between the elements of the SU system. In parallel, the active subcarriers of the SUs are used for finalizing the on-going transmissions and providing further signalling information for re-organizing the SU system (assuming, of course, that the PU is at a power level which allows the SU to operate).

To complete the description of the concept, the role of the different SU system elements in the co-operative sensing process needs to be discussed. We consider here a base-station (BS) ruled system, so, naturally, the fusion center is located at the base station. The size and mobility/portability of the SU BS may be different in different applications, but at least in some scenarios, the BS may be equipped with antenna(s) above to roof-top level and could thus be free of shadow fading. In such cases, the BS is able to reach relatively high sensitivity in spectrum sensing, depending of course on the characteristics of the PU system (this reasoning fails, for example, when the PU system operates locally indoors only). But also in these scenarios, additional sensing devices might be needed at the cell edge areas.

If the PU system has effective uplink power control, the BS is in good position for sensing also in the sense that the dynamic range of the UL signals is well under control. Then, for example, the PA spectral regrowth effects are not very critical. On the other hand, the elements of other SU systems operating nearby, spectrally and geographically, might have significant effect on the dynamic range of the signals seen by the BS under consideration. The used DSA scheme has great effect on this issue.

Let us then consider the signal dynamic range observed by the mobile stations (MS'es). Clearly, MS'es close to the BS usually receive the downlink signal at a high power level, and have difficulties in spectrum sensing. This depends naturally on the DL multiple access scheme and possible existence of downlink power control. On the other hand, in an isolated SU system, MS'es

at the cell edge region are in a good position for spectrum sensing. Again, this depends on the DSA scheme and on the possible existence of other SU systems operating in the same region.

The key elements of this concept have been developed and tested, or they have been introduced based on literature, in the above sections. However, validation of this overall concept, as well as various details and more complete analytical and simulation based performance studies remain topics for future work.

5 Filter Bank based Multiband Spectrum Sensing for Cognitive Radio Networks

In filter bank based multicarrier transmission, two classes of filter banks can be distinguished

- filter banks with overlapping filters. The 3dB-passband of the prototype filter equals the sub-channel frequency spacing. The PHYDYAS reference filter belongs to this class, which leads to maximum transmission speed.
- filter banks with non-overlapping filters. The main lobe of the prototype filter frequency response is contained in the sub-channel frequency spacing, so that neighbouring sub-channels do not overlap. This is the most widely used class in past and present communication systems. In the nineties, the corresponding scheme was called “filtered multitone” (FMT).

In the context of cognitive radio, filter banks improve the resolution of the real time spectrum analyzer, with respect to the FFT. In fact, this was one of the main motivations for developing the PHYDYAS project. Due to the non-overlapping property, FMT systems are likely to provide better spectrum sensing performance than systems based on overlapping filters.

In this chapter, we investigate a multiband detection architecture based on Polyphase Filter Bank (PFB), which aims to reliably sense multiple active bands by exploiting the low leakage property of PFB. The objective of the present chapter is to quantify some sensing parameters, namely detection and false alarm probabilities, and compare the results obtained for the FMT and PHYDYAS approaches. The straightforward design technique of the PHYDYAS prototype filter can be applied to the design of non-overlapping filters as well. However, in order to maximize the challenge to the overlapping filter, the Nyquist transmission constraint is dropped and the FMT prototype filter is designed according to the prolate technique and is denominated “prolate sequence window” (PSW) filter. The prolate principle consists of maximizing the in-band energy to out-of-band energy ratio. For the sake of completeness, the FFT is included in the comparison, under the term “periodogram spectrum estimator” (PSE). The difference in performance between PSE and the filter banks allows putting in perspective the difference between the two filter bank approaches

Spectrum sensing on a single frequency band has a relatively rich literature. However, the literature of multiband sensing which monitors multiple frequency bands simultaneously is very limited. Generally, the spectrum sensing schemes fall into three categories: energy detection, matched filter detection and cyclostationary feature detection. The basic concept of multiband sensing is to firstly estimate the power spectral density (PSD) and then power detection (which is simple and can locate spectrum occupancy information quickly) is applied in the frequency domain based on the observed power spectrum. In [Hur06], a wideband dual-stage sensing technique: a coarse and a fine spectrum sensing architecture was proposed. These two sensing stages collaborate with each other to enhance the accuracy of spectrum sensing performance. In [Che09], three widely used spectrum estimation methods: weighted overlapped segment averaging approach, multi-taper spectrum estimator and multiple signal classification algorithm were introduced and compared for wideband detection. The authors in [Qua09] considered making joint decisions over multiple frequency bands. The spectrum sensing problem is formulated as a class of optimization problems in interference limited cognitive radio networks. In [Tas09], a novel approach called segmented periodogram for wideband spectrum segmentation is proposed. The proposed scheme is based on the posterior expectation of the piece-

wise flat realizations of the underlying signal spectrum, which is obtained using the reversible jump Markov chain Monte Carlo technique. According to the estimated segmented periodogram, the wideband detection performance can be improved compared to conventional periodogram.

However, few of the aforementioned studies consider the PSD estimation applying Polyphase Filter Bank (PFB) [Sio02][Bel08]. PFB was proposed as an efficient tool for spectral analysis [Far08] without additional cost since each secondary user can be equipped with PFB as the receiver front end. This means that the PFB structure for communication will offer a new opportunity for sensing at no extra cost. Furthermore, the complexity issues associated with PFB for spectrum sensing were investigated in [Mah08], and a new low complexity PFB architecture for multi-standard cognitive radios was presented. The previous works using PFB and energy detector for multiband sensing can be found in [She09][Kim09]. In these papers, the performance of the PFB based multiband sensing was evaluated in comparison with conventional periodogram spectrum estimator (PSE), and the final simulation results demonstrated the significant advantage of the PFB multiband sensing compared to conventional PSE. Nevertheless, both of these papers employ an optimal prolate sequence window (PSW) as a prototype filter of the PFB. This PSW prototype filter as a spectral analysis cannot be reused for communicating.

In this section, our motivations for multiband sensing are firstly focused on the PFB based on the prototype filter of the projet PHYDYAS. Theoretical expressions of detection and false alarm probabilities for PFB and PSE based detectors are derived. Thereby, proper threshold levels for different detectors can be achieved to ensure a fair comparison. Specifically, the PFBs using the prototype filter of PHYDYAS and PSW are investigated and compared with the conventional PSE, and experimental results verify the theoretical analysis and reveal that PFB is a better spectrum analyzer instead of PSE.

5.1 System model and multiband sensing architecture

5.1.1 System model

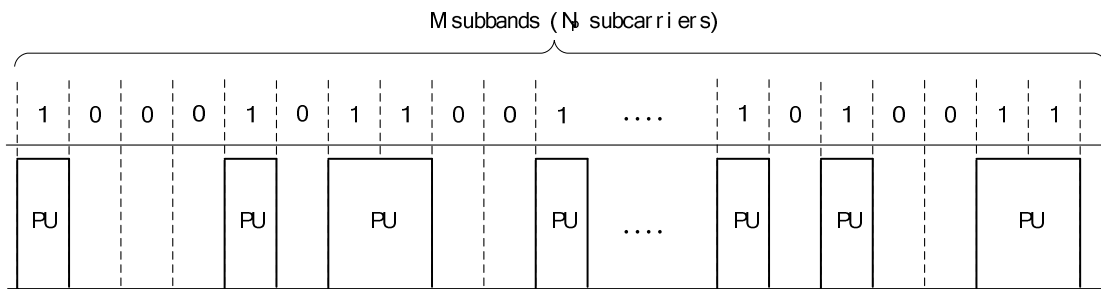


Fig. 5.1: Primary channel distribution

In the context of cognitive radio network, a primary system operating over a wideband channel with " N_p " subcarriers is considered. As illustrated in Fig. 5.1, the whole frequency band licensed to the primary users (PU) is divided into " M " nonoverlapping subbands with " L " subcarriers per subband. In a particular time interval or geographical region, some of the " M " subbands might not be occupied by the PUs and are available for secondary users (SU). Fig. 5.1 displays the primary channel distribution in some time interval, wherein the subbands occupied by primary users are referred to as "1", whereas the available subbands for SUs are referred to as "0".

According to the assumed primary model, the crucial task of SU is to sense the " M " subbands and identify available subbands for opportunistic use. The basic multiband sensing scheme will be introduced in the next subsection.

5.1.2 Multiband sensing architecture

In our study, we take into account the detection of PUs for multiple frequency subbands instead of considering one single band at a time. The basic multiband sensing architecture is shown in Fig. 5.2. It is noted that the accomplishment of the multiband sensing comprises of two basic parts: power estimation and energy detection. Every secondary node in the cognitive radio network is equipped with a FFT or a PFB based spectrum analyzer for the power estimation over the band of interest. On the basis of the estimated power density spectrum, the simple energy detector is then applied in different subbands.

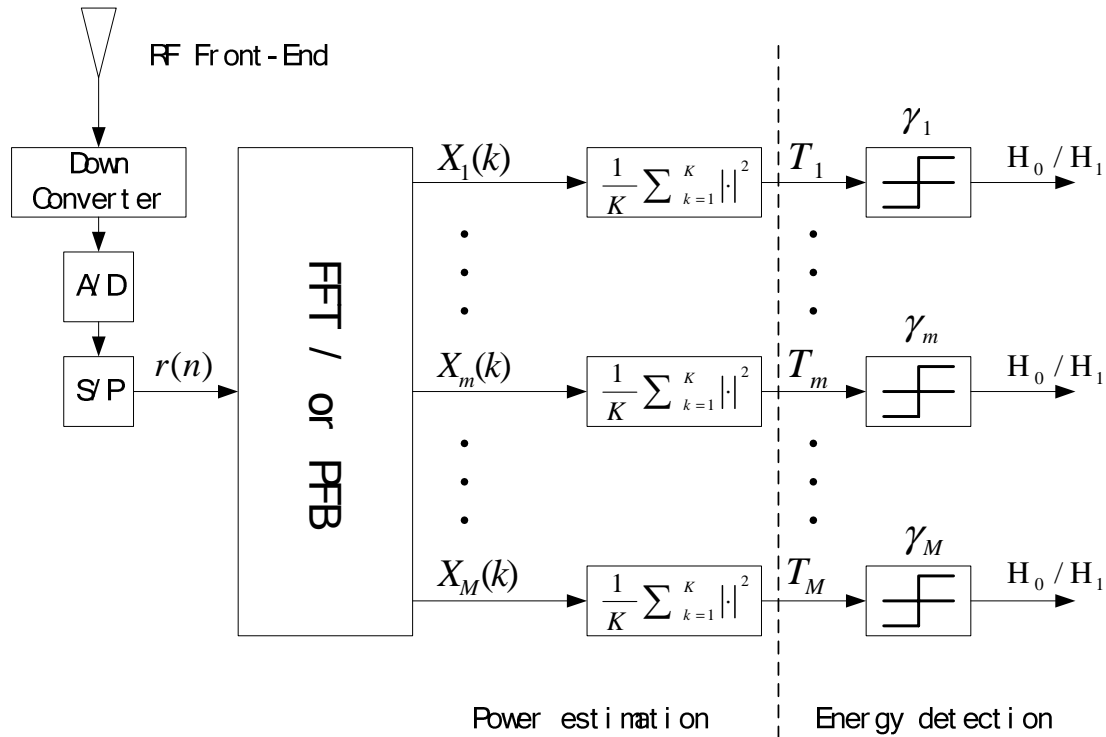


Fig. 5.2: Multiband sensing architecture: joint power estimation and energy detection

For simplicity, the PU signal affected by an AWGN channel is considered herein, and we assume that the noise variance σ_n^2 is perfectly known at the receiver due to the measurements when signal is absent. The binary test hypotheses at the m^{th} subband are

$$\begin{aligned} H_0 : r_m(n) &= w_m(n) \\ H_1 : r_m(n) &= s_m(n) + w_m(n) \end{aligned} \quad (5.1)$$

where $s_m(n)$ and $w_m(n)$ are the primary transmitted signal and the band limited noise signal at the m^{th} subband, respectively.

The received wideband signal $r(n) = \sum_{m=1}^M r_m(n)$ including all subbands' information is firstly processed by SU to estimate the frequency spectrum X_m in all the subbands using M point FFT

$$X_m = \sum_{n=0}^{M-1} r(n) e^{-j2\pi \frac{mn}{M}}, \quad m = 0, 1, \dots, M-1 \quad (5.2)$$

and then the test statistic for the m^{th} subband is given

$$T_m = \frac{1}{K} \sum_{k=1}^K |X_m(k)|^2 \quad (5.3)$$

where $K = N/M$, and N is the samples of received signal. Given the threshold γ_m , the detection rule is: $T_m \geq \gamma_m \rightarrow H_1$, $T_m < \gamma_m \rightarrow H_0$.

5.2 Theoretical sensing performance

In this subsection, the wideband sensing performance are investigated from a theoretical point of view. Three different spectrum analyzers are considered: conventional PSE, PHYDYAS based PFB and PSW based PFB.

When PHYDYAS based PFB or PSE spectrum analyzers are applied, the frequency estimation $X_m(k)$, $k = 1, 2, \dots, K$, are complex independent observations.

Given the complex frequency estimation $X_m(k)$ with zero mean and variance $\sigma_{H_{0(1)}}^2$, the modulus of $X_m(k)$ satisfies a Rayleigh distribution

$$|X_m(k)| \approx \text{Rayleigh}(\sqrt{\sigma_{H_{0(1)}}^2/2}) \quad (5.4)$$

The two-order and four-order raw moments of $|X_m(k)|$ can be therefore calculated as

$$E(|X_m(k)|^2) = \sigma_{H_{0(1)}}^2, \quad E(|X_m(k)|^4) = 2 \cdot \sigma_{H_{0(1)}}^4 \quad (5.5)$$

by which the variance of $|X_m(k)|^2$ is obtained accordingly

$$\text{Var}(|X_m(k)|^2) = \sigma_{H_{0(1)}}^4 \quad (5.6)$$

According to the central limit theorem (assuming K is sufficiently large), the distributions of T_m in the absence (H_0) and the presence (H_1) of primary signal are subject to Gaussian approximation

$$H_0: T_m \approx \mathcal{N}(\sigma_{H_0}^2, \frac{1}{K} \sigma_{H_0}^4)$$

$$H_1 : T_m \approx N(\sigma_{H_1}^2, \frac{1}{K} \sigma_{H_1}^4) \quad (5.7)$$

here $\sigma_{H_0}^2$ and $\sigma_{H_1}^2$ are the variances of $X_m(k)$ in the absence and the presence of primary signal, respectively.

With respect to PSW based PFB, the central limit theory is no longer valid since $X_m(k)$ are complex correlated observations due to the correlated property of PSW.

For this special case, the frequency estimation $|X_m(k)|^2$ are a sequence of dependent and identically distributed random observations each having finite values of expectation $\sigma_{H_0(1)}^2$ and variance $\sigma_{H_0(1)}^4$. With a sufficiently large number of random variables, the test statistic T_m can be approximately normally distributed, then the mean and the variance of T_m are given by

$$\begin{aligned} E(T_m) &= E\left(\frac{1}{K} \sum_{k=1}^K |X_m(k)|^2\right) = \sigma_{H_0(1)}^2 \\ \text{Var}(T_m) &= \frac{1}{K^2} \text{Var}\left(\sum_{k=1}^K |X_m(k)|^2\right) \\ &= \frac{1}{K^2} \left[\sum_{k=1}^K \text{Var}(|X_m(k)|^2) \right. \\ &\quad \left. + 2 \cdot \sum_{i < j} \text{Cov}(|X_m(i)|^2, |X_m(j)|^2) \right] \\ &\approx \frac{1}{K^2} [K \sigma_{H_0(1)}^4 + 2K(R(1) - \sigma_{H_0(1)}^4)] \\ &\approx \frac{2}{K} \sigma_{H_0(1)}^4 \end{aligned} \quad (5.8)$$

where $R(1)$ is the autocorrelation between $|X_m(k)|^2$ and $|X_m(k+1)|^2$, $k = 1, 2, \dots, K-1$. In order to facilitate our theoretical analysis, the test statistic T_m using PSW based PFB is approximately treated as Gaussian distribution for a large K , and the distributions in the absence and the presence of primary signal can be written as

$$\begin{aligned} H_0 : T_m &\approx N(\sigma_{H_0}^2, \frac{2}{K} \sigma_{H_0}^4) \\ H_1 : T_m &\approx N(\sigma_{H_1}^2, \frac{2}{K} \sigma_{H_1}^4) \end{aligned} \quad (5.9)$$

In the literature [She09][Kim09-2], the variances $\sigma_{H_0}^2$ and $\sigma_{H_1}^2$ in (5.7) and (5.9) were easily regarded as the noise variance σ_n^2 and the signal-plus-noise variance $\sigma_n^2 + \sigma_s^2$, respectively, and thus the same theoretical threshold was used to implement the subband detection for both windowed FFT and filter bank based spectrum analyzer. For more precise detection and fair detection performance comparison, more stringent requirement of defining a proper detection threshold for various spectrum analyzers should be considered.

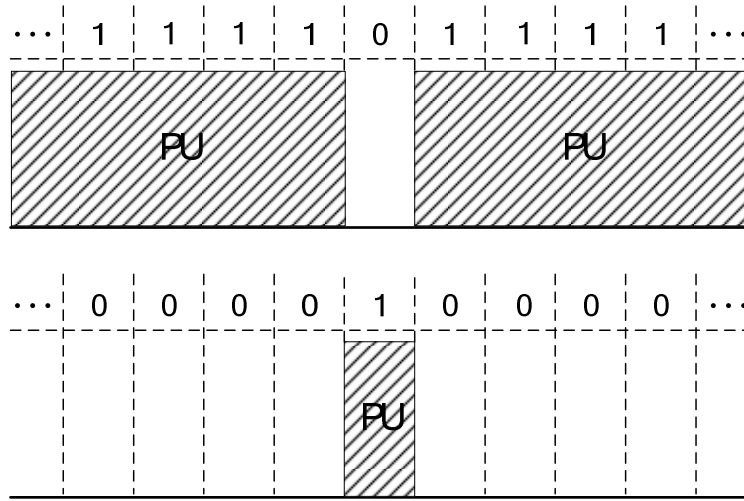


Fig. 5.3: Two extreme cases corresponding the absence and the presence of primary signal

Next, we attempt to achieve the corresponding variance values $\sigma_{H_{0(1)}}^2$ of the frequency estimation $X_m(k)$ for conventional PSE, PHYDYAS based PFB and PSW based PFB. In the first instance, our analysis is based on two extreme cases, as illustrated in Fig. 5.3. It is important to note that the spectrum estimation disparity between these two extreme cases is envisaged to be the smallest. In the absence of primary signal, the extreme (worst) case is in such a way that the detected subband (referred to as "0" in the top graphic of Fig. 5.3) is fully surrounded by primary users, which contribute somewhat interfering power to the power estimation result. Conversely, in the presence of primary signal, the worst detection result of the detected subband (referred to as "1" in the bottom graphic of Fig. 5.3) emerges when there is no primary users in the neighborhood.

The detection performance of each detected subband could be well guaranteed provided that the detection requirement of the subbands in the two extreme cases are satisfied. For this reason the theoretical detection threshold can be yielded by analyzing the statistic property of these two extreme cases.

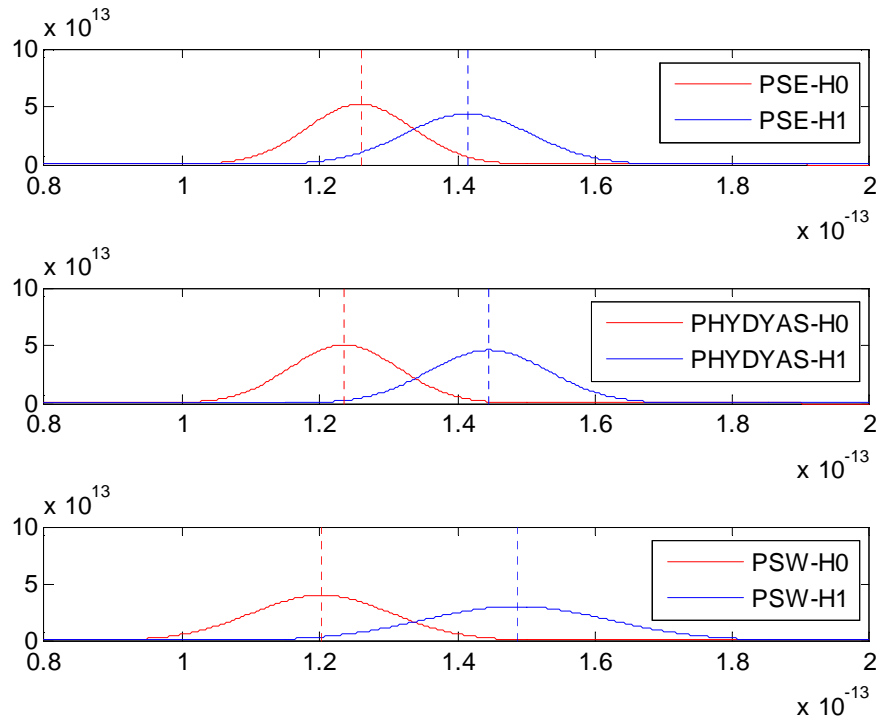


Fig. 5.4: The probability density functions of the variable T_m for three different spectrum analyzers

In order to facilitate the analysis, normalization is carried out. The variances of $X_m(k)$ can be expressed as

$$\begin{aligned}\sigma_{H_0}^2 &= \sigma_n^2 + C_0 \cdot \sigma_s^2 \\ \sigma_{H_1}^2 &= \sigma_n^2 + C_1 \cdot \sigma_s^2\end{aligned}\quad (5.10)$$

where the coefficient values of C_0 and C_1 corresponding to different prototype filters can be calculated by the simulated probability density functions, as illustrated in Fig. 5.4. The estimated values of C_0 and C_1 for different prototype filters are presented in Table 5.1.

On the basis of (5.7)(5.10), the probabilities of false alarm and detection can be theoretically calculated by

$$\begin{aligned}P_f &= Q\left(\frac{\gamma_m - (\sigma_n^2 + C_0 \cdot \sigma_s^2)}{\sqrt{\frac{1}{K}(\sigma_n^2 + C_0 \cdot \sigma_s^2)}}\right) \\ P_d &= Q\left(\frac{\gamma_m - (\sigma_n^2 + C_1 \cdot \sigma_s^2)}{\sqrt{\frac{1}{K}(\sigma_n^2 + C_1 \cdot \sigma_s^2)}}\right)\end{aligned}\quad (5.11)$$

Table 5.1: Estimated values of C_0 and C_1 for different prototype filters

Prototype filters	PSE	PHYDYAS	PSW
C_0	22.48%	12.57%	0%
C_1	77.52%	87.43%	100%

5.3 Simulations

In the following, we numerically evaluate the multiband sensing scheme from a practical point of view. Assuming a 30MHz licensed system containing " $N_p = 8192$ " subcarriers where the wideband channel is equally separated into " $M = 128$ " subbands with " $L = 64$ " subcarriers per subband. It is also assumed that the channel is AWGN with zero mean and noise power density - 174dBm/Hz . The primary system load rate is 50%. The length of the prototype filters of PFB is " $\beta = 4M = 512$ ". The center frequency is " $f_c = 3.6\text{GHz}$ ". The received RF signal by RF Front-End is down-converted without frequency offset. " $K = 250$ " groups of sampled signals with 128 samples per group are used for simulating the multiband sensing.

At the first stage, we analyze one detected subband which suffers from the extreme situations demonstrated in Fig. 5.3. From a cognitive radio perspective, one of the main challenges is how to deal with an optimal tradeoff between the throughput of secondary system (SS) and the interference from SS to primary system (PS). Normally, the PS has the spectrum use priority so the SS should try to avoid introducing severe interference to PS. The amounts of throughput and interference are associated with the false alarm probability and the detection probability, respectively. In other words, low false alarm probability serves to maintain high throughput and high detection probability guarantee the QoS (Quality-of-Service) of PS. Therefore, both detection probability performance and false alarm probability performance are simulated.

Given a fixed false alarm probability " $P_f = 5\%$ ", a theoretical threshold can be computed, and then this threshold is used to compute the probability of detection. Similarly, the probability of false alarm can be computed for a given detection probability " $P_d = 95\%$ ". The performance curves of the detection probability and the false alarm probability versus SNR level are plotted in Fig. 5.5 and Fig. 5.6, respectively. Each decision statistic is implemented over 10^3 simulation runs. We can observe that the simulated results match well with the theoretical results. Besides, the performance of PFB (PHYDYAS and PSW) exhibits a significant improvement (at maximum 25% performance gain) relative to PSE because of the low spectral leakage property of PFB. It is interesting to find that PHYDYAS performs slightly better than PSW, which can be explained by the fact the variance of PSW based frequency estimation variable is twice as large as that of PHYDYAS (see (5.4)(5.5)). Next, we compare the experimental results of more general case (as shown in Fig. 5.1) by averaging the detection and the false alarm probabilities over all the detected subbands. In this case, the same detection thresholds determined in the extreme cases are employed to ensure " $P_f \leq 5\%$ " and " $P_d \geq 95\%$ ". Fig. 5.7 and Fig. 5.8 show the detection probability and the false alarm probability versus SNR level for the general case, respectively. As expected, PHYDYAS and PSE in the general case can achieve better performances than their counterparts in the extreme cases because of the average effect. However, PSW has the same performance in both extreme and general cases due

to its well localized frequency spectrum (see Fig. 5.4 and Table 5.1). Compared with the extreme cases, the performance gap between PHYDYAS and PSE decreases (at maximum 15% performance gain), but the performance difference between PHYDYAS and PSW increases especially for the probability of false alarm.

In order to examine the detection performance more practical, the frequency offset effect stemming from the oscillator stability is demonstrated in Fig. 5.9 and Fig. 5.10 for the general case with a fixed " $SNR = -6dB$ ". The change of an oscillator in frequency, usually measured in parts per million (ppm). Assuming the oscillator used for the down-conversion has a stability range between 0 and 30 ppm. We observe that the amount of frequency offset has an influence on the detection performance. A large amount of frequency offset leads to a significant performance degradation. At the same time, it can be seen that PFB always outperforms the PSE at different frequency offset levels. In addition, the performance curve of PSW follows the different variation rule from those of PHYDYAS and PSE. The reason lies in the special frequency response of PSW (Fig. 5.4), which gives perfect sideband rejection.

Lastly, we analyze the effect of primary system load rate on the detection performance. In Fig. 5.11 and Fig. 5.12, we show the probabilities of detection and false alarm as a function of primary system load rate with a fixed " $SNR = -6dB$ ". It should be noted that PSW is invulnerable to the system load rate because of its perfect sideband rejection. With regard to PHYDYAS and PSE, the detection probability performance improves as the rate of system load increases. On the contrary, the false alarm probability performance degrades as the increase of system load rate. In particular, the performance of PHYDYAS dominates PSE over all the different load rates as illustrated in Fig. 5.11 and Fig. 5.12, wherein we observe that the large performance disparity of detection probability between PHYDYAS and PSE can be achieved in a low system load rate, whereas the large performance gap of false alarm probability is achieved in a high loaded system.

5.4 Conclusion

In this section, we have investigated the PFB based spectrum analyzer to show its applicability for multiband sensing in cognitive radio context. Our study includes theoretical and experimental analysis for three kinds of spectrum analyzers: conventional PSE, PHYDYAS based PFB and PSW based PFB with non-overlapping filters. The simulation results reveal that PSE based spectrum analyzer is sensitive to the spectral leakage. Conversely, PFB demonstrates more efficient and reliable detection performance by taking advantage of its low spectral leakage property, which further enhances the multiband sensing application of PFB in cognitive radio networks. Furthermore, we have shown that due to the ISI at the output of the PSW filter bank, the false alarm detection and detection probability of PHYDYAS based PFB are better compared to PSW. From the view of computational complexity, the performance gain obtained by PFB doesn't come with the penalty of increased complexity due to the inherent parallel structure of PFB.

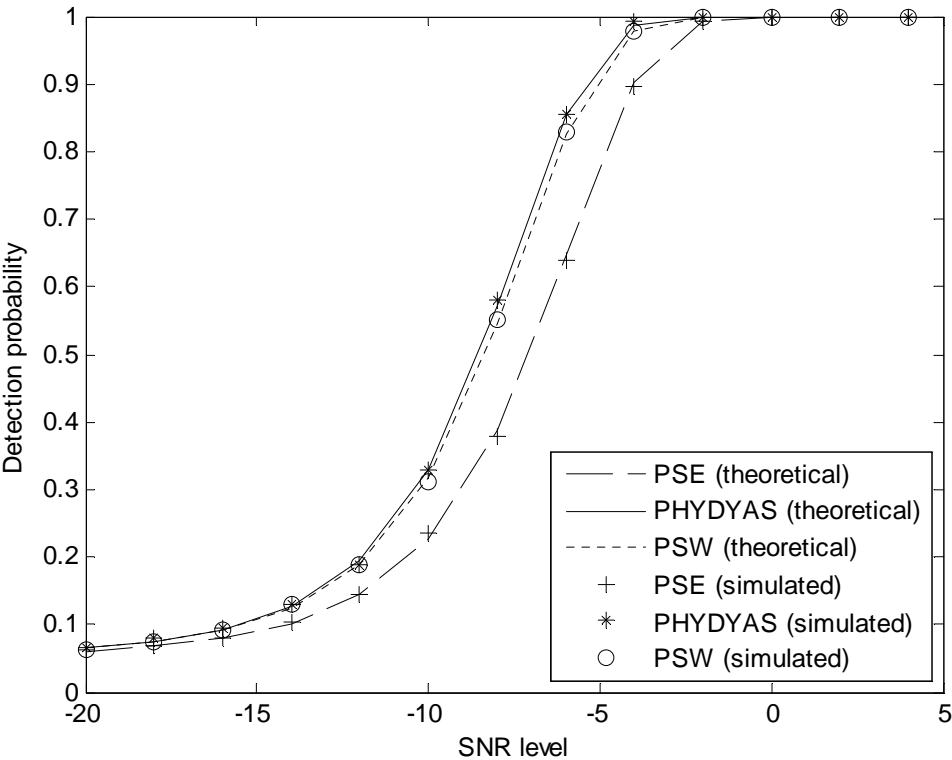


Fig. 5.5: Probability of detection vs. SNR level for the extreme cases

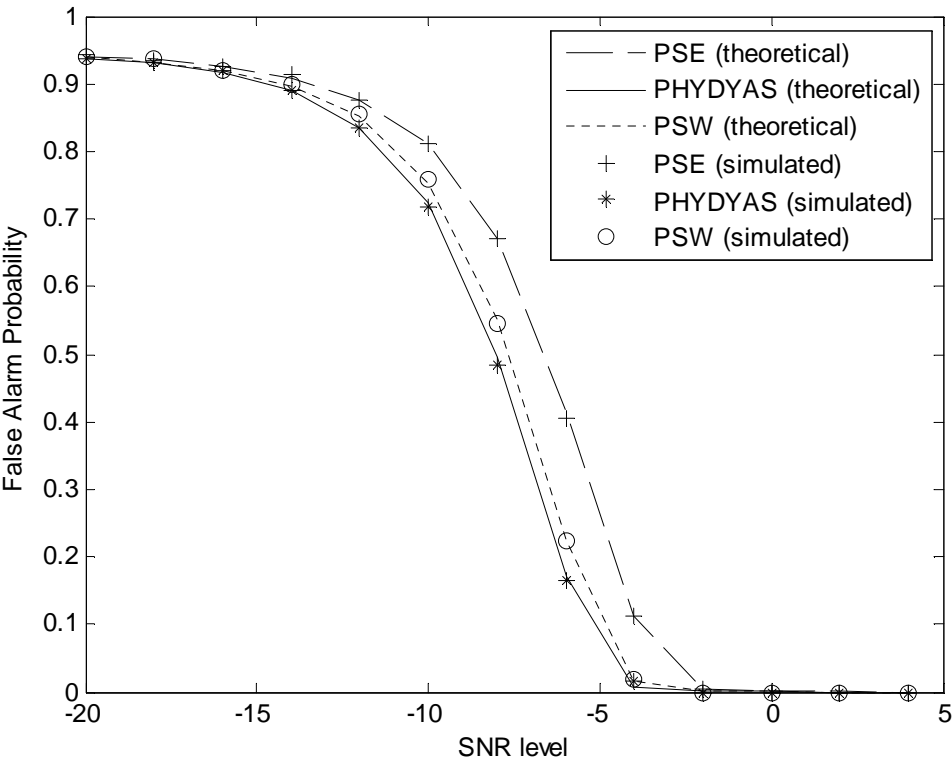


Fig. 5.6: Probability of false alarm vs. SNR level for the extreme cases

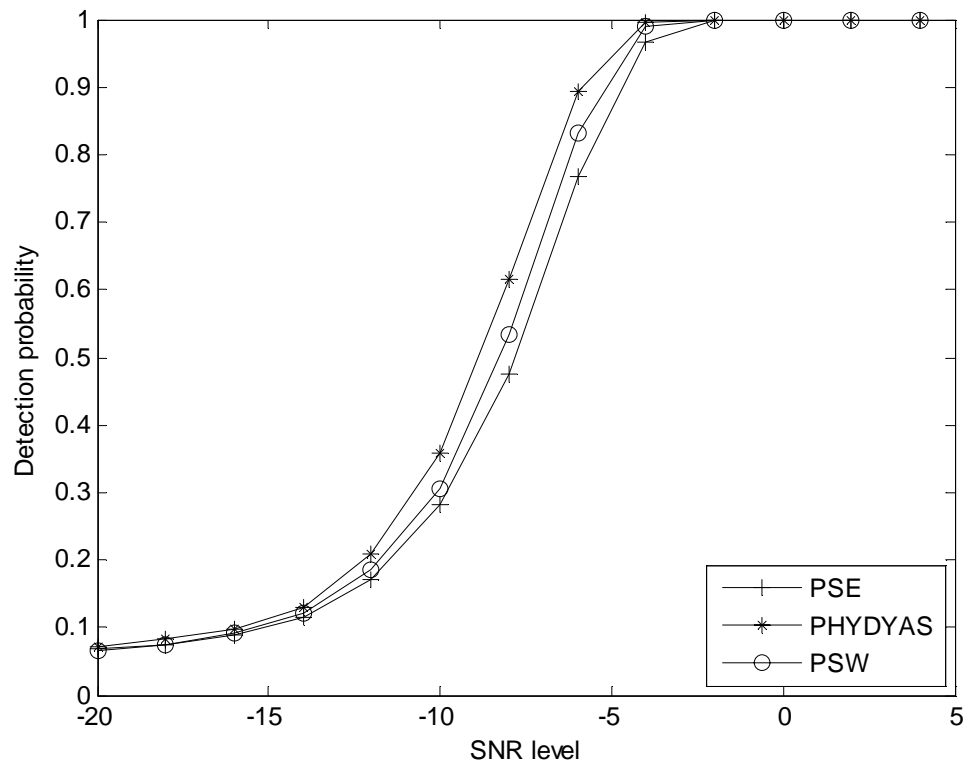


Fig. 5.7: Probability of detection vs. SNR level for the general case

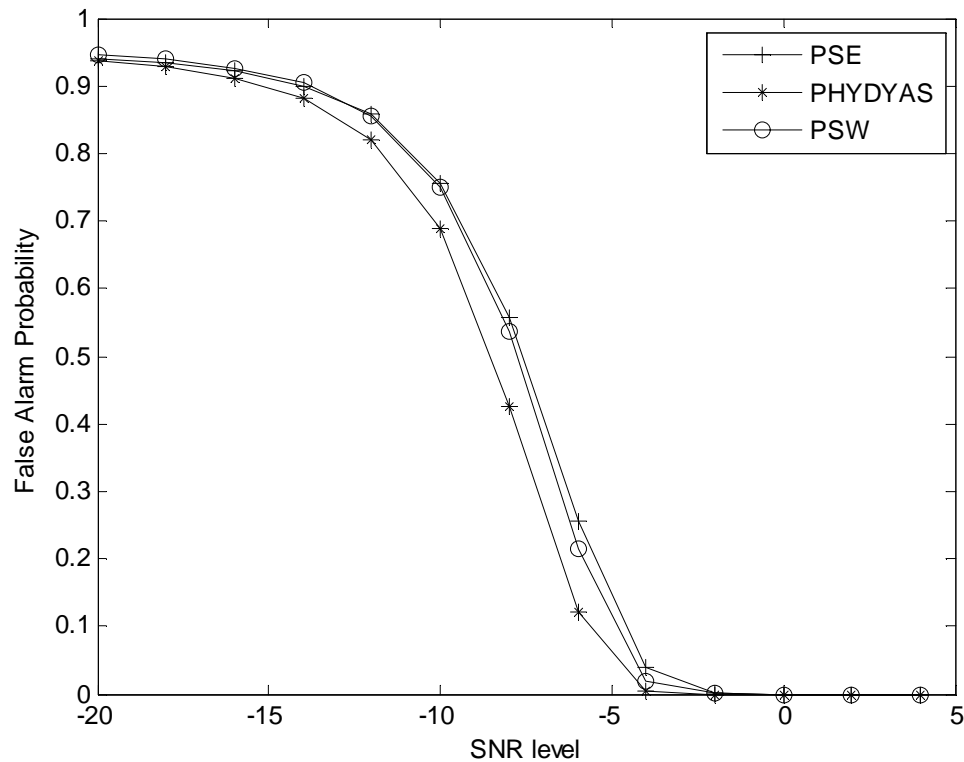


Fig. 5.8: Probability of false alarm vs. SNR level for the general case

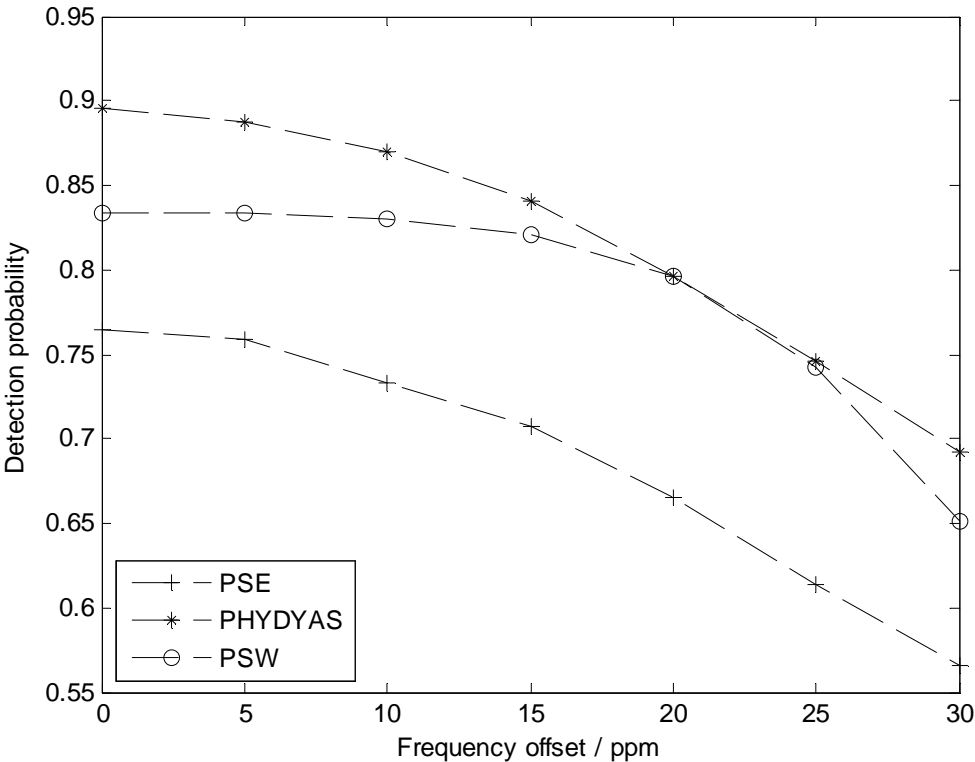


Fig. 5.9: Probability of detection vs. frequency offset level with a fixed SNR=-6dB

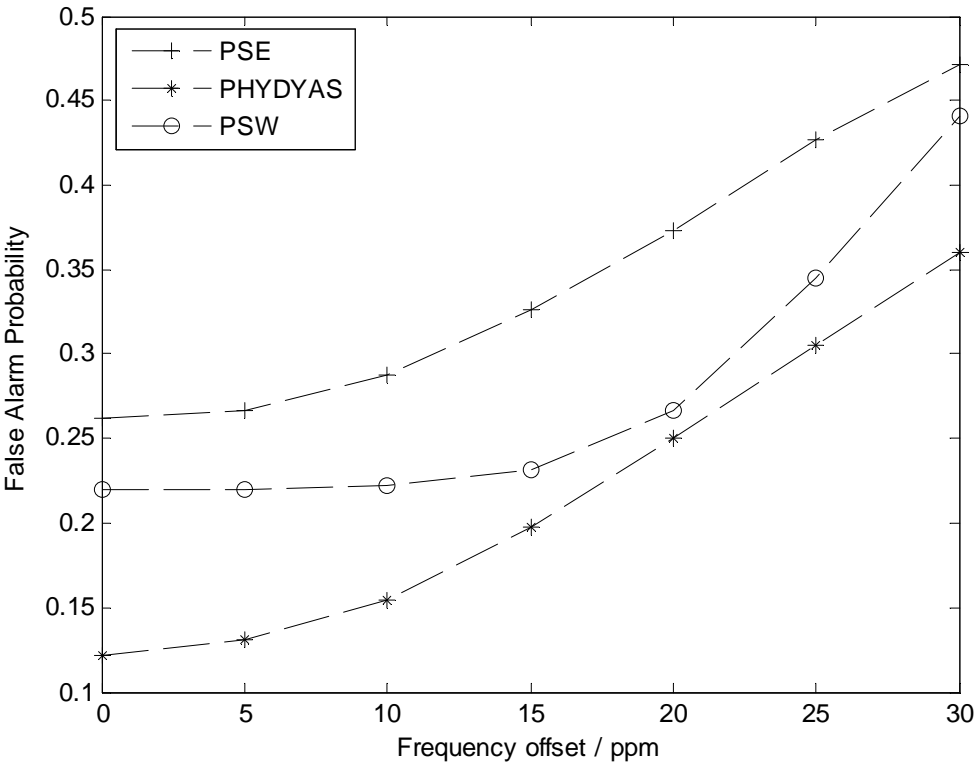


Fig. 5.10: Probability of false alarm vs. frequency offset level with a fixed SNR=-6dB

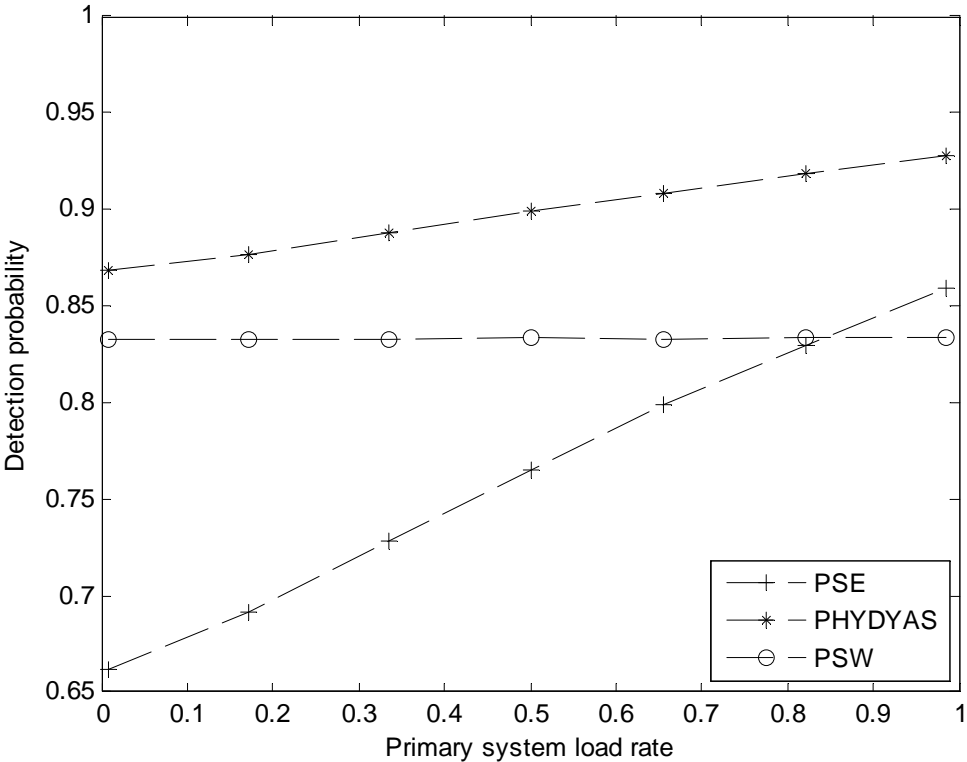


Fig. 5.11: Probability of detection vs. primary system load rate with a fixed SNR=-6dB

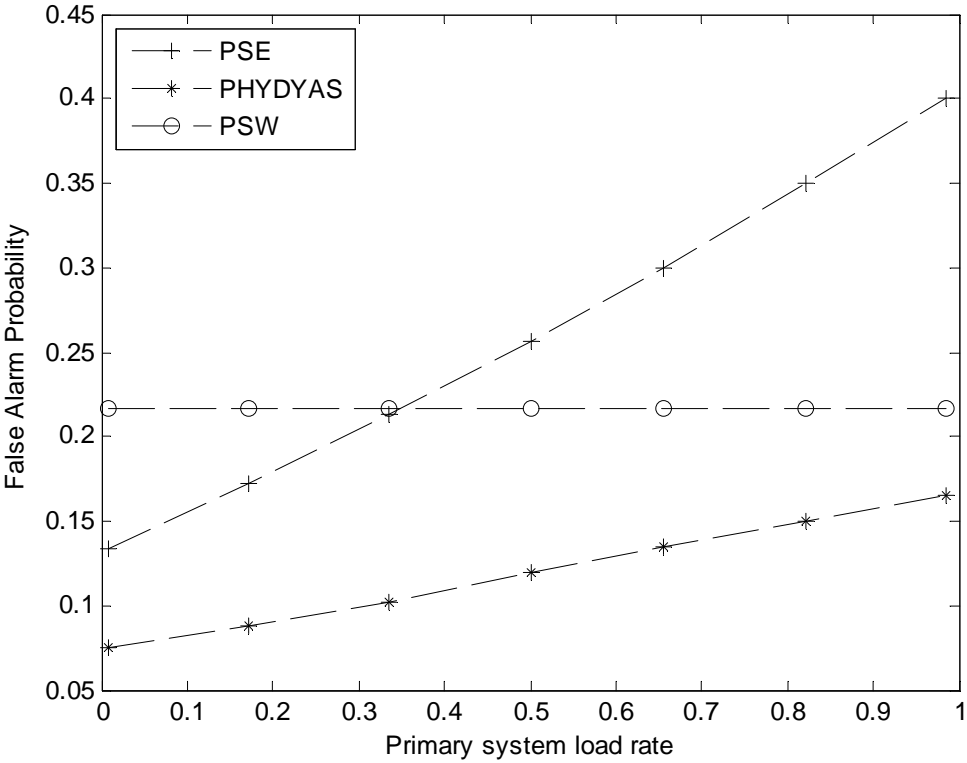


Fig. 5.12: Probability of false alarm vs. primary system load rate with a fixed SNR=-6dB

6 Candidate Spectral Estimation Based on Filterbank for FBMC Spectrum Sensing in Cognitive Radio

6.1 Problem formulation

The deficiencies in our current model of spectrum allocation originated in the economics/law/public-policy literature in the seminal papers by [Coa59] in 1959 and de Vany et. al. [Van69] in 1969, and more recently by Goodman in [Goo04]. The focus was mostly on making sure that spectrum was efficiently allocated to the socially most important uses. The work of Mitola [Mit00] introduced the idea of “cognitive radios” that are more intelligent and autonomous than the dumb radios of yesterday. The subsequent Spectrum Policy Task Force report [FCC04] of the FCC generated technical interest in the topic. This report revealed that the inefficiency of the current allocation system went beyond the issue of assigning bands to inefficient uses— the current system has a dramatic underuse of spectrum since much of it is simply not used at all in most places/times. It has been argued that this waste is an inevitable consequence of the current static approach to spectrum access [Tan04]. The limited “snap-shot” spectrum occupancy studies that have been undertaken [Coa59 – Tan04] suggest that there is still an abundance of real spectrum available and that the current issue is more related to our fixed, time independent approach to spectrum allocation, than it is to any real lack of spectrum from a time space continuum perspective.

A potential market model would be the deployment by existing or new operators of spectral monitoring equipment which broadcast to potential secondary users the spectral vacancies in terms of time available and frequency ranges. When a secondary user agrees to use the available spectrum with the operator, it starts transmission with some economic compensation for the operator for opening its spectrum to secondary users. Regardless this model is accepted or not, there is no way to avoid the proper spectrum monitoring and labelling of primary users in any vision of a CR scenario [Van69] Furthermore, we believe that, together with cross-layer technologies to match the frequency vacancies to the CR applications, spectral estimation tools have to be revisited to detect spectral signatures rather than mere spectral occupancy.

Persuaded that the spectral signature/shape estimation is one of the pillars for cognitive radio deployment, it constitutes one of the main challenges still to take up. In this section we analyze the use of a new spectral sensing procedure for Filter Banks Multicarrier system (FBMC). The technique is based on filter bank approach for spectral estimation. The proposed procedure is able to detect and label power and central frequency location for any spectral signature (candidate) with noise signal existence, and co-channel interference with different modulation format.

6.2 Different approaches on Spectrum sensing based on transmitter detection

Several widely held spectrum sensing solutions are discussed in [Cab04]. The four typical practical sensing approaches are described below:

- *Matched filter*: A matched filter maximizes the signal to noise ratio at the sampling time, if the transmission waveform of the primary user is known. This requires the secondary user to have a priori knowledge of the primary user such as the modulation type and order, the pulse shaping, and packet format. Due to the coherent nature of the matched filter, detection can be very fast.
-

But if there are multiple types of primary users, the secondary user have to be equipped with multiple dedicated receivers.

- *Energy detection:* An energy detector is a non coherent detector that avoids the complicated coherent receivers required by a matched filter, and can be implemented using spectrum analysing tools such as fast Fourier transform (FFT). The main drawbacks of this technique are; first the spectrum sensing speed is relatively slow. Second, the threshold for detection is very vulnerable to the noise level and in band interference. Third, the energy detector cannot differentiate modulated signals, noise and interference. Fourth, the primary (candidate) user and the secondary user cannot be distinguished, while only the primary user's transmission should be protected (not very suitable for Spread Spectrum signals).
- *Cyclostationary feature detection:* The modulated signals are usually cyclostationary, since in general built in periodicity often occurs in training sequence, cyclic prefix, etc. This periodicity is introduced in the transmitting signal of the primary users so that the receivers can exploit it for timing, etc. This periodicity could be used to detect the candidate user. The basic approach is based on the autocorrelation function of the power spectrum density. Often, information required is the carrier frequency, and the cyclic frequency of the primary user, that most coincide with the modulation rate or baud rate. Nevertheless, only a non-parametric version of cyclic spectral estimation is reported. This non parametric character implies low resolution together with a low quality performance versus complexity trade-off. Since the sample size needed to obtain a reliable detection in spectrum sensing has to be low, the low resolution and the need of long data records constitute the major drawback of cyclo-stationary based methods.
- *Wavelet detection:* It is well known that the spectrum usage can cause irregularities in the power spectrum density, an attractive mathematical tool for analyzing singularities and irregular structure is the wavelet transform, which can investigate the local regularities of signals. The wavelet approach [Tia06] provides advantages for wideband spectrum sensing over the conventional use of multiple narrow band filter band in terms of implementation cost and flexibility.

To overcome the above mentioned drawbacks in [Roj08] we propose a new procedure for spectral estimation that is able to detect the presence of a given spectral shape defined by it proper autocorrelation matrix \mathbf{R}_c at baseband, in a given data signal record.

6.2.1 Filter bank spectral estimation

The filter bank approach is based on a dedicated filter design, which steered to a given frequency aims to minimize spectral leakage from the rest of frequencies. The estimate is given by the measured output power of the filter (power level), divided by the bandwidth of the analysis filter (power density). In order to gets a mathematical formulation of spectral estimation for PSD using filter banks, we need to find the relationship between filter's output and Power Spectral Density of $x(n)$. Let $x(n)$ be a zero mean wide-sense stationary (WSS) random process with a PSD equal to $S(w)$ and $h(n)$ a ideal passband filter with bandwidth B_N at central frequency w_0 .

$$|H(w_0)| = \begin{cases} 1, & |w - w_0| \leq B_N / 2 \\ 0, & \text{otherwise} \end{cases} \quad (6.1)$$

If the signal $x(n)$ is filtering with $h(n)$ at w_0 , then the PSD of the output process $y_{w_0}(n)$ is

$$S_x(w_0) = S_x(w) \left| H_{w_0}(w) \right|^2 \quad (6.2)$$

And the power in $y_{w_0}(n)$ is $P(w_0) = E \left\{ \left| y_{w_0}(n) \right|^2 \right\} = \frac{1}{2\pi} \int_{-\pi}^{+\pi} S_x(w) \left| H(w_0) \right|^2 dw$. if we consider the bandwidth B_N small enough so that $S_x(w)$ can be considered approximately constant over the filter pasband then the power became

$$P(w_0) = S_x(w) B_N \quad (6.3)$$

Therefore, it is possible to estimate the PSD of $x(n)$ around at central frequency w_0 from filtered process by estimating the power in $y_{w_0}(n)$ and dividing by the filter bandwidth, B_N

$$\hat{S}_x(w) = \frac{P(w_0)}{B_N} \quad (6.4)$$

Based on the above theoretical introduction the response of the filter to a sinusoidal signal of frequency w is determined by the filter's frequency response; $A(w) = \sum_{k=0}^m a_k e^{-jkm} = \mathbf{A}^H \mathbf{S}(w)$.

Now, If we want to make the filter as selective as possible for a frequency band around w_0 then we have to minimize the power $P(w_0)$ in (6.5) subject to a constraint. This constraint implies that the filter frequency response must be equal 1 at central frequency and 0 otherwise, usually formulated as in [Lag08] [Lar02] by

$$\mathbf{A}^H \mathbf{R} \mathbf{A} |_{\min}, \text{ subject to } \mathbf{A}^H \mathbf{S} = 1 \quad (6.5)$$

Having $\mathbf{S} = [1 \ e(jw) \dots e(j(Q-1)w)]^T$ is the steering frequency vector with w equal to $(2\pi f)$, \mathbf{A} contains the FIR Q filter coefficients $[a_1 \ a_2 \ , \dots, \ a_Q]$, and \mathbf{R} is the correlation matrix of the input signal.

As concerns with the constraint, it is clear that the response of zero dB at the steering frequency refers to the magnitude only and not necessarily over the filter phase, that does not impact in the resulting power level estimate. When setting the magnitude constrain only, (6.5) is reformulated as (6.6).

$$\mathbf{A}^H \mathbf{R} \mathbf{A} |_{\min}, \text{ subject to } \mathbf{A}^H [\mathbf{S} \mathbf{S}^H] \mathbf{A} = 1 \quad (6.6)$$

The solution of (6.6) is given by the solution of (6.7), where λ is the Lagrange multiplier.

$$(\mathbf{R} - \lambda \mathbf{S} \mathbf{S}^H) \mathbf{A} = 0 \quad (6.7)$$

Clearly λ represents how much power we can remove from data at the steering frequency, such that the remaining matrix preserves its positive definite character. This value, for a rank-one subtraction can be derived directly and reduces to be λ_{\min} of the generalized eigenvalue problem. The unitary null eigenvector is also easy to derive. Both, eigenvector and λ_{\min} are:

$$\underline{\underline{\mathbf{A}}} = \frac{\underline{\underline{\mathbf{R}}}^{-1} \underline{\underline{\mathbf{S}}}}{\sqrt{\underline{\underline{\mathbf{S}}}^H \underline{\underline{\mathbf{R}}}^{-2} \underline{\underline{\mathbf{S}}}}} \quad \lambda = \frac{1}{\underline{\underline{\mathbf{S}}}^H \underline{\underline{\mathbf{R}}}^{-1} \underline{\underline{\mathbf{S}}}} \quad (6.8)$$

Note that the power level estimate coincides with the one derived from the use of the magnitude and phase constrain. And that when adjusting the unitary eigenvector to the constraint the filter also reduces to the same as in the traditional method. In summary nothing has changed, just it is a different view but much richer than the traditional one as we will see. In fact, (6.7) suggest a reformulation of the nonparametric spectral estimation problem. The problem can be viewed as follows: First, the power level estimate is just how much power we can remove of a single line contribution to the data autocorrelation matrix, yet preserving its positive definite character. Second, the analysis bandwidth can be defined as the bandwidth of the filter producing the same power either introducing the single line or the data autocorrelation matrix. This is the eigenvector of (6.9).

$$\underline{\underline{\mathbf{R}}} \cdot \underline{\underline{\mathbf{A}}} = \lambda \underline{\underline{\mathbf{S}}} \cdot \underline{\underline{\mathbf{S}}}^H \underline{\underline{\mathbf{A}}} \quad (6.9)$$

The noise bandwidth of the eigenvector will be:

$$B_N = \frac{1}{\underline{\underline{\mathbf{A}}}^H (\underline{\underline{\mathbf{S}}} \cdot \underline{\underline{\mathbf{S}}}^H) \underline{\underline{\mathbf{A}}}} \quad (6.10)$$

Finally, the spectral density will be estimated by the power level λ divided by B_N .

$$\hat{s}(w) = [\underline{\underline{\mathbf{A}}} \underline{\underline{\mathbf{S}}} \cdot \underline{\underline{\mathbf{S}}}^H \underline{\underline{\mathbf{A}}}] \lambda \quad (6.11)$$

In summary, this complicated manner of looking to a well known and solved, problem resumes as: Compute λ_{min} in (6.7) for power level estimate and the corresponding eigenvector; then use (6.11) for spectral density. The motivation for this complex view of filter-bank spectral estimation is appreciated in the next section.

6.2.2 Spectrum sensing using Candidate Spectral Estimation (CASE)

Formula (6.7), as mentioned before, reveals that looking for a single carrier contribution in data autocorrelation matrix is just a problem of spectral subtraction. Furthermore, the concept of a basic candidate that it modulated from zero frequency to any other frequency can be formulated as the basic zero frequency line with candidate correlation equal to $(\underline{\underline{\mathbf{1}}} \underline{\underline{\mathbf{1}}}^H)$, where “ $\underline{\underline{\mathbf{1}}}$ ” denotes the vector of ones on every entry, which is modulated to the scanned frequency as (12), where \odot indicates element wise product.

$$\underline{\underline{\mathbf{R}}}_{sc} = (\underline{\underline{\mathbf{S}}} \cdot \underline{\underline{\mathbf{S}}}^H) \odot (\underline{\underline{\mathbf{1}}} \underline{\underline{\mathbf{1}}}^H) \Rightarrow \underline{\underline{\mathbf{R}}}_{sc} = (\underline{\underline{\mathbf{S}}} \cdot \underline{\underline{\mathbf{S}}}^H) \odot \underline{\underline{\mathbf{R}}}_c \quad (6.12)$$

$\underline{\underline{\mathbf{R}}}_{sc}$ here represent the candidate autocorrelation matrix. The matrix of ones, aiming to determine in which frequency it is located and what is its power level, $\underline{\underline{\mathbf{R}}}_c$ is a basedband matrix. At this moment we are ready to solve the CR problem. Let us assume that the licensed user is, for example, a BPSK modulation signal with four samples per symbol and rectangular pulse shape. The candidate

correlation will be a Toeplitz matrix containing $[1 \ 0.75 \ 0.5 \ 0.25 \ 0 \ 0]$ as its first row. Then the power level estimate of this signature at a given frequency will be the minimum eigenvalue of (6.13).

$$(\underline{\mathbf{R}} - \lambda (\underline{\mathbf{S}} \cdot \underline{\mathbf{S}}^H) \odot \underline{\mathbf{R}}_c) \underline{\mathbf{A}} = 0 \quad (6.13)$$

Next, using the corresponding eigenvector, the density of the candidate will be (6.14).

$$\hat{s}(w) = \left[\underline{\mathbf{A}}^H \left((\underline{\mathbf{S}} \cdot \underline{\mathbf{S}}^H) \odot \underline{\mathbf{R}}_c \right) \underline{\mathbf{A}} \right] \lambda \quad (6.14)$$

Note that for the same symbol rate, any M-QAM signal, with rectangular pulse signalling, will be detected as candidate. When the symbol's rate (bauds) is not equal, the number of samples per symbol will change and, in consequence, it will not be recognized as the candidate which is at a rate, relative to our sampling rate, of four samples per symbol.

6.3 Spectrum sensing having FBMC signal using candidate spectrum estimate

This section describes briefly the two procedures to be evaluated in the simulations section, i.e. the candidate detector described in the previous section and the cyclo detector as it is reported in [Gho06]. Subcarriers using BPSK modulation, a narrowband interference (an unmodulated carrier) is present with 10 dB SNR with 20 MHz system bandwidth, and with $N=256$ subcarriers. The filter order of the candidate estimate is denoted as Q and it will be set equal to 40 in the simulations section. The number of samples of the signal used for detection M , will be set to 2560.

The sample autocorrelation matrix will be computed using the forward and backward method [Hon98] formulated as (6.15)

$$\underline{\underline{R}} = \frac{1}{2(N-Q)} \sum_{n=Q+1}^N \{ X(n) X^H(n) + \underline{\underline{J}} X^*(n) X^T(n) \underline{\underline{J}} \} \quad (6.15)$$

where upper indexes $(.)^H$, $(.)^T$ and $(.)^*$ denote hermitic, transpose and complex conjugate respectively, X_n is a column vector arranging Q consecutive samples of the data signal from $x(n)$ down to $x(nQ+1)$, finally matrix $\underline{\underline{J}}$ denotes the exchange matrix with main cross diagonal elements equal to one and the rest entries equal to zero.

Since our aim is to prove the superiority of the candidate approach versus the cyclo-stationary approach, the second is summarized briefly herein. A non-stationary cyclic random process, as it is the case for the most used linear modulation schemes, presents an autocorrelation function as given in (6.16)

$$r(t, \tau) = r(\tau) + \sum_{\alpha \in \Psi} R(\alpha, \tau) e^{j2\pi\alpha t} \quad (6.16)$$

having

$$R(\alpha, \tau) = \lim_{T \rightarrow \infty} \frac{1}{T} \int_{-T/2}^{T/2} r(t, \tau) e^{-j2\pi\alpha t} dt \quad (6.17)$$

which is named the cyclic autocorrelation function, a is the cyclic frequency and Ψ is the total set of cyclic frequencies. Applying the principle of synchronized averaging [Gho06] to (6.16) and using the sampled version of the original signal $x(t)$, the autocorrelation function is (6.17),

$$\hat{r}^{(N)}(n, \tau) = \frac{1}{N} \sum_{k=0}^{N-1} x(n + kT_0) x(n + kT_0 + \tau) \quad (6.17)$$

where T_0 is any cyclic period and N is the number of symbols of the signal.

6.3.1 Algorithm description

Finally the complete procedure of CASE detector can be resumed in the following algorithm. We proposed an algorithm for detection of specific primary user's signal based on autocorrelation matrix. The spectral autocorrelation matrix properties of different communications signal are usually unique, CASE detector takes this advantage to differentiate between a particular primary user and other users or interferences. The general algorithm for CASE detector is detailed in the following

Step1: Sensing the candidate user (primary user) including the noise and the interference effects

Step2: Define the autocorrelation matrix of received signal using equation (6.15)

Step3: Define based autocorrelation Matrix of primary user, \mathbf{R}_c at unit power level and baseband frequency

Step4: find the minimum eigenvalue and eigenvector associated of

$$\left(\underline{\underline{R}} - \lambda \left(\underline{\underline{S}} \cdot \underline{\underline{S}}^H \right) \odot \underline{\underline{R}}_c \right) \underline{\underline{A}} = 0$$

Step5: Compute power level estimate

6.3.2 Robustness against the SNR increase

First we show the claimed performance of the candidate power level estimation. For this purpose the high SNR scenario depicts clearly the behaviour of the candidate estimate, the FBMC is here set to 11 dB of SNR. Figure 6.1 presents the periodogram estimate, i.e. the response of an energy detector, and the traditional Capon's estimate capabilities. Note that the candidate spectral estimate (CASE) is able to provide a clear peak at the actual frequency location of the FBMC signal (at 90 MHz) with a value of 10.6 dB as power level estimate.

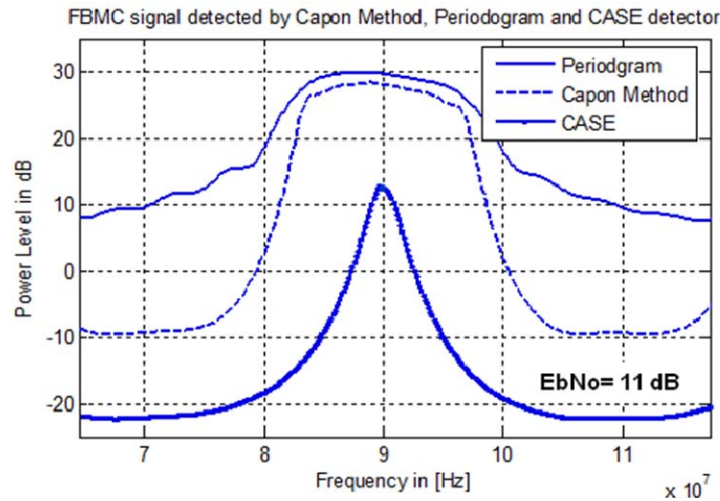


Figure 6.1. The periodgram estimate, i.e in the response of an energy detector, the traditional Capon's estimate and the developed CASE detector, having a FBMC signal, with $N=256$ carriers, $B_w=20$ MHz of bandwidth, and $f_c=90$ MHz frequency carrier, at 10dB of E_b/N_o . The used sample size is $M=2560$ with an estimate order of $Q=40$.

In Figure 6.2, we are testing the robustness of the CASE detector against the increase of the SNR value, we could note that candidate is still detected in a robust manner despite its contamination with different SNR values (-5 dB, 2 dB, 9 dB). The FBMC signal is perfectly located with 16.4 dB as power level.

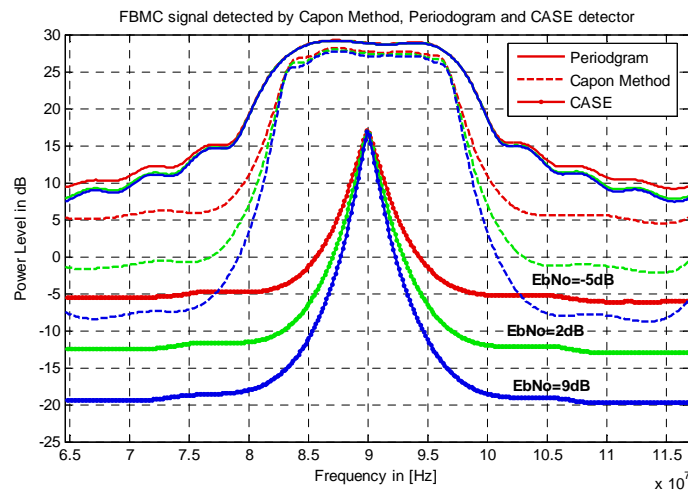


Figure 6.2. The periodgram estimate, i.e in the response of an energy detector, the traditional Capon's estimate and the developed CASE detector, Having a FBMC signal, with $N=256$ carriers, $B_w=20$ MHz of bandwidth, and $f_c=90$ MHz frequency carrier and having different values E_b/N_o dBs $\{9, 2, -5\}$. The used sample size is 2560 with an estimate order of $Q=40$.

6.3.3 System capabilities with narrow band interferences to FBMC signal

First we show the claimed performance of the candidate power level estimation. For this purpose the high SNR scenario depicts clearly the behaviour of the candidate estimate, the filter bank multicarrier signal is set to 10 dB of SNR at 90 MHz, together with a narrowband interference

located at 80 MHz (see Figure 6.3), with the same SNR, in white Gaussian noise. The sample size was 2560 samples ($M=2560$) and the estimates order is 40 ($Q=40$).

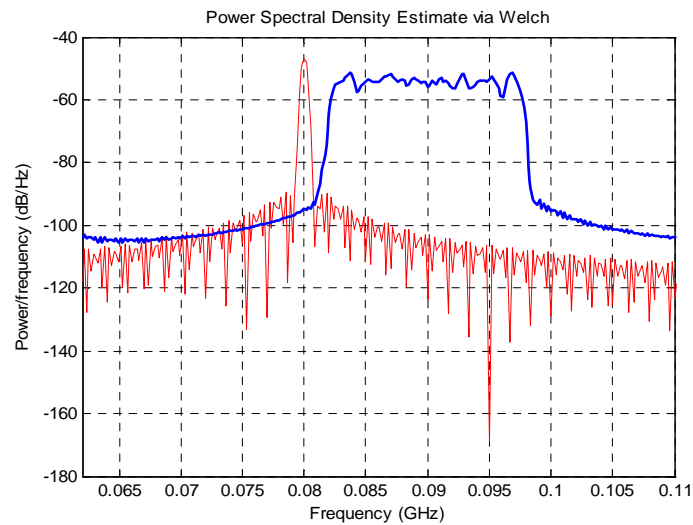


Figure 6.3. Primary user (blue line) is a FBMC signal, $N=256$ carriers, $B_w=20$ MHz, $f_c=90$ MHz, with 10 dB of SNR, we used PHYDYAS's filter parameters with $K=4$, the sample size was 2560, and estimate order $Q=40$. We have also a narrow band interference (red line) located at 80 MHz with same SNR, in white Gaussian noise.

Figure 6.4 presents the periodogram estimate, i.e. the response of an energy detector, and the traditional Capon's estimate. Note that the candidate is robust against interference or narrowband secondary users' transmissions. At the same time it provides a clear peak at the actual frequency location of the FBMC signal. Clearly the candidate only reacts to the presence of the candidate in the signal. Also note that even in-band narrowband interferences do not affect severely the accuracy of the FBMC power level estimate.

We can note that the candidate spectral estimate (CASE) is able to provide a clear peak at the actual frequency location of the FBMC signal (90 MHz frequency carrier f_c) with a 8.87 dB as power level estimate even having secondary user transmission interference.

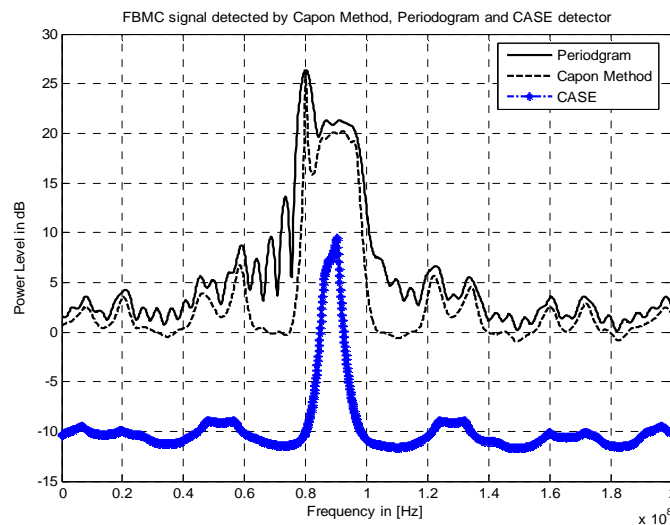


Figure 6.4. CASE detector capability, having narrow band interference does not affect severely the accurate of the FBMC power level estimate.

6.3.4 ROC performance (Probability of detection vs. probability of false alarm)

Without the presence of a narrow interference

In order to test the candidate estimate in realistic CR scenarios, the ROC performance, i.e. probability of detection versus probability of false alarm, for SNR ranging will be analysed. Figure 6.5 depict the ROC performances having a FBMC system with same characteristics described in Section 6.3.3 but this time without presence of narrow interference. The analysed SNR ranging includes the values $\{-15, -13, -11 \text{ and } -9\}$ dBs. We can observe that even having -9 dB of SNR still the system have very good possibilities in terms of probability of detection.

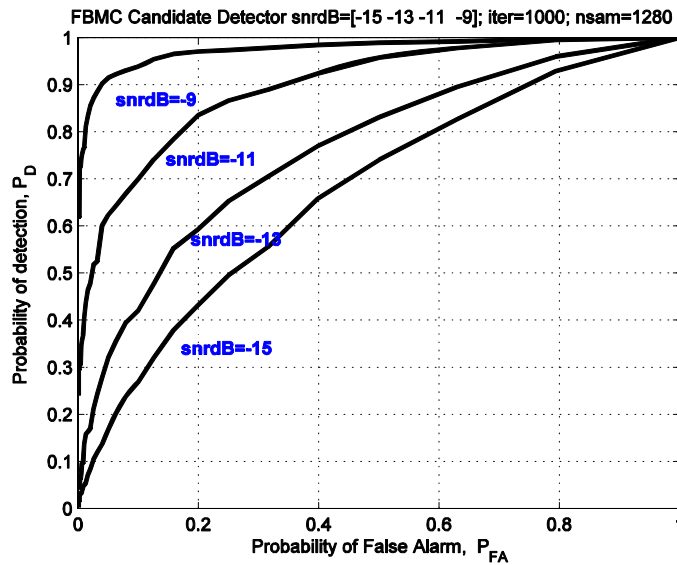


Figure 6.5. The ROC performance, i.e. Probability detection P_D versus probability of false alarm P_{FA} having an SNR ranging from $\{-15, -13, -11, -9\}$ dB, without narrow interference. The number of iterations is 1000, with 1280 samples.

With the presence of a narrow interference

Figure 6.6 shows the ROC curves for the same SNR range and FBMC signal than in previous Figure 6.5, but in the presence of a narrowband interference of from -13 dB to -6 dB and 80 MHz interference with SNR 10 dB above the primary user power level. This performance is in accordance with the low sensitivity of the candidate estimate. Despite of a narrow interferer the system achieves good performances in terms of probability of detection. Of course the CASE detector experiment a small loss compared with case of Figure 6.5.

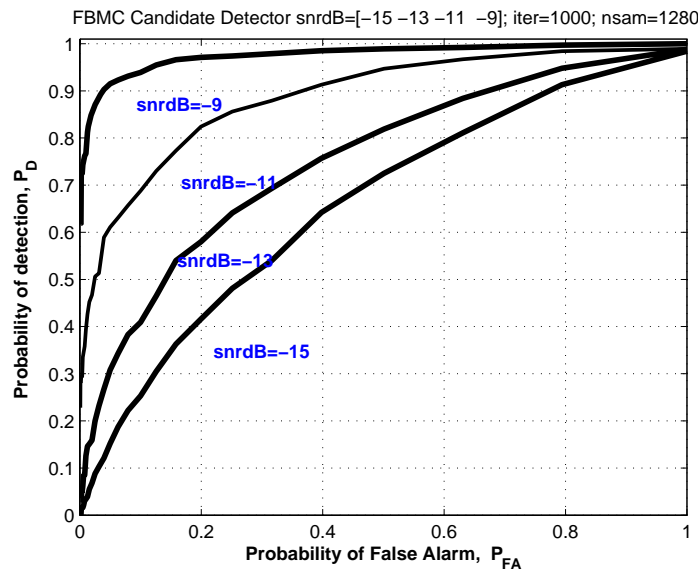


Figure 6.6. The ROC performance, i.e. Probability detection P_D versus probability of false alarm P_{FA} having an SNR ranging from $\{-15, -13, -11, -9\}$ dB, with narrow interference of 10 dB. The number of iterations is 1000, with 1280 samples.

6.4 Conclusions

The performance of the so-called Candidate detector, based on generalized spectral subtraction, is reported for FBMC signals with same characteristics defined in [deliverable 3.1]. The FBMC signal, considered as the primary user signature in a cognitive radio scenario, is detected in presence of narrowband interferers that may correspond to secondary users and in SNR regimes ranging from -15 up to -9 dB that correspond to realistic scenarios. Requiring only the spectral shape of the primary user, the Candidate detector (CASE) stays always with superior quality than traditional energy detectors for the cyclo-stationary based methods. The candidate detector provides accurate power level estimates and central frequency location, even in the presence of severe narrow band interferences.

7 Complexity Assessment of Analysis Filter Banks

This Section presents an overview of the investigation we performed around the complexity of analysis filterbanks. The approach is compared with the classical windowed DFT approach. Section 7.1 gives an overview of the DFT approach and its limitations. Section 7.2 introduces the filterbank based approach while Section 7.3 aims at comparing the two schemes. Finally, conclusions are drawn in Section 7.4.

7.1 Windowed DFT based approach

Introductory remark: Throughout this report, we will always refer to DFT (Discrete Fourier Transform). In practice, its implementation is usually done in most cases through an FFT (Fast Fourier Transform) whose complexity is much lower but requires a number of points amounting to a power of two, e.g. 512 or 1024.

7.1.1 Spectral leakage

Blocks of K samples with T [seconds] between each sample are assumed. Hence one block of K samples is captured in KT [seconds]. The DFT kernel can be seen as an orthogonal trigonometric basis. From the continuum of possible frequencies, only those which coincide with the basis will project onto a single basis vector; all other frequencies will exhibit non zero projections on the entire basis set. This is often referred to as spectral leakage and is the result of processing finite-duration records [Har78].

An intuitive approach to leakage is the understanding that signals with frequencies other than those of the basis set are not periodic in the observation window. The periodic extension of a signal not commensurate with its natural period exhibits discontinuities at the boundaries of the observation. The discontinuities are responsible for spectral contribution (or leakage) over the entire basis set. The forms of discontinuity are demonstrated in Figure 7.1 [Har78].

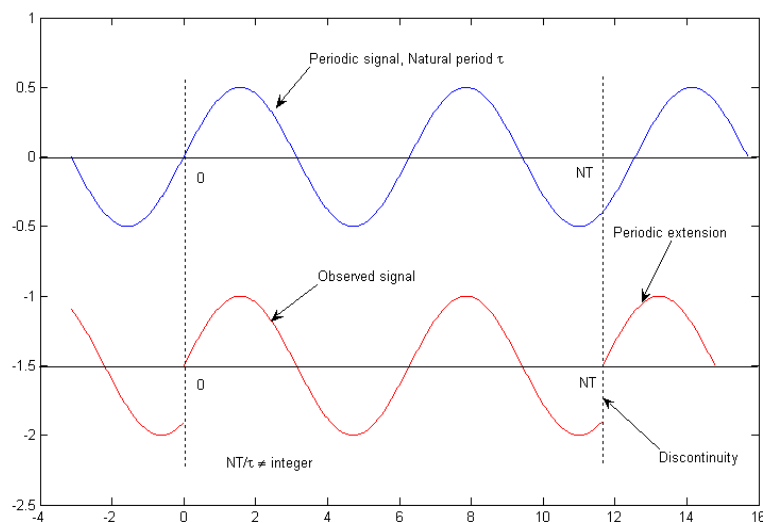


Figure 7.1. Periodic extension of sinusoid not periodic in observation interval.

7.1.2 Windowing

To reduce the effects of spectral leakage, windowing is usually applied and leads to the block-scheme of the so-called Short-Time (or Short Term) Fourier Transform (STFT) illustrated through Figure 7.2.

Windows are weighting functions applied to data to reduce the spectral leakage associated with finite observation intervals [Har78].

From one viewpoint, the window is applied to data (as a multiplicative weighting) to reduce the order of the discontinuity at the boundary of the periodic extension. This is accomplished by matching as many orders of derivative (of the weighted data) as possible at the boundary. Thus windowed data are smoothly brought to zero at the boundaries so that the periodic extension of the data is continuous in many orders of derivative [Har78].

From another viewpoint, the window is multiplicatively applied to the basis set so that a signal of arbitrary frequency will exhibit a significant projection only on those basis vectors having a frequency close to the signal frequency [Har78].

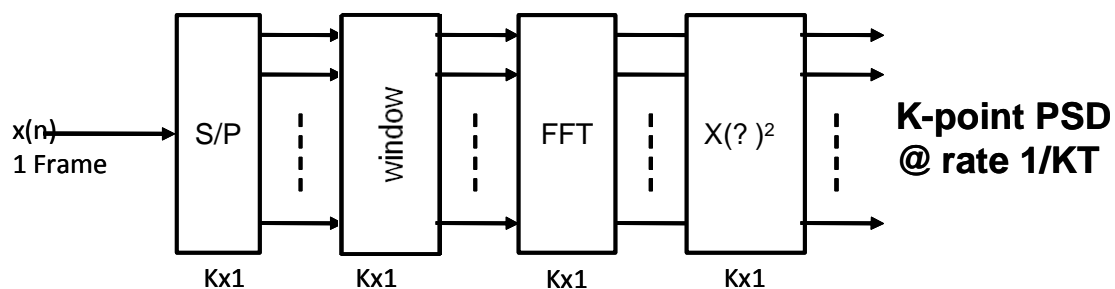


Figure 7.2. Block scheme for Short-Time (or Short-Term) Fourier Transform (STFT).

Multiple windows can be applied like Dirichlet, Bartlet, Hamming or Blackman windows. The choice of the window may vary for a specific application. For example, the Hann window is the window of choice in application requiring high resolvability. We refer the user to [Har78] for a detailed analysis.

Windowing reduces the spectral leakage but only at the expense of broadening the main lobe. Spectral width of the window's spectral main lobe is responsible for the minimum separation required between two frequency components of similar amplitude to assure reliable detection of distinct signal components. This minimum separation reduces the capability of detecting weak frequency components near strong components.

7.1.3 Overlapping and averaging

According to Figure 7.2, one spectral representation is computed every K samples. The update rate is then given by $1/KT$. Very often blocks of K samples are overlapped as illustrated by Figure 7.3 where a 50% overlap is displayed.

The first obvious effect of overlapping is an increased update rate of the spectral image. In the 50% overlap case, two spectral images are computed every KT seconds compared to only one in the non overlapping case.

In addition, remember that most window functions tend to zero at the start and at the end of the time record to mitigate the spectral leakage effect. Hence the points close to the borders will have a very limited influence on the spectral image compared to the points at the center of the time records. By overlapping, these border points are “re-used” and appear as well as middle points in other time records. Doing so, all of the points will have virtually the level of impact of the spectral images.

Besides overlapping, averaging several PSDs (periodograms) is often used as a means to decrease the variance of the estimate relative to a single periodogram. This scheme usually referred as Bartlett method is illustrated by Figure 7.4 in which no overlap is assumed. The drawback of the method is reduction of the update rate by a factor N .

In the sequel and as overlapping can similarly applied both on the classical windows+DFT method and on the filterbank method, we will not consider it in the comparison of the two approaches.

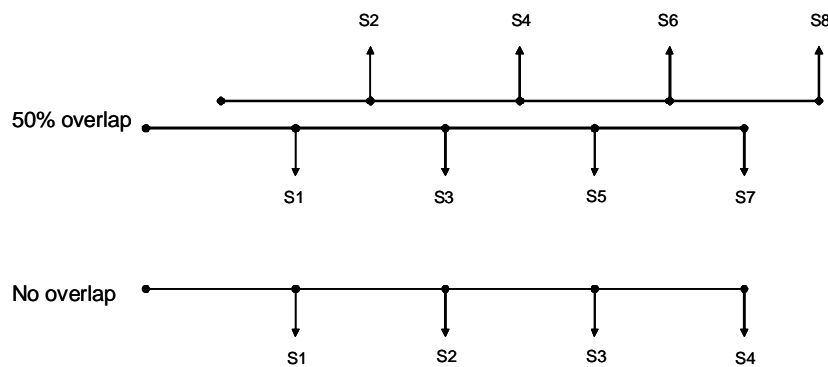


Figure 7.3. Overlapping principle.

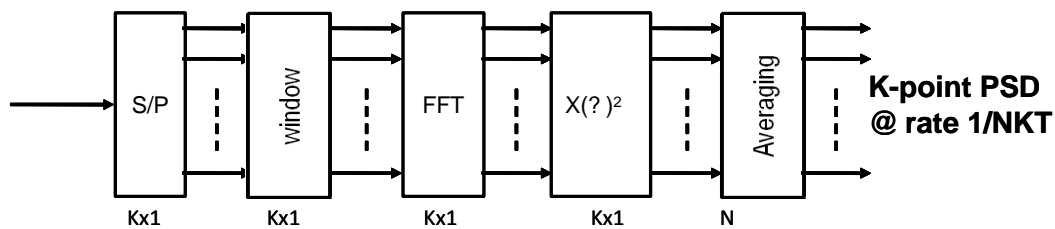


Figure 7.4. Bartlett averaging method.

7.2 Filterbanks based analysis

The widely used STFT discussed supra and the related algorithms like for example the Welch method may be viewed as Filter Bank Spectral Estimators (FBSEs) with relatively simple prototype filters. See also [Far09], [D5109] for other discussions on filterbank architectures and complexity analysis.

7.2.1 Architecture

The filterbank-based architecture is detailed through Figure 7.5 and Figure 7.6 in which the polyphase filter structure is displayed. The factor $l=K/M$ is the oversampling ratio, where K is the decimation factor and M the number of subbands. This structure only allows integer ratios.

The polyphase filter resamples the signal by a factor of K , to alias the spectral terms residing at multiples of the output sample rate to baseband. This means that, for the standard polyphase filter, the output rate is the same as the subband spacing. Operating at this sample rate permits aliasing of the band edges into the down-sampled passband.

The DFT (or FFT) performs the task of separating the channels after the polyphase filter so the transform size is locked to the number of channels. Also the filterbandwidth is determined by the weights of the low-pass prototype and that this bandwidth and spectral shape is common to all the channels.

Note that the polyphase filter is of size $K \times N$ which forces the output rate to be N times slower than for the STFT case.

At last, we emphasize the backward compatibility with the classical approach which corresponds to the $N=1$ case.

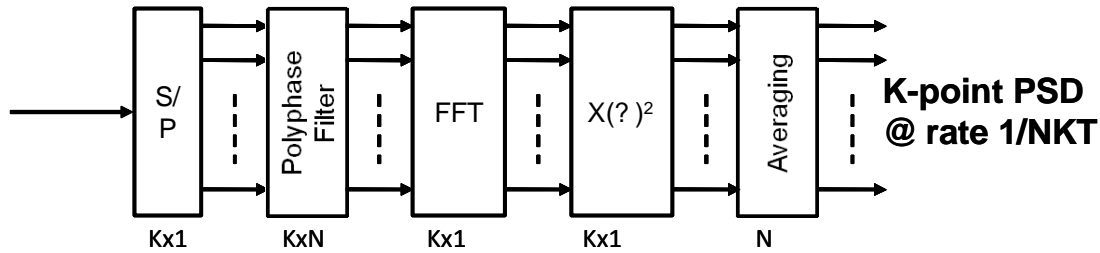


Figure 7.5. Filterbank based architecture.

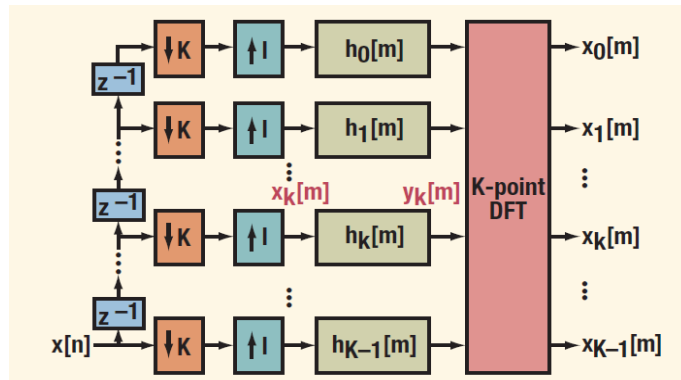


Figure 7.6. Polyphase DFT filter bank.

7.2.2 Analysis and prototype filter

In filter bank estimation every point in power or frequency spectrum is considered as the output of single filter (or multiple filters operating at the same band). Hence, the frequency spectrum is

considered as the output of multiple filters (operating at different bands). The analysis can now easily be performed by calculating short-term averages of the signal power at the outputs of the filter bank. Due to better magnitude response of its prototype filter, the filter bank introduces lower leakages compared to periodogram methods at the expense of extra computation complexity.

Error! Reference source not found. displays a magnitude response for a given filterbank and for a rectangular. In this case, the FB wins both in terms of resolution (main lobe) and dynamic range.

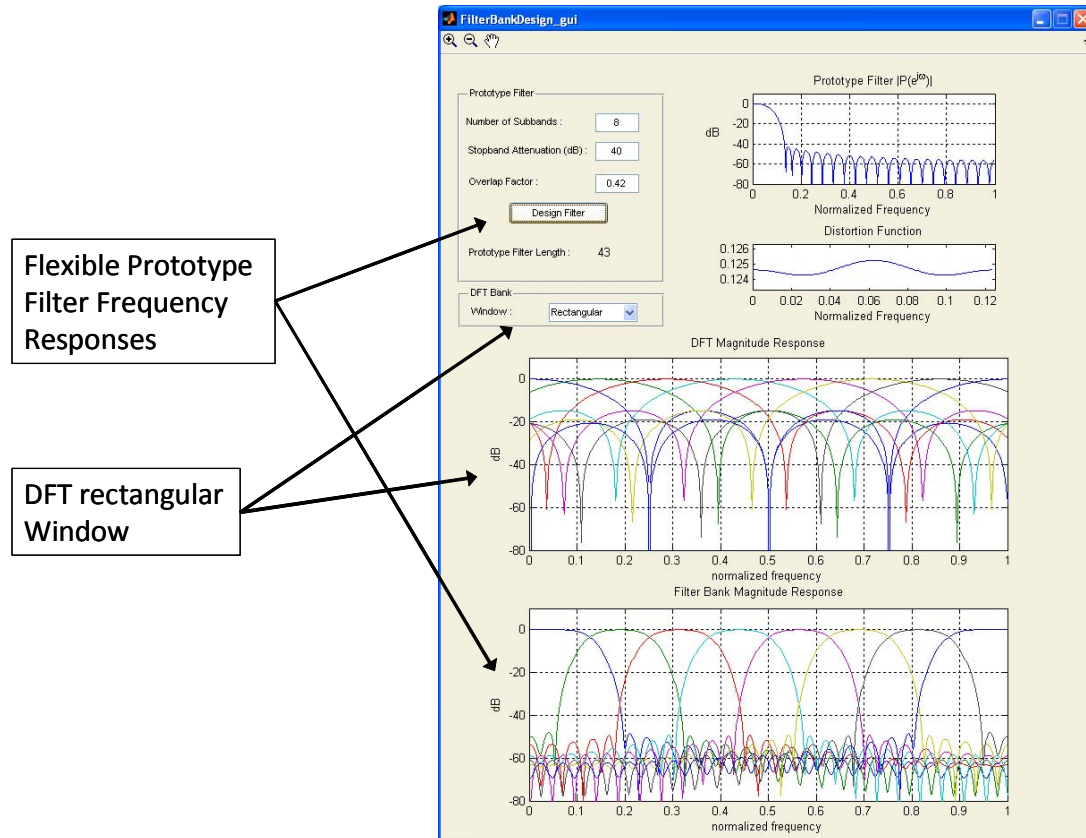


Figure 7.7. Prototype filter vs rectangular window.

7.3 Comparison

In the sequel, the two approaches are compared both in terms of complexity and performance. As stated earlier, no overlap is assumed. Furthermore, DFT is assumed to be implemented through FFT.

7.3.1 Complexity comparison

The computational complexity of the filterbank structure is equivalent to a realization of an FIR prototype filter of size $(N \times K)$ and one FFT of size K which amounts to:

$$\text{Compl. FB} = O(K \log_2 K + NK).$$

As for the classical windowed approach, it is equivalent to an FFT and the windowing operation, that is:

$$\text{Compl. } W = O(K \log_2 K + K).$$

Table 7.1 below lists different scenarios in terms of number of operations.

Table 7.1: Complexity comparison (number of operations).

	K	512	1024	2046	4096	8192
O	Win FFT	5120	11264	24549	53248	114688
	FB (N=2)	5632	12288	26624	57344	122880
	FB (N=4)	6656	14336	30720	65536	139264
	FB (N=6)	7680	16384	34816	73728	155648
	FB (N=8)	8704	18432	38912	81920	172032
	FB (N=10)	9728	20480	42963	90112	188416
	FB (N=12)	10752	22528	47055	98304	204800
	FB (N=13)	11264	23552	49101	102400	212992

Hence we notice that the complexity of the filterbank approach compared to the windowed FFT increases with increasing N as follows:

FB ($N=2$) is 9% more complex

FB ($N=4$) is 27% more complex

FB ($N=8$) is 64% more complex.

7.3.2 Illustrative examples

The simulation scenario is constituted of three sinusoids among which two of them are close to each other in frequency (111Hz and 116Hz). The challenge is to resolve these two.

- *Case A: Performance comparison with same FFT size (Figure 7.8):*

Figure 7. illustrates a performance comparison between the two schemes assuming a same FFT size of $K=512$ for the two schemes. Clearly, the classical approach is unable to resolve the two nearby frequencies while the filterbank based approach clearly separates the two frequencies. The price paid is a reasonable greater complexity ($N=2$) in this case.

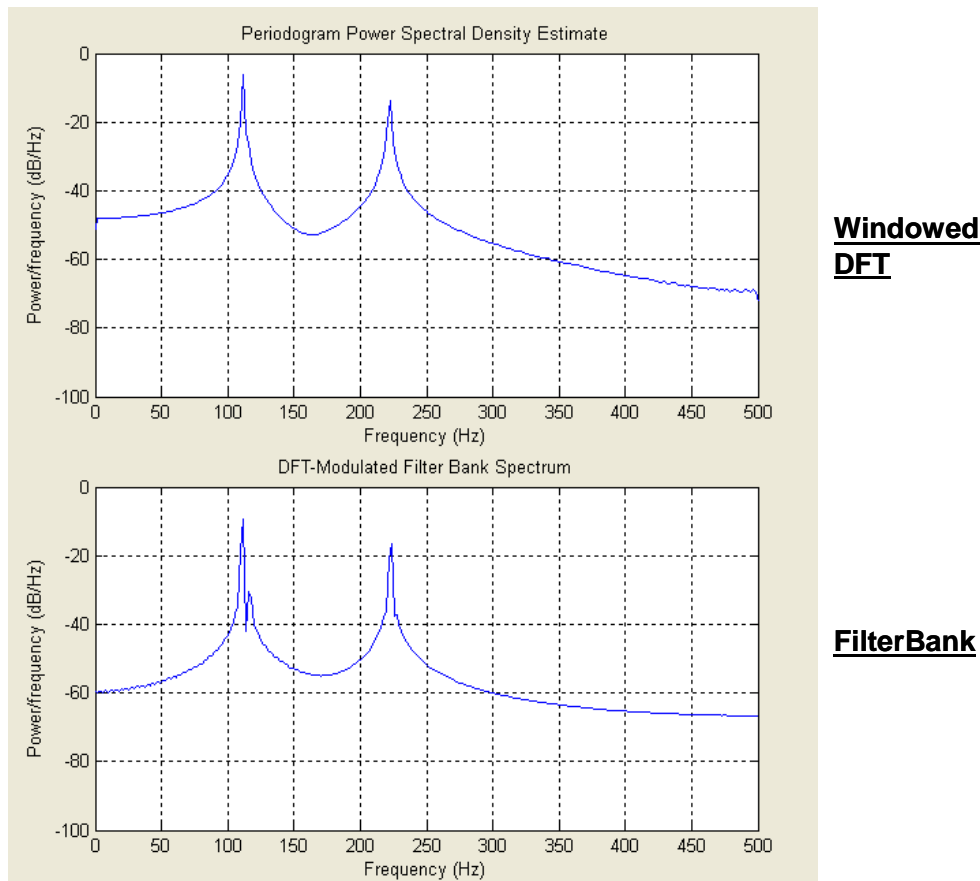


Figure 7.8. Simulation results: Case A.

- *Case B: Gaussian window (Figure 7.9):*

Here, the difference with the previous setup is the usage of a Gaussian window in place of the rectangular window in the classical case. Clearly, it can be seen that the dynamic range is improved but the approach still fails in identifying the two sinusoids.

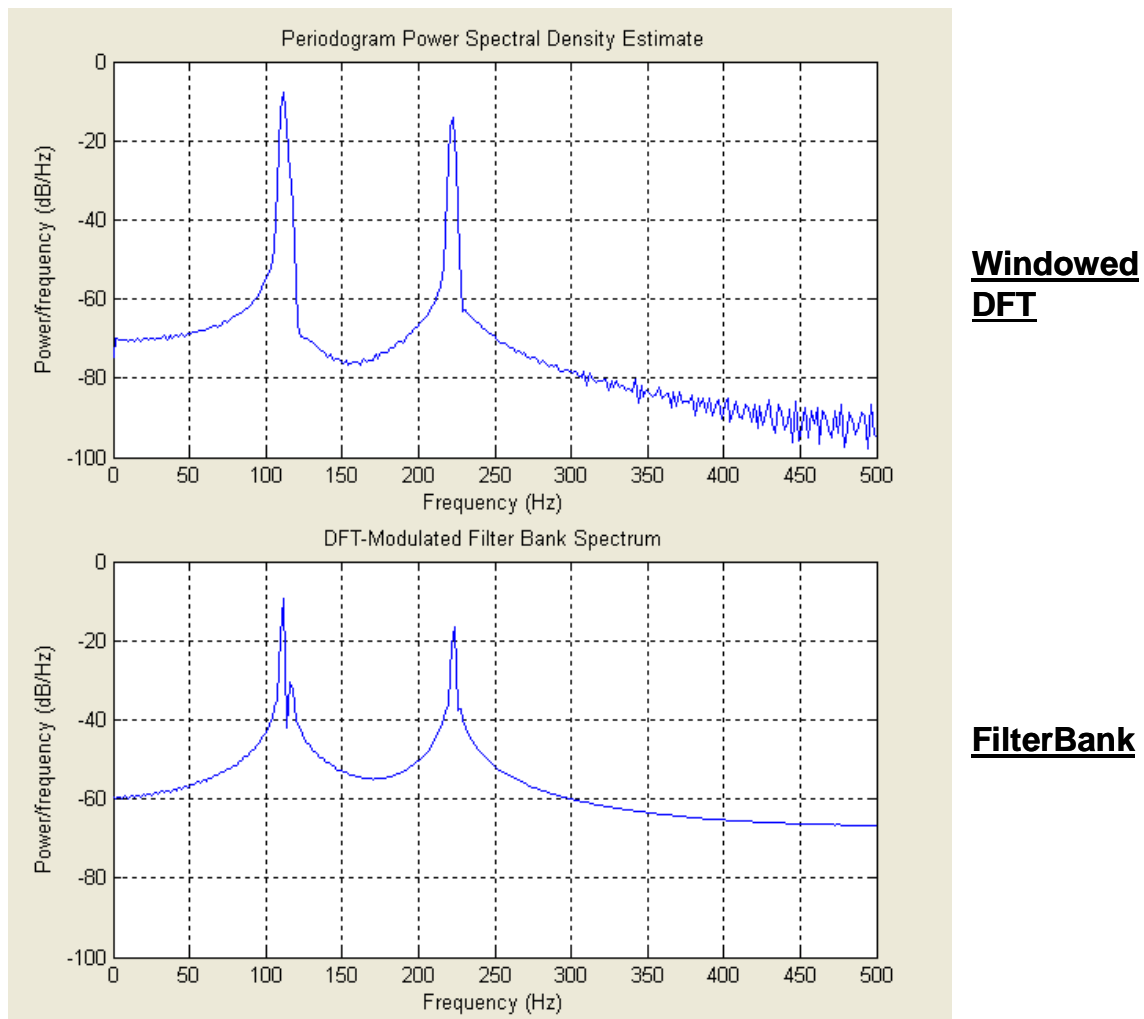


Figure 7.9. Simulation results: Case B.

- *Case C: Different FFT sizes* (Figure 7.10):

A greater FFT size ($K=1024$) is here used in the classical approach to increase the resolution (A Gaussian window is assumed). The FB FFT is kept to the initial $K=512$.

Clearly, both methods resolve the two frequencies, but their complexity is significantly different due to the increased size of the FFT in the classical case.

- Windowed FFT: $O(11264)$
- FB: $O(5632)$

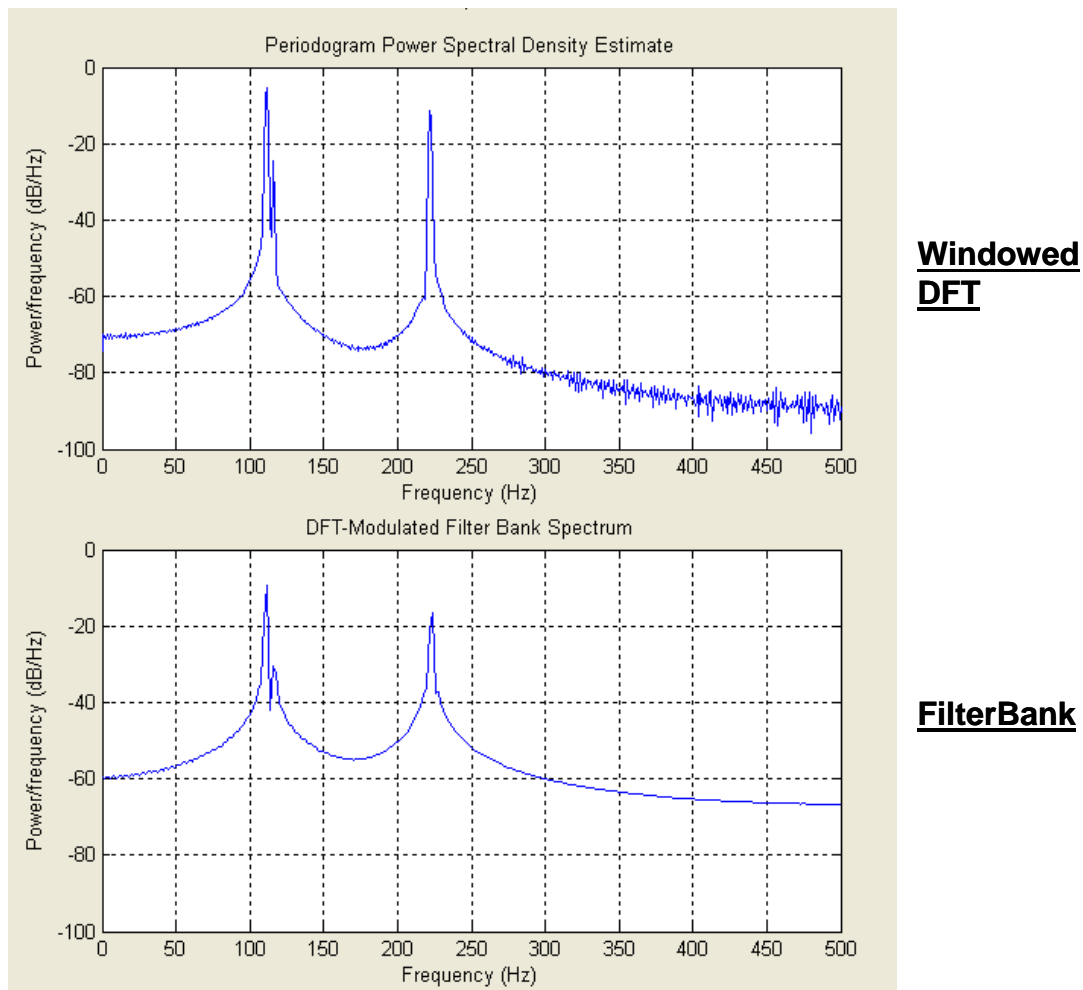


Figure 7.10. Simulation results: Case C.

- *Case D: Analysis at same complexity* (Figure 7.11):

Here, the size of the filterbank (number of slices) is increased to reach the same complexity as the windowed FFT methods: $O(11264)$.

While both methods resolve the two sinusoids, the increased size of the FB leads to a significant increase in the dynamic range.

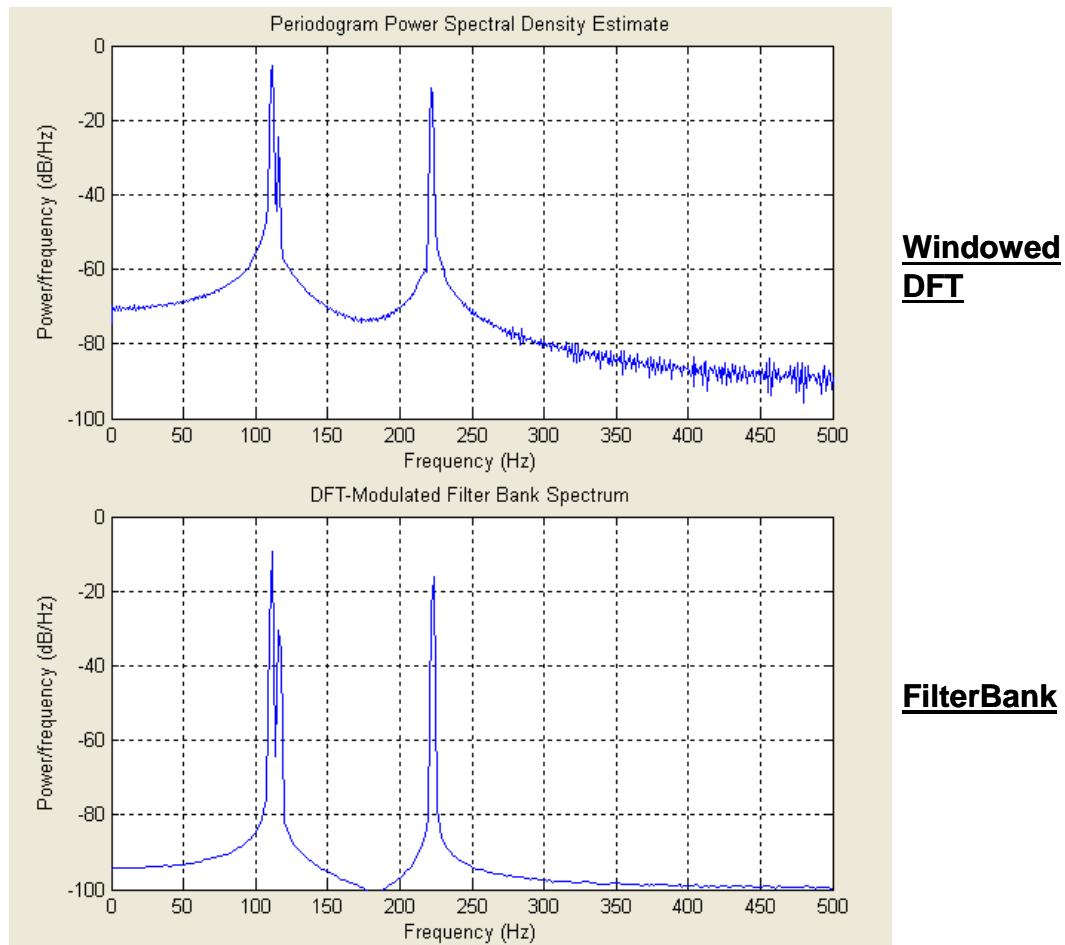


Figure 7.11. Simulation results: Case D.

- *Case E: Addition of noise* (Figure 7.12):

The same setup as in case D is considered with noise added.

It is clear seen from the picture that, thanks to averaging ($N=13$), the noise performance of the filter is significantly better than for the window-based approach.

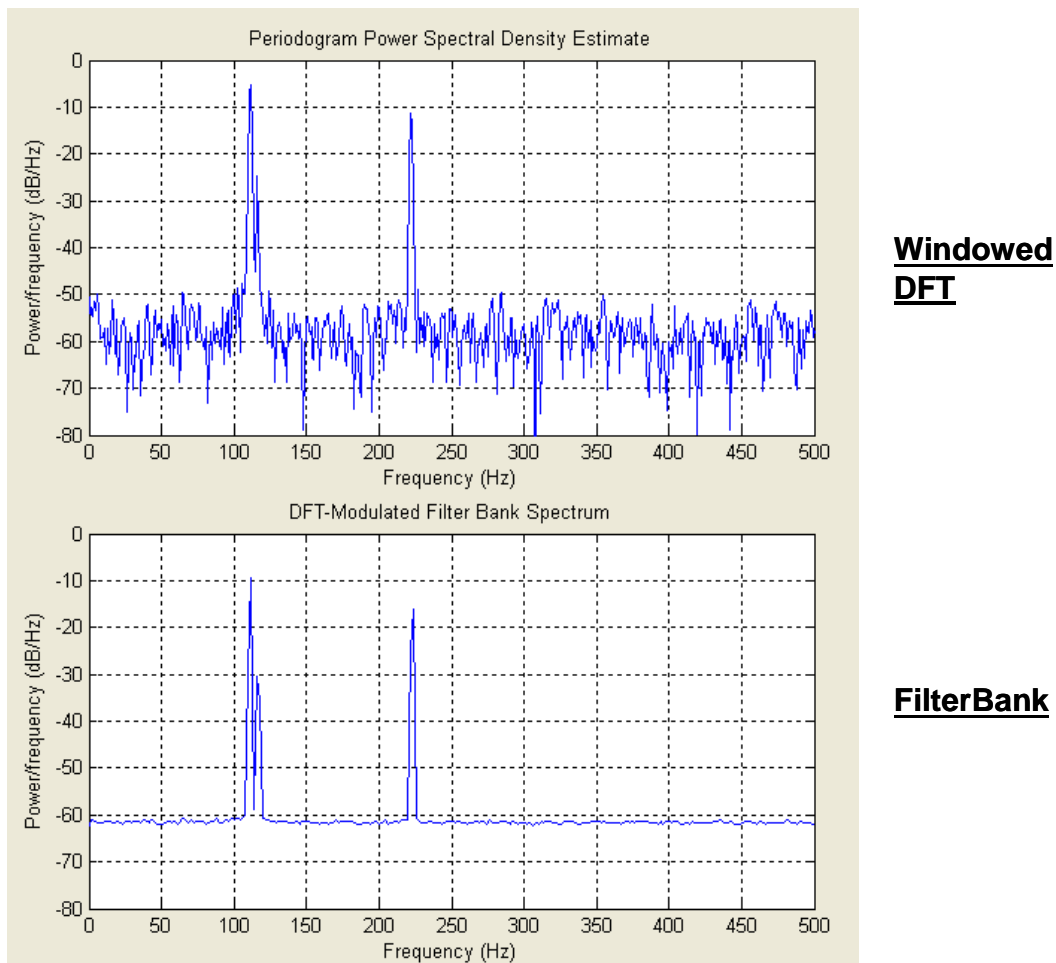


Figure 7.12. Simulation results: Case E.

- *Case F: Averaging in the classical method case* (Figure 7.13):

Here, a significant noise variance reduction in the classical approach by averaging $N=13$ spectral images.

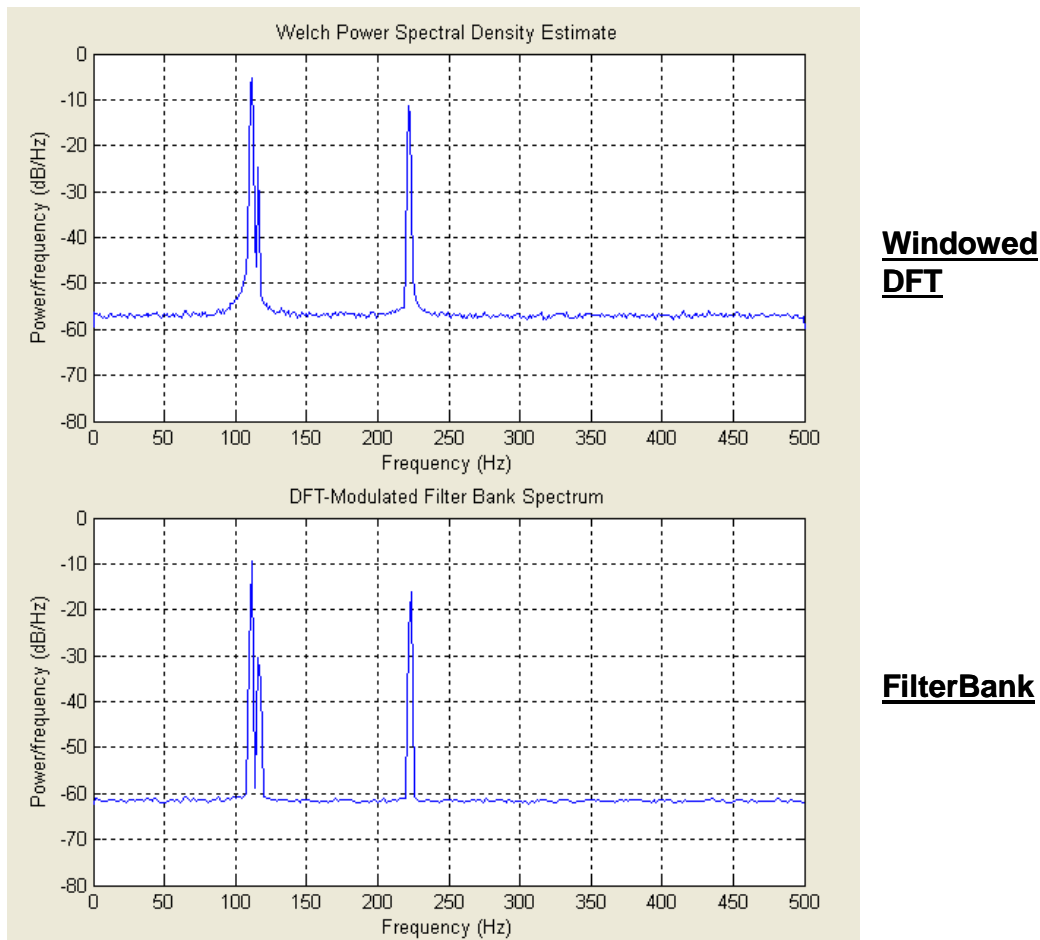


Figure 7.13. Simulation results: Case F

7.4 Conclusions

In this work, we have reviewed both the classical windowed DFT approach and a filterbank based approach. We have seen that the windowed DFT analysis is limited by the rectangular window length (window length = FFT length). While more advanced windowing (Gaussian, Hann...) will improve the dynamic range (reduced spectral leakage), it will on the other hand reduce the resolution. Overlapping / Averaging (Welch method) improves the variance but not the resolution. To improve the latter, an increased FFT size is required.

Conversely, we have seen that filterbanks have a higher complexity than the windowed DFT approach.

Both schemes are of interest, the choice between the two should be conducted accordingly to the application targeted.

8 Decentralized Dynamic Spectrum Allocation in Uncoordinated Cognitive Radio Networks Based on Adaptive Antenna Array Interference Mitigation Diversity: Finite Amount of Data Spectrum Sensing Effects

In this Section, we continue investigation of the interference mitigation (IM)-based dynamic spectrum allocation (DSA) algorithms introduced and studied in [D8109], [Kuz08], [Kuz09-1], [Kuz09-2], [Abr09], [Kuz10-1], [Kuz10-2], and [Kuz10-3]. The basic scenario assumes a number of uncoordinated and unsynchronized wireless subsystems sharing spectrum in the same geographical area. It is shown in [D8109] that OFDM is spectrally inefficient PHY in this scenario and FBMC could be much better solution for uncoordinated spectrum sharing and cognitive radio (CR) networks. A “good neighbour” (GN) approach proposed in [D8109] can be considered as some kind of rule-regulated cooperation between spectrum sharing subsystems without explicit data exchange between them. The IM-based DSA algorithms are studied in [D8109] and the indicated papers by means of the theory of absorbing Markov chains and simulations assuming that local second-order statistics is known at each subsystem. Now, we are going to introduce spectrum sensing algorithms at each spectrum sharing subsystem to estimate these statistics and study finite amount of data effects for the GN IM-based DSA.

It is worth emphasizing that this chapter is devoted to horizontal CR, where spectrum sharing systems equally compete for spectrum. In Section 8.7.3 [D8109], we have demonstrated application of our approach to vertical CR networks with PU. In this case, spectrum monitoring of the PU presence addressed in Sections 2, 3, 5, and 6 is required additionally to the local spectrum sensing considered in this Section. Particularly, the free of PUs bands available for spectrum sharing systems need to be found at each of them. This can be achieved by narrowband (Sections 2 and 3) or multiband (Section 5) PU detection taking into account the PU features as proposed in Section 6 (candidate detection).

In Section 8.1, we describe the system model and formulate the problem. Section 8.2 presents a modified GN algorithm based on locally estimated second-order statistics. In Section 8.3 we introduce a spectrum sensing protocol for estimation of the statistics required for the algorithm in Section 8.2. Section 8.4 is devoted to Markov chain analysis of low-dimension IM-based DSA networks taking into account the finite amount of data spectrum sensing effects. Section 8.5 presents the simulation results for higher-dimension DSA networks. Advanced spectrum sensing solutions based on adaptive averaging over a number of sensing intervals are proposed and studied in Section 8.6. Conclusions are given in Section 8.7.

8.1 System model and problem formulation

As in [D8109], the considered system consists of N independent subsystems containing base stations BS_n , $n=1, \dots, N$ and corresponding users SS_{nm} , $m=1, \dots, M$, where M is the number users per BS. A spectrum sharing version (no primary users) of the system model is illustrated in Fig. 8.1 for $N = M = 3$. Users transmit data to their BSs using one of the $F \geq M$ available

frequency channels. BSs have full control of their own users. In particular, they can estimate propagation channels and interference statistics in all the available bands and allocate the individual bands and transmit powers to their own users. Assuming for simplicity narrowband channels, the signal received by an antenna array of K elements for the n th subsystem can be expressed as follows:

$$\mathbf{x}_{nf}(t) = \sum_{l=1}^N \sum_{m=1}^M \delta_{fd_{lm}q_{lm}} \mathbf{h}_{d_{lm}m\ln} s_{lm}(t) + \mathbf{z}_{nf}(t), n=1, \dots, N, f=1, \dots, F, \quad (8.1)$$

where $\mathbf{x}_{nf}(t)$ is the $K \times 1$ vector of the signal received at BS _{n} in the f th band at the t th time instant, $\mathbf{h}_{fm\ln}$ is the $K \times 1$ vector of propagation channel to BS _{n} in the f th band from the m th user of the l th subsystem, $s_{nm}(t)$ is the SS _{nm} transmitted signal with $\sigma_s^2 = E\{|s_{nm}(t)|^2\} = 1$ and q_{nm}^2 is its power with constraint $\sum_{m=1}^M q_{nm}^2 = Q$, $n=1, \dots, N$, $\mathbf{z}_{nf}(t)$ is a $K \times 1$ vector of AWGN with $E\{\mathbf{z}_{nf}(t)\mathbf{z}_{nf}^*(t)\} = \sigma^2 \mathbf{I}_K$, d_{nm} is the nm th element of the $N \times M$ decision matrix \mathbf{D} denoting the frequency band assigned to SS _{nm} , $E\{\cdot\}$ is the averaging operator, $(\cdot)^*$ is the conjugate transpose operation, \mathbf{I}_K is the $K \times K$ unity matrix, and

$$\delta_{ij} = \begin{cases} 1 & \text{if } i = j \\ 0 & \text{if } i \neq j \end{cases} \quad (8.2)$$

Figure 8.1. System model for horizontal CR scenario (spectrum sharing)

A global performance metric, which cannot be estimated locally at each BS _{n} , is defined as the data rate for the weakest link in the system

$$\gamma = \min_{m=1, \dots, M, n=1, \dots, N} \log_2 [1 + \text{SINR}(\mathbf{D})], \quad (8.3)$$

where

$$\text{SINR}(\mathbf{D}) = \mathbf{h}_{d_{nm}mn}^* \mathbf{R}^{-1} \mathbf{h}_{d_{nm}n} \quad (8.4)$$

is the SINR at the output of the optimal spatial filter for the nm th user and

$$\mathbf{R}_{d_{nm}n} = \sum_{\substack{i=1 \\ i \neq n}}^N \sum_{j=1}^M \delta_{d_{nm}d_{ij}} \mathbf{h}_{d_{ij}jin} \mathbf{h}_{d_{ij}jin}^* + \sigma^2 \mathbf{I}_K \quad (8.5)$$

is the $K \times K$ interference covariance matrix at BS_n in the band occupied by SS_{nm} .

For the given performance threshold γ_0 , the basic GN IM-based DSA algorithm developed in [D8109] is as follows:

- Sensing interval

Step 1a: Calculate for $m = 1, \dots, M$

$$\mathbf{w}_{nm} = \frac{\mathbf{R}_{d_{nm}^{(0)}n}^{-1} \mathbf{h}_{d_{nm}^{(0)}mnn}}{\mathbf{h}_{d_{nm}^{(0)}mnn}^* \mathbf{R}_{d_{nm}^{(0)}n}^{-1} \mathbf{h}_{d_{nm}^{(0)}mnn}}, \quad (8.6)$$

$$\gamma_n = \log_2 \left(1 + \min_{m=1, \dots, M} \mathbf{h}_{d_{nm}^{(0)}mnn}^* \mathbf{R}_{d_{nm}^{(0)}n}^{-1} \mathbf{h}_{d_{nm}^{(0)}mnn} \right), \quad (8.7)$$

where $d_{nm}^{(0)}$ is the m th element of the current band allocation vector $\mathbf{d}_n^{(0)}$ before the current sensing interval at BS_n .

Step 1b: If $\gamma_n \geq \gamma_0$, then go to the “Data interval” stage without updating \mathbf{d}_n ; otherwise, go to Step 2;

Step 2: Update the band allocation vector \mathbf{d}_n

$$\mathbf{d}_n = \arg \min_{m=1, \dots, M; f_m \in \Phi; f_m \neq f_q, q=1, \dots, M, q \neq m} \sum_{m=1}^M |\text{sign}(f_m - d_{nm}^{(0)})| \quad (8.8)$$

subject to

$$\log_2 (1 + \mathbf{h}_{f_m mnn}^* \mathbf{R}_{f_m n}^{-1} \mathbf{h}_{f_m mnn}) \geq \gamma_0, \quad (8.9)$$

Step 3: Calculate the optimal weight vector

$$\mathbf{w}_{nm} = \frac{\mathbf{R}_{d_{nm}n}^{-1} \mathbf{h}_{d_{nm}mnn}}{\mathbf{h}_{d_{nm}mnn}^* \mathbf{R}_{d_{nm}n}^{-1} \mathbf{h}_{d_{nm}mnn}}, m = 1, \dots, M. \quad (8.10)$$

- Data interval

SS_{nm} , $m = 1, \dots, M$ transmit data in bands assigned in \mathbf{d}_n ;

BS_n receives data with the optimal weight vectors \mathbf{w}_{nm} , $m = 1, \dots, M$ for interference suppression.

The general system assumptions are:

- BSs allocate different bands for all users in their subsystems, i.e., all rows in matrix \mathbf{D} contain different elements.
- Rayleigh propagation channels \mathbf{h}_{fmln} are stationary independent random Gaussian vectors

$$\mathbf{h} \propto CN(0, \sigma_h^2 \mathbf{I}_K), \quad (8.11)$$

where $\sigma_h^2 = 1$ is assumed to emphasize interference limited scenario and simplify comparison with [D8109]. In Section 8.7.2 [D8109], σ_h^2 is a random variable according to the pathloss and shadowing models for particular system geometry.

- For simplification, constant power $q_{nm}^2 = Q/M$ for all users in the system is assumed, i.e., locally selected frequency bands are the only adjustable parameters. Power control was discussed in Section 8.4 in [D8109]. Furthermore, exhaustive minimum switch (MinSwitch) local search in (8.7), (8.8) is assumed to be feasible. Higher-dimension networks require simplified optimization algorithms already addressed in Section 8.3.2 in [D8109].

The main assumption in [D8109] was that the all subsystems know their own second order statistics, i.e.,

- BS_n knows \mathbf{R}_{fn} and \mathbf{h}_{fmmn} for $n = 1, \dots, N$, $m = 1, \dots, M$, $f = 1, \dots, F$, and has no information on \mathbf{R}_{fl} and \mathbf{h}_{fmln} for $l \neq n$.

Now, we concentrate on the finite amount of data spectrum sensing effects and assume that

- Space-time spectrum sensing is implemented at each BS_n to estimate the weight vectors and SINR in all the available bands. To do this, we assume that users transmit the pilot symbols during the sensing intervals and data signals during the data intervals. Furthermore, focusing on the cognitive radio effects, we assume that the sensing intervals for different subsystems do not overlap. A low probability of overlapping of the sensing intervals can be achieved, for example, by means of random duration of the data intervals as illustrated in Fig. 8.2 in [D8109].

The following problems need to be addressed:

- modify the basic GN algorithm using estimated second-order statistics,
 - design a space-time spectrum sensing protocol that allows such estimation,
 - study the IM-based DSA algorithms developed in [D8109] taking into account the finite amount of data effects,
 - propose and investigate modified spectrally efficient IM-based DSA algorithms that allow minimization of the required amount of the training data.
-

8.2 “Good neighbour” DSA algorithm based on locally estimated second order statistics

The main difference compared with the case of known second-order statistics is that the weight vectors and IM efficiency in terms of SINR or potential data rates have to be estimated over the final number of pilot symbols. Assuming that T pilots are available for each user during a sensing interval for the n th subsystem and taking into account that $\sigma_s^2 = 1$, the weight vector and SINR can be estimated as follows:

$$\hat{\mathbf{w}}_{nm} = \hat{\mathbf{R}}_{d_{nm}n}^{-1} \hat{\mathbf{g}}_{d_{nm}n}, m = 1, \dots, M, \quad (8.12)$$

$$\hat{v}_{nm} = \text{SINR}_{nm} = \frac{1}{1 - \hat{\mathbf{w}}_{nm}^* \hat{\mathbf{R}}_{d_{nm}n} \hat{\mathbf{w}}_{nm}} = \frac{1}{1 - \hat{\mathbf{g}}_{d_{nm}n}^* \hat{\mathbf{R}}_{d_{nm}n}^{-1} \hat{\mathbf{g}}_{d_{nm}n}}, m = 1, \dots, M, \quad (8.13)$$

$$\hat{\mathbf{R}}_{fn} = T^{-1} \sum_{t=1}^T \mathbf{x}_{fn}(t) \mathbf{x}_{fn}^*(t), \quad (8.14)$$

$$\hat{\mathbf{g}}_{fn} = T^{-1} \sum_{t=1}^T \mathbf{x}_{fn}(t) s_p^*(t), \quad (8.15)$$

where $\hat{\mathbf{g}}_{fn}$ is the estimated propagation channel \mathbf{h}_{fmmn} of the m th user in the f th band, $s_p(t)$ is the pilot symbol, $\mathbf{x}_{fn}(t)$ is the $K \times 1$ vector of the received signal in the f th band.

Then, the basic GN algorithm summarized in Section 8.1 can be expressed as follows:

- Sensing interval

Step 1a: For the current band allocation $d_{nm}^{(0)}$ calculate $\hat{\mathbf{w}}_{nm}$ according to (8.12) and

$$\hat{\gamma}_n = \log_2 \left(1 + \min_{m=1, \dots, M} \hat{v}_{nm} \right), \quad (8.16)$$

where \hat{v}_{nm} is defined in (8.13);

Step 1b: If $\hat{\gamma}_n \geq \hat{\gamma}_0$, where $\hat{\gamma}_0$ is the threshold that takes into account the finite amount of data effects (to be defined later), then go to the “Data interval” stage without updating \mathbf{d}_n , otherwise, go to Step 2;

Step 2: Update the band allocation vector \mathbf{d}_n according to (8.8) subject to

$$\log_2(1 + \hat{v}_{nm}) \geq \hat{\gamma}_0, \quad (8.17)$$

Step 3: Calculate the optimal weight vector according to (8.12).

- Data interval

SS_{nm} , $m=1,\dots,M$ transmit data in bands assigned in \mathbf{d}_n ;

BS_n receives data with the optimal weight vectors \mathbf{w}_{nm} , $m=1,\dots,M$ for interference suppression.

8.3 Spectrum sensing protocol

Now, we need to design a spectrum sensing protocol that allows implementation of the GN algorithm presented in Section 8.2.

For simplification we assume that users can simultaneously transmit the same pilots in all available bands. This may be difficult to implement, but this is not a critical issue. Furthermore, we note that transmission of the pilots in the currently occupied bands does not change the interference environment for other subsystems. On the contrary, pilot transmission in all available bands does change the interference environment. This means that pilot transmission in all the available bands must be avoided in the stationary regime after convergence of the decentralized DSA network.

The proposed spectrum sensing protocol is shown in Fig. 8.2.

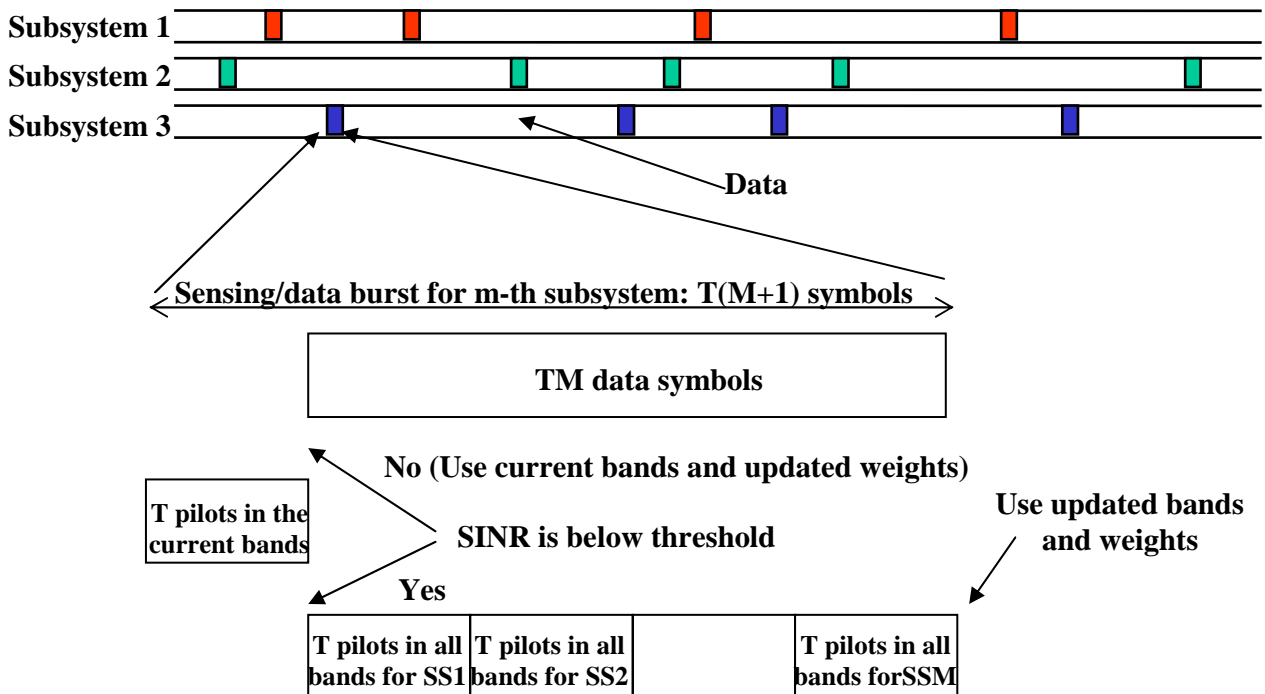


Figure 8.2. Space-time spectrum sensing protocol

At the beginning of the sensing interval all users of the sensing subsystem transmit T pilots in their currently allocated bands without changing the interference scenario for other subsystems. If SINR

estimated over the training interval is above the threshold, then all users transmit TM data symbols, again without any changes to the interference environment. If the estimated SINR is below the threshold, then all users sequentially transmit pilots in all available bands to allow estimation of the decision statistics to apply the MinSwitch search in the GN algorithm. In this case, the interference environment is affected, but this is expected anyway because of updates in band allocation in the end of spectrum sensing interval.

The total duration of the sensing interval during convergence stage is $T_{\text{tot}} = T(M + 1)$ symbols. For high number of users $M \gg 1$, the required T_{tot} may be quite high. In this situation, development of efficient algorithms that allow reduction of T and correspondingly T_{tot} , becomes critically important. To develop such algorithms, first, we need to study the GN DSA performance depending of the number of pilots T .

8.4 Markov chain modelling of IM-based DSA with estimated propagation channels and interference statistics

The main difference of the considered finite amount of data case compared to the known second order statistics situation in [D8109] is that band allocation decision has to be taken based on the SINR (potential data rate) estimated over T pilot symbols. Clearly, this significantly changes the threshold requirements and Markov chain model developed in Section 8.5 [D8109]. To specify all these changes we need to derive probability distribution for SINR estimated over T pilot symbols.

8.4.1 Probability density function of the SINR estimated over a single interval with T i.i.d. complex Gaussian training samples

Here we consider the problem of SINR estimation over a single training interval that consists of $T \geq K + 1$ i.i.d. Gaussian training samples. As in [Kuz06], we replace deterministic training sequence by a realization of a circular Gaussian samples and consider the $(K + 1)$ -dimensional problem, where K is the number of antenna elements. For simplification, in this section we omit indexes corresponding to the scenario in Fig. 8.1 and use conventional for array processing [Mon80] dimension-based notations.

The actual $(K + 1) \times (K + 1)$ covariance matrix \mathbf{R}_{K+1} of the extended $(K + 1) \times 1$ input signal $\tilde{\mathbf{x}}(t) = [s_p(t), \mathbf{x}^T(t)]^T$ has a structure

$$\mathbf{R}_{K+1} = \begin{bmatrix} 1 & \mathbf{h}^* \\ \mathbf{h} & \mathbf{R}_K \end{bmatrix}, \quad (8.18)$$

where \mathbf{h} is the channel “steering vector” for the useful signal, and \mathbf{R}_K is the $K \times K$ covariance matrix of the received signal.

The adaptive $(K + 1) \times 1$ extended weight vector can be expressed as

$$\hat{\mathbf{w}}_{K+1} = \frac{\hat{\mathbf{R}}_{K+1}^{-1} \mathbf{e}_1}{\mathbf{e}_1^T \hat{\mathbf{R}}_{K+1}^{-1} \mathbf{e}_1} = \begin{bmatrix} 1 \\ -\hat{\mathbf{w}}_K \end{bmatrix}, \quad (8.19)$$

where $\hat{\mathbf{R}}_{K+1} = T^{-1} \sum_{t=1}^T \tilde{\mathbf{x}}(t) \tilde{\mathbf{x}}^*(t)$, \mathbf{e}_1 is the first column vector of the $(K+1) \times (K+1)$ unit matrix, and $\hat{\mathbf{w}}_K$ is the conventional minimum mean square (MMSE) weight vector as in (8.12).

Correspondingly, the SINR estimate (8.13) can be expressed as:

$$\hat{\nu} = \left(\hat{\mathbf{w}}_{K+1}^* \hat{\mathbf{R}}_{K+1} \hat{\mathbf{w}}_{K+1} \right)^{-1} = \mathbf{e}_1^T \hat{\mathbf{R}}_{K+1}^{-1} \mathbf{e}_1. \quad (8.20)$$

Now, we are interested in the probability distribution of the ratio

$$\hat{\eta} = \frac{\hat{\nu}}{\nu_{\text{opt}}} = \frac{\mathbf{e}_1^T \hat{\mathbf{R}}_{K+1}^{-1} \mathbf{e}_1}{\mathbf{e}_1^T \mathbf{R}_{K+1}^{-1} \mathbf{e}_1}, \quad (8.21)$$

where $\nu_{\text{opt}} = \mathbf{e}_1^T \mathbf{R}_{K+1}^{-1} \mathbf{e}_1$, and $T\hat{\mathbf{R}}_{K+1}$ has the complex Wishart distribution [Ree74], i.e.,

$$T\hat{\mathbf{R}}_{K+1} \propto \text{CW}(T, K+1, \mathbf{R}_{K+1}). \quad (8.22)$$

It is shown in [Ree74] that statistics of $\hat{\eta}$ depends only on K and T , and does not depend on scenario, i.e., on the covariance matrix \mathbf{R}_{K+1} . Furthermore, the relative SINR estimate can be expressed as

$$\hat{\eta} = \frac{T}{d_{11}}, \quad (8.23)$$

where $d_{11} = c_{11} - \mathbf{c}_{12} \mathbf{C}_{22}^{-1} \mathbf{c}_{12}^*$, $\hat{\mathbf{C}}_0 = \begin{bmatrix} c_{11} & \mathbf{c}_{12} \\ \mathbf{c}_{21} & \mathbf{C}_{22} \end{bmatrix} \propto \text{CW}(T, K+1, \mathbf{I}_{K+1})$, and the probability density function (p.d.f.) of d_{11} is

$$w(d_{11}) = \frac{1}{\Gamma(T-K)} d_{11}^{T-K-1} e^{-d_{11}}, \quad (8.24)$$

where $\Gamma(a)$ is the gamma function [Gra94].

According to [Gra94], the l th moment of $\hat{\eta}$ can be expressed as

$$\text{E}\{\hat{\eta}^l\} = \frac{T^l}{\Gamma(T-K)} \int_0^\infty x^{T-K-1-l} e^{-x} dx = \frac{T^l (T-K-1-l)!}{(T-K-1)!}. \quad (8.25)$$

Particularly, the mean value of $\hat{\eta}$ is

$$E\{\hat{\eta}\} = \frac{T}{T-K-1}. \quad (8.26)$$

One can see from (8.26) that $E\{\hat{\eta}\} > 1$ and $E\{\hat{\eta}\} \rightarrow 1$ for $T \rightarrow \infty$, as expected.

The cumulative distribution function (c.d.f.), i.e., the probability that $\hat{\eta} < \gamma$, can be found as follows [Gra94]:

$$\beta(\delta, T, K) = \text{Prob}(\hat{\eta} < \delta) = \text{Prob}\left(\frac{T}{\delta} < d_{11}\right) = 1 - \frac{1}{\Gamma(T-K)} \int_0^{T/\delta} x^{T-K-1} e^{-x} dx = e^{-\frac{T}{\delta}} \sum_{t=0}^{T-K-1} \frac{1}{t!} \left(\frac{T}{\delta}\right)^t. \quad (8.27)$$

Fig. 8.3 illustrates c.d.f. (8.27) for the fixed $K=4$ and variable T . One can see that the SINR estimated over a short training interval is very likely to be much higher than the actual SINR for the known second order statistics. Clearly, this situation significantly changes the algorithm behaviour in general and the threshold selection in particular. Now, we can study these effects analytically using the estimated SINR statistics (8.26), (8.27).

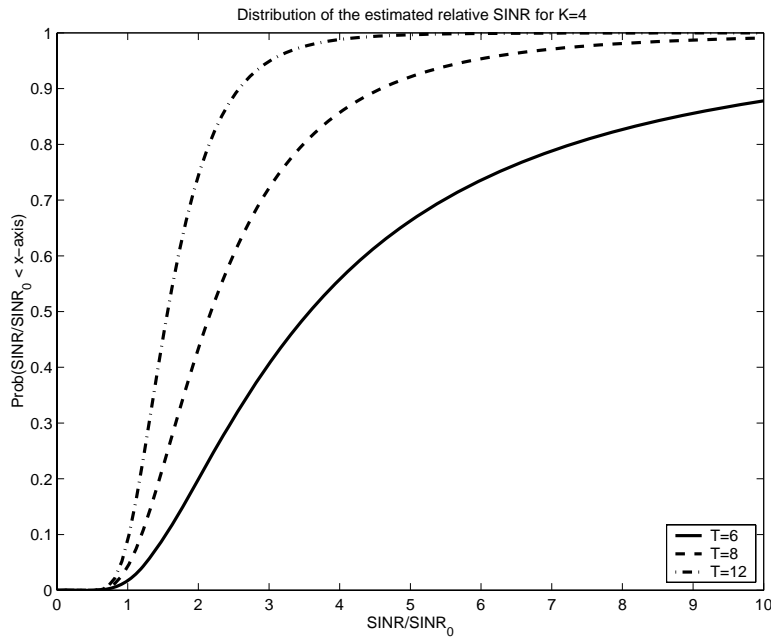


Figure 8.3. c.d.f. of $\hat{\eta}$ for $K=4$ and $T=[6,8,12]$

8.4.2 Markov chain modelling of the IM-based DSA with locally estimated second order statistics

Markov chain analysis of the IM-based DSA with the known local second order statistics is presented in Section 8.5 in [D8109]. It is based on the absorbing Markov chain model, which assumes that the absorbing states exist with zero probability to leave them if they are reached from

some transient states. It is clear that the considered case of estimated second order statistics significantly changes the underlying Markov chain model.

As in [D8109], to formulate a Markov model we assume that all possible $I = (A_M^F)^N$, $A_M^F = F!/(F-M)!$ different allocation matrices \mathbf{D}_i , $i = 1, \dots, I$ form states of the Markov chain. At each sensing interval, we assume that one randomly selected subsystem is sensed with probability $p_{\text{sens}} = N^{-1}$. Then, the $I \times I$ transition probability matrix $\mathbf{P} = \{p_{ij}\}$ can be defined as generalization of the similar procedure for the basic algorithm with the locally known second order statistics [D8109]:

$$\{p_{ij}, i = 1, \dots, I, j = 1, \dots, I\} = p_0(i)\delta_{ij} + p_{\text{sense}}[1 - p_0(i)] \sum_{n=1}^N \sum_{q=1}^Q p_1(i, n, q)\delta_{jj_{inq}}, \quad (8.28)$$

where $Q = A_M^F$ is the number of all possible band allocations for one subsystem; $p_0(i)$ is the probability that $\hat{\gamma}_n(i) \geq \hat{\gamma}_0$ for all $n = 1, \dots, N$, where $\hat{\gamma}_n(i) = \log_2[1 + \min_{m=1, \dots, M} \hat{\nu}_{nm}(i)]$ for the current state \mathbf{D}_i ; $p_1(i, n, q)$ is the probability to select the q th out of Q possible band allocations as the outcome of sensing at the n th subsystem for the i th current state \mathbf{D}_i ; j_{inq} is the corresponding state; and δ_{ij} denotes the Kronecker delta function.

Taking into account that if $a_i \geq \alpha$ for all $i \in I$ then $\min_{i \in I} a_i \geq \alpha$, $p_0(i)$ can be found using (8.27) as follows:

$$p_0(i) = \prod_{n=1}^N \prod_{m=1}^M \left[1 - \beta\left(\frac{\hat{\nu}_0}{\hat{\nu}_{nm}(i)}, T, K\right) \right], \quad (8.29)$$

where $\hat{\nu}_0 = 2^{\hat{\gamma}_0} - 1$ is the SINR threshold.

Unfortunately, it is difficult to get an analytical expression for $p_1(i, n, q)$ in (8.28) because it involves a constrained search according to the GN algorithm. One option could be to use a semi-analytical approach, which is based on the observation that (8.24) actually is the χ^2 distribution with $2(T-K)$ degrees of freedom. This means that d_{11} can be simulated as

$$d_{11} = \sum_{j=1}^{T-K} |z_j|^2, \quad (8.30)$$

where $z_j \sim CN(0,1)$ are independent random complex Gaussian variables with zero mean and unit power. Then, $p_1(i, n, q)$ can be estimated by means of averaging over J trials in which the estimated SINR is simulated as $\hat{\nu} = \nu \frac{T}{d_{11}}$, where ν is the SINR calculated for the given second order statistics and d_{11} is generated according to (8.30) independently for each estimated SINR. In each trial, the MinSwitch search of the GN algorithm for the given \mathbf{D}_i and the n th sensing

subsystem can be applied for the $F \times M$ matrix of estimated SINRs with registration of the band allocation outcome, which is one of the $q=1, \dots, Q$ options. Then, $p_1(i, n, q)$ for the corresponding states j_{inq} can be calculated by means of averaging over all $J \gg 1$ trials.

Now, the transition probability matrix \mathbf{P} is a sparse $I \times I$ stochastic matrix with maximum $A_M^F N - N + 1$ nonzero elements in a row, such that $\sum_{j=1}^I p_{ij} = 1$ for $i=1, \dots, I$, which completely defines Markov model of the considered system.

The main difference compared with the case of the known second order statistics addressed in [D8109] is that the number of nonzero elements is much higher in the estimated case and the absorbing points formally disappear in the corresponding Markov chain because $\beta(\delta) > 0$ for $\delta > 0$, although, $\beta(\delta)$ may be very low for $\delta < 1$ as it can be seen in (8.27) and Fig. 8.3. An illustration of this situation is given in Fig. 8.4, which shows the transition matrices for the known (left) and estimated with $T=12$ pilots second order statistics (right) for the same channel realizations for the following system configuration: $N=5$, $M=2$, $F=3$, $K=4$, $\sigma_s^2=1$, $SNR=20$ dB, $\gamma_0=5$ bits/symbol, and $J=1000$. Taking into account that the estimated SINR is likely to be higher than the actual SINR (see Fig. 8.3), we use the following threshold for the estimated version of the GN algorithm:

$$\hat{\nu}_0 = \nu_0 \frac{T}{T-K-1}, \quad (8.31)$$

or in terms of potential data rate

$$\hat{\gamma}_0 = \log_2 \left[1 + \frac{T(2^{\gamma_0} - 1)}{T-K-1} \right], \quad (8.32)$$

where $\frac{T}{T-K-1}$ is the mean value of the relative estimated SINR for the given K and T according to (8.26).

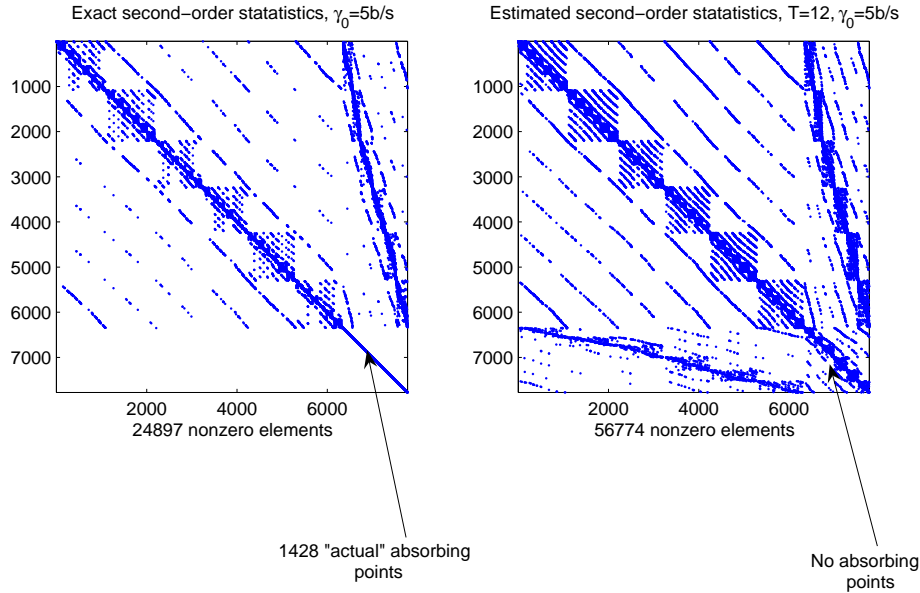


Figure 8.4. Example of the actual (left) and estimated (right) canonical form of the transition probability matrices for the given propagation channels for $T = 12$, $N = 5$, $M = 2$, $F = 3$, $K = 4$, $\sigma_s^2 = 1$, $SNR = 20$ dB, $\gamma_0 = 5$ bits/symbol, and $J = 1000$

For example, the particular 7000th row (the absorbing state in the left matrix) in the right matrix is as follows: $p(7000, 6999) = 3.99 \cdot 10^{-2}$, $p(7000, 7000) = 0.96$, $p(7000, 7033) = 4.2407 \cdot 10^{-6}$, $p(7000, 7255) = 9.7537 \cdot 10^{-5}$.

One can see that, indeed, the number of nonzero elements is much higher in the estimated case and some of them may be very small. Further illustration of this situation is presented in Fig. 8.5, which shows c.d.f. of $\alpha = 1 - p_0(i)$, where $p_0(i)$ is the probability to exceed the threshold for the i th state defined in (8.29) for the states that are the absorbing ones in the actual transition matrix. In fact, this is c.d.f. of the probability to leave the states corresponding to the absorbing states of the actual transition probability matrix calculated over 200 hundred independent channel realizations for different numbers of pilot symbols in the spectrum sensing protocol.

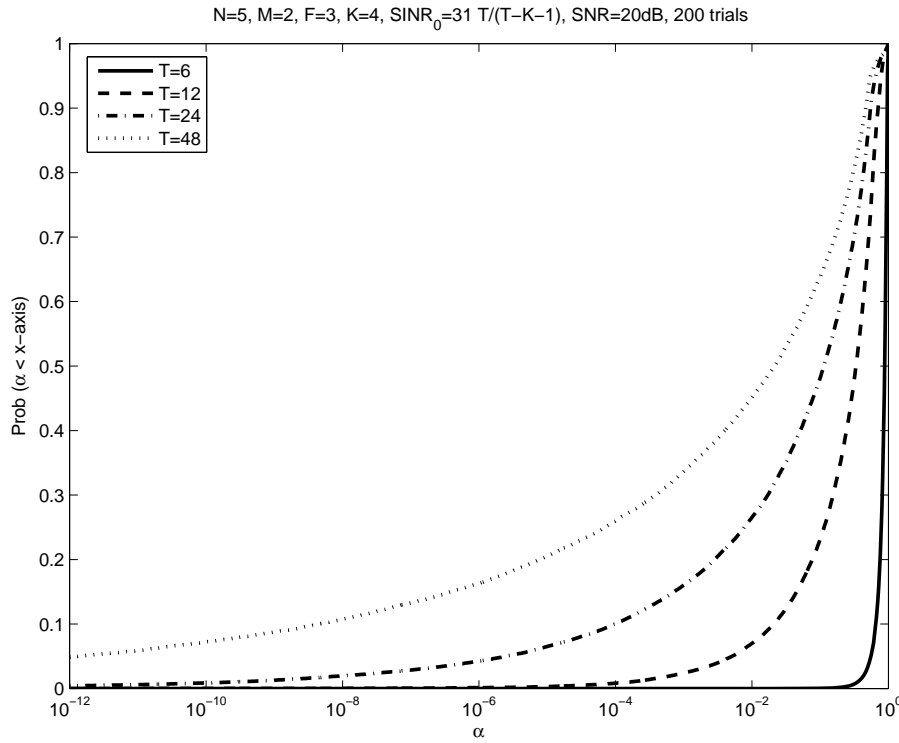


Figure 8.5. Probability to leave the “actual” absorbing points for different number of pilots

One can see in Fig. 8.5 that although probability to leave many of the “actual” absorbing states may be very high, some of them remain very close to absorbing ones. For example, for $T = 12$ almost 5% of the “actual” absorbing states have probability to leave less than 10^{-2} , and for $T = 48$ almost 15% of these states have less than 10^{-6} probability to leave.

8.4.3 Markov chain analysis of the IM-based DSA with locally estimated second order statistics

The fact that some of the states of the defined Markov chain may be very close to absorbing points in terms of $p_{ii} \geq 1 - \alpha$, $\alpha \ll 1$, but $p_{ii} < 1$ for all $i = 1, \dots, I$, means that the theory of absorbing Markov chains [Kem66] is formally not applicable any more. At the same time, the theory of ergodic Markov chains [Fel57] is not practically applicable as well because some elements of the transition probability matrix may be very small that makes practically impossible finding and physical interpretation of the fixed vector as well as other characteristics of the chain in practically singular situations.

Our proposal to overcome this difficulty is to consider a simplified Markov chain modelling, where the states with $p_{ii} \geq 1 - \alpha_0$ for the given $\alpha_0 \ll 1$ are replaced with the absorbing states with $p_{ii} = 1$. This simplification allows us to apply the theory of absorbing Markov chains [Kem66] to the simplified models, calculate the corresponding fundamental matrices, and eventually find average absorption times for all the initial states. In the considered application, this performance can be useful to describe the finite amount of data effect in the IM-based DSA because it can be interpreted

as the average number of sensing intervals before reaching the states with probability to leave them less than $\alpha_0 \ll 1$.

The simplified absorbing Markov models in the same situation as in Fig. 8.4 are shown in Fig. 8.6 for $\alpha_0 = 10^{-3}$ (left) and $\alpha_0 = 10^{-4}$ (right).

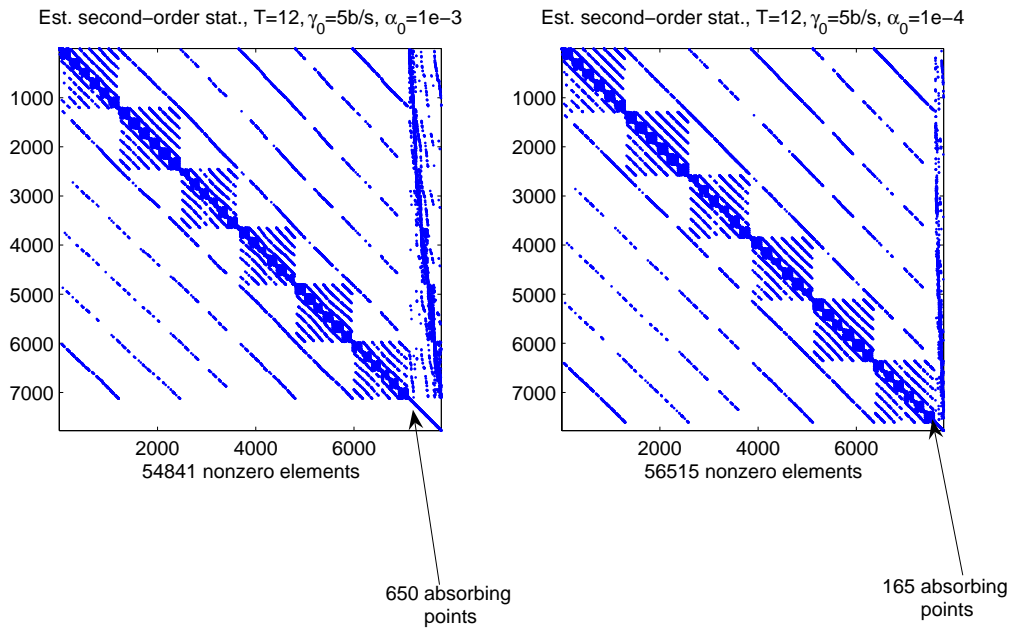


Figure 8.6. Simplified absorbing models of the estimated Markov chain in Fig. 8.4 for $\alpha_0 = 10^{-3}$ (left) and $\alpha_0 = 10^{-4}$ (right)

As expected, the number of absorbing points in the simplified Markov model is lower compared with the number of the “actual” absorbing points in the underlying model (Fig. 8.4 (left)) for the same channel realizations. Furthermore, it is decreasing with decreasing of α_0 as can be seen in Fig. 8.6.

The average number of iterations before reaching the absorbing points of the simplified model from all the initial states can be found similarly to Section 8.5.1 in [D8109]:

$$\mathbf{t}_{av} = \mathbf{C}\mathbf{1}, \quad (8.33)$$

$$\bar{\mathbf{P}}_a = \begin{bmatrix} \mathbf{A} & \mathbf{B} \\ \mathbf{0} & \mathbf{I} \end{bmatrix}, \quad (8.34)$$

where $\mathbf{C} = (\mathbf{I} - \mathbf{A})^{-1}$ is the fundamental matrix of $\bar{\mathbf{P}}_a$ after collapsing the ergodic sub-chains in to the absorbing chains if they exist as described in [D8109], and $\mathbf{1}$ is a vector of all ones.

C.d.f. of t_{av} calculated according to (8.33) for the particular simplified Markov chain shown in Fig. 8.6 (left) is presented in Fig. 8.7.

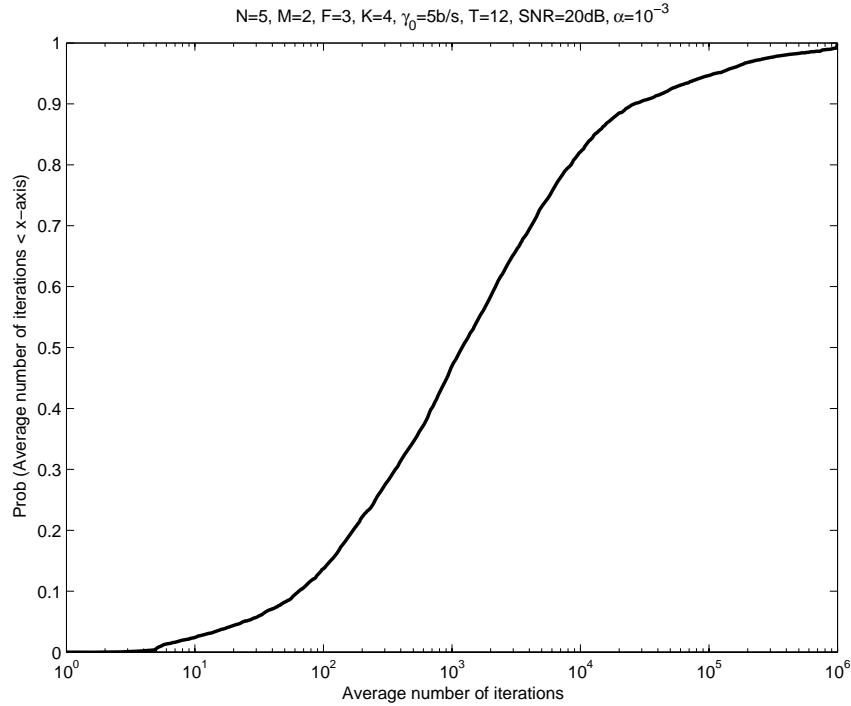


Figure 8.7. C.d.f. of the average number of sensing intervals before reaching the states with probability to leave them less than 10^{-3} for the Markov chain in Fig. 8.6 (left)

One can see in Fig. 8.7 that convergence from some initial states still can be very fast, e.g., for 10% of the initial transient states it is less than 80 iterations on average. Other initial states may experience much slower convergence. Particularly, 20% of initializations require 10^4 and more iterations to reach states with probability to leave less than 10^{-3} in this scenario. A typical example of long-term behaviour of the GN algorithm in this scenario is illustrated in Fig. 8.8 and Fig. 8.9, which presents the initial fragment of Fig. 8.8.

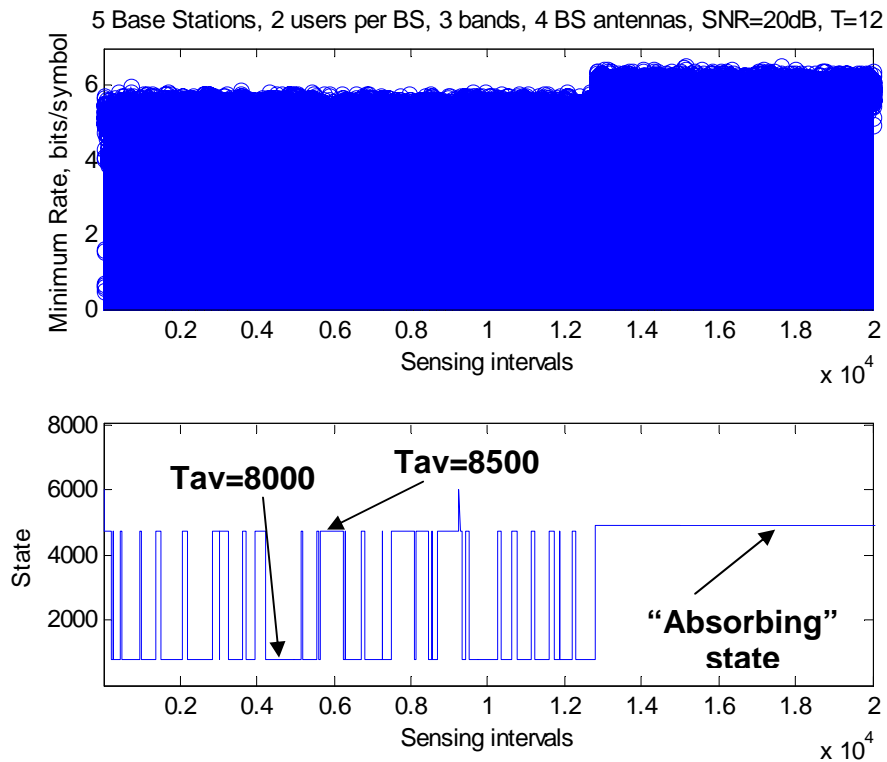


Figure 8.8. Typical example of long-term behaviour

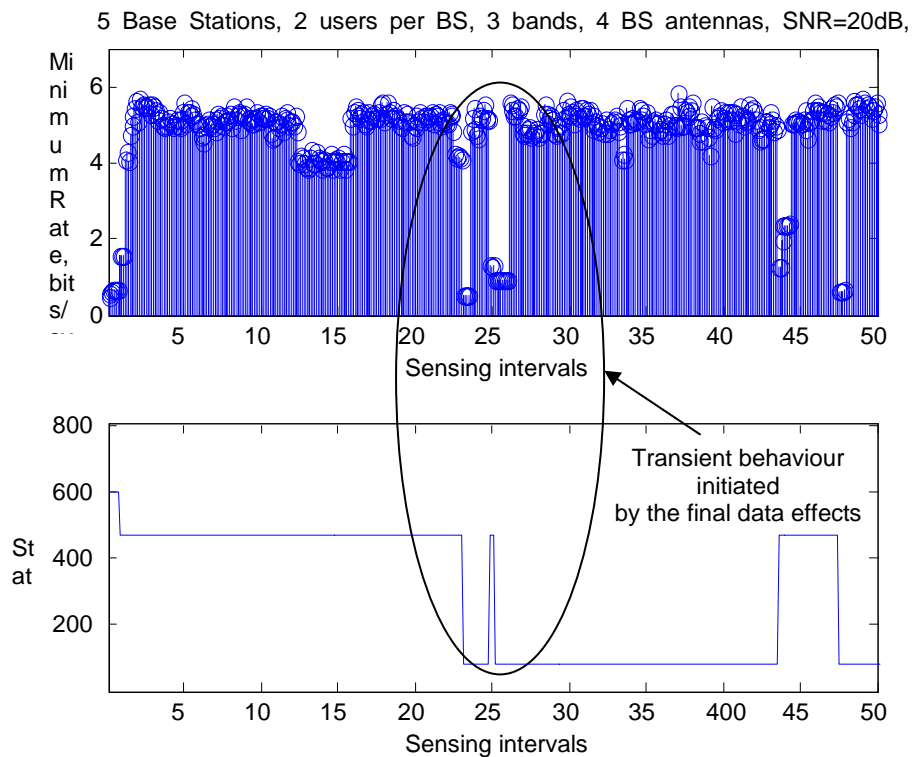


Figure 8.8. The initial fragment of the long-term example in Fig. 8.8

Figs. 8.8 and 8.9 present the simulation results in the same format as in [D8109]. One can see a very slow convergence to the state with very low probability to leave. This state is marked “absorbing”

in Fig. 8.8, but it is important to emphasize that the system will leave it eventually because of the estimation effects if it is observed sufficiently long time.

Although the data rate picture in Fig. 8.8 looks good because of relatively long stationary intervals, the zoom in Fig. 8.9 shows that actually, the system demonstrates an undesirable transient long-term behaviour before reaching the “absorbing” point leading to some performance degradation. This performance degradation is clearly initiated by the finite amount of data effects in the considered stationary propagation conditions.

Generally, the presented simplified absorbing Markov chain modelling allows a quantitative and qualitative analysis of the final amount of data effects in low-dimensional IM-based DSA networks. Higher-dimension networks can be studied by means of simulations still taking into account the effects and trends established by the proposed analysis.

8.5 Simulation results for higher dimension networks

The long-term transient behaviour because of the estimation effects predicted by the Markov chain analysis in Section 8.4 and illustrated in Fig. 8.9 for low dimension networks can be expected for more complicated systems as well. Fig. 8.10 presents the minimum data rate simulation results over 1000 data intervals in 100 stationary channel realizations for $N = 5$, $M = 5$, $F = 7$, $K = 4$, $\sigma_s^2 = 1$, $SNR = 20$ dB, $\gamma_0 = 5$ bits/symbol, and variable $T = [6, 8, 12]$.

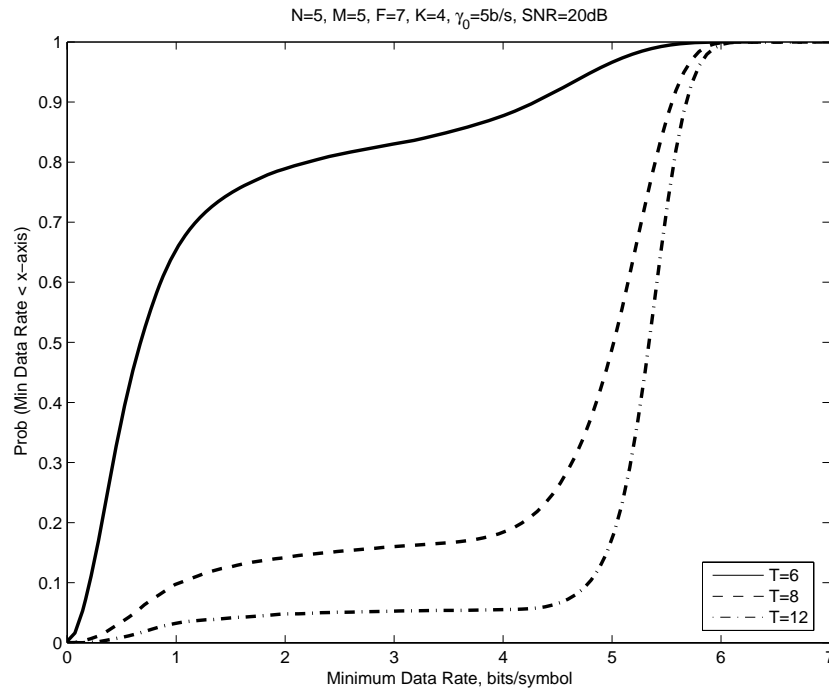


Figure 8.10. Minimum data rate performance over 1000 data intervals in 100 trials for $N = 5$, $M = 5$, $F = 7$, $K = 4$, $\sigma_s^2 = 1$, $SNR = 20$ dB, $\gamma_0 = 5$ bits/symbol, and variable T

In Fig. 8.10, one can see that the spectrum sensing effects make the critical impact on the network performance. Particularly, increasing the pilot interval by 2 times from $T = 6$ to $T = 12$ reduces the number of data intervals with minimum data rate below 4.5 bits/symbol from 90% to 5%. Obviously, the doubled overhead is the price to be paid for this performance improvement.

Furthermore, further performance improvement requires even more pilot symbols leading to spectrum efficiency degradation because of the spectrum sensing effects.

8.6 Adaptive averaging for spectrum sensing algorithms in GN IM-based DSA

In many practical situations with quasi-stationary environment the pilot data could be averaged over a number of sensing intervals leading to reduced requirements for the pilot support and higher efficiency of spectrum sensing algorithms. A new adaptive averaging (AA) spectrum sensing solution for the GN IM-based DSA is developed and investigated in this Section.

8.6.1 Modified GN algorithm

The main idea is that at any new sensing interval a stationarity test should be applied to decide if the new pilot data of T symbols is received in the same environment as the ET pilot symbols received at the previous E sensing intervals or not. Then the GN algorithm in Section 8.2 should be modified as follows:

- If “yes” for the stationarity test, then the pilot data from the “whole” stationary sensing interval of $(E+1)T$ pilot symbols is used at Steps 1a and 1b in the algorithm in Section 8.2. Particularly, the threshold in Step 1b becomes an updated version of (8.32):

$$\hat{\gamma}_0 = \log_2 \left[1 + \frac{(E+1)T(2^{\gamma_0} - 1)}{(E+1)T - K - 1} \right]. \quad (8.35)$$

- If “no” for the stationarity test or $\hat{\gamma}_n$, then the algorithm on Section 8.2 remains unchanged with the threshold defined in (8.32) for both Steps 1b and 2.

This AA modification of the GM algorithm should allow better performance in slowly changing scenarios for the given number of pilots, still demonstrating ability to react to fast changes in the environment. Clearly, an effective stationarity test is the critical requirement for AA in GN IM-based DSA.

8.6.2 Stationarity test for spectrum sensing with adaptive averaging

We apply a stationarity test from [Abr92] that is based on comparison of antenna array interference mitigation efficiency estimated over the last T and previous ET training symbols:

$$\hat{\eta}_E = \frac{1}{E} \frac{\mathbf{e}_1^T \hat{\mathbf{R}}_{K+1}^{-1} \mathbf{e}_1}{\mathbf{e}_1^T \hat{\mathbf{R}}_{K+1}^{-1} \hat{\mathbf{R}}_{K+1}^{-1} \hat{\mathbf{R}}_{K+1}^{-1} \mathbf{e}_1}, \quad (8.36)$$

where $\hat{\mathbf{R}}_{K+1}$ is the $K+1$ -dimension covariance matrix defined after (8.19) over the last sensing interval of T pilots, $\hat{\mathbf{R}}_{K+1} = \sum_{e=1}^E \sum_{t=1}^T \tilde{\mathbf{x}}_e(t) \tilde{\mathbf{x}}_e^*(t)$, is the $K+1$ -dimension covariance matrix defined

over the previous E sensing intervals of ET pilots, and $\tilde{\mathbf{x}}_e(t) = [s_p(t), \mathbf{x}_e^T(t)]^T$ is the extended $(K+1) \times 1$ input signal received at the e th sensing interval defined similarly to $\tilde{\mathbf{x}}(t)$ in (8.18) over the last $(E+1)$ th sensing interval.

The idea is that if all $E+1$ intervals correspond to a stationary interference environment, then probability to find $\hat{\eta}_E \ll 1$ should be very low especially for high E . On the contrary, if the interference scenario at the last sensing interval is different compared with the one during the previous E intervals, then this outcome can be found with much higher probability.

In [Abr92], c.d.f. of $\hat{\eta}_E$ is found as an extension of the corresponding statistic (8.27) derived in [Ree74]:

$$\beta_E(\delta, E, T, K) = \text{Prob}(\hat{\eta}_E < \delta) = \frac{1}{(1+E\delta)^T} \frac{(ET)![(E+1)-K]!}{(ET-K)!(T-1)![(E+1)T]!} \times \sum_{l=0}^{ET-K+1} \frac{(T+1-l)!}{l!} \left(\frac{E\delta}{1+E\delta} \right)^l {}_2F_1 \left[T+l, K; (E+1)T+1; \frac{1}{1+E\delta} \right] \quad (8.37)$$

where

$${}_2F_1(a, b; c; z) = \frac{\Gamma(c)}{\Gamma(b)\Gamma(c-b)} \int_0^1 t^{b-1} (1-t)^{c-b-1} (1-tz)^{-a} dt \quad (8.38)$$

is the hypergeometric function [Gra94].

Now, expressions (8.37) and (8.38) allow us to calculate the variable threshold $\delta_0(E)$ to be compared with $\hat{\eta}_E$, such that $\beta_E[\delta_0(E), E, T, K] = \beta_0$ for some given probability threshold $\beta_0 \ll 1$. An example of $\delta_0(E)$ for $K=4$, $\beta_0=10^{-5}$, and different $T=[6,8,12]$ is shown in Fig. 8.11.

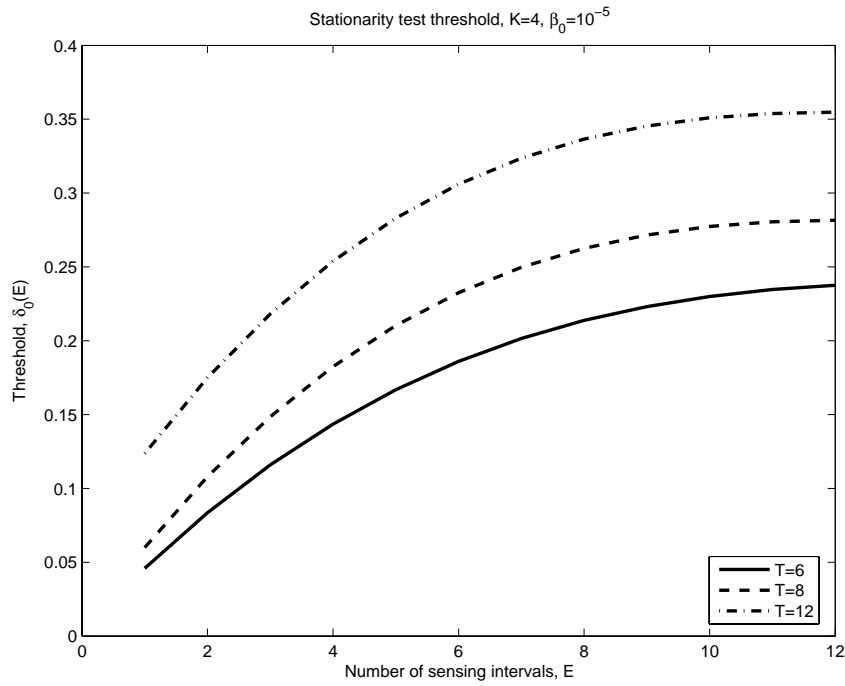


Figure 8.11. Threshold for the stationarity test

Application of the stationarity test in the modified GN IM-based DSA is as follows:

- For the current sensing interval, calculate $\hat{\eta}_E$ as in (8.36), where E is the number of successive sensing intervals with “yes” decision on stationarity;
- if $\hat{\eta}_E > \delta_0(E)$, then decide “yes” and update $E = E + 1$;
- if $\hat{\eta}_E \leq \delta_0(E)$, then decide “no” and update $E = 1$ for the next sensing interval for the given subsystem;
- follow the modified GN algorithm summarized in Section 8.6.1.

8.6.3 Simulation results

Fig. 8.12 shows the long-term simulation results for both versions of the GN algorithm with and without AA in the same stationary scenario as in Fig. 8.10 with the AA threshold given in Fig. 8.11. Examples of the long term behaviour are presented in Fig. 8.12 for $T = 6$ and Fig. 8.13 for $T = 12$ pilot symbols. In the middle of the simulations in Figs. 8.12 and 8.13, the propagation conditions in one out of five subsystems are randomly changed to simulate a non-stationary environment.

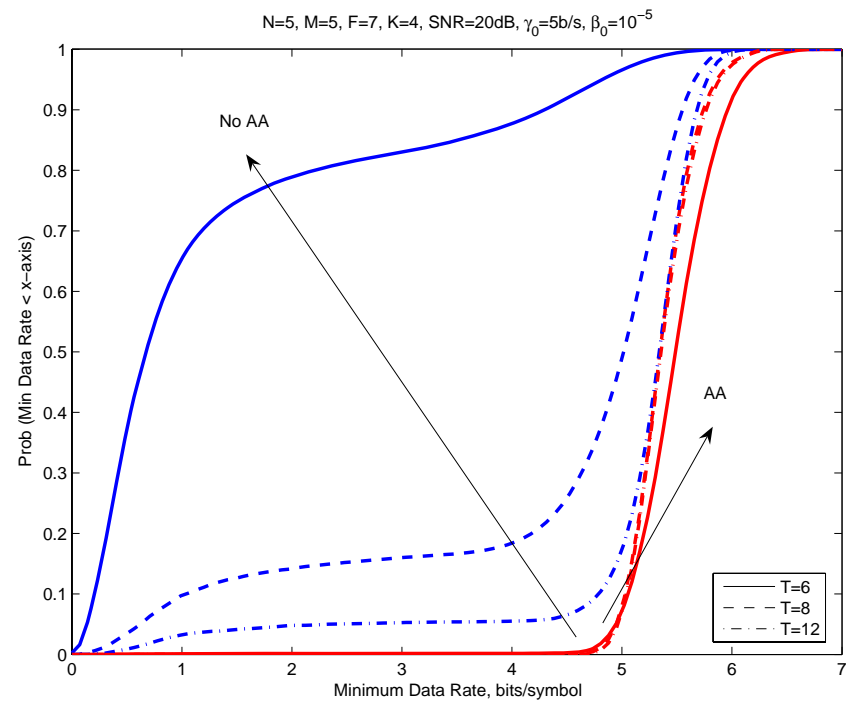


Figure 8.12. Comparison of the AA and non AA results in stationary environment

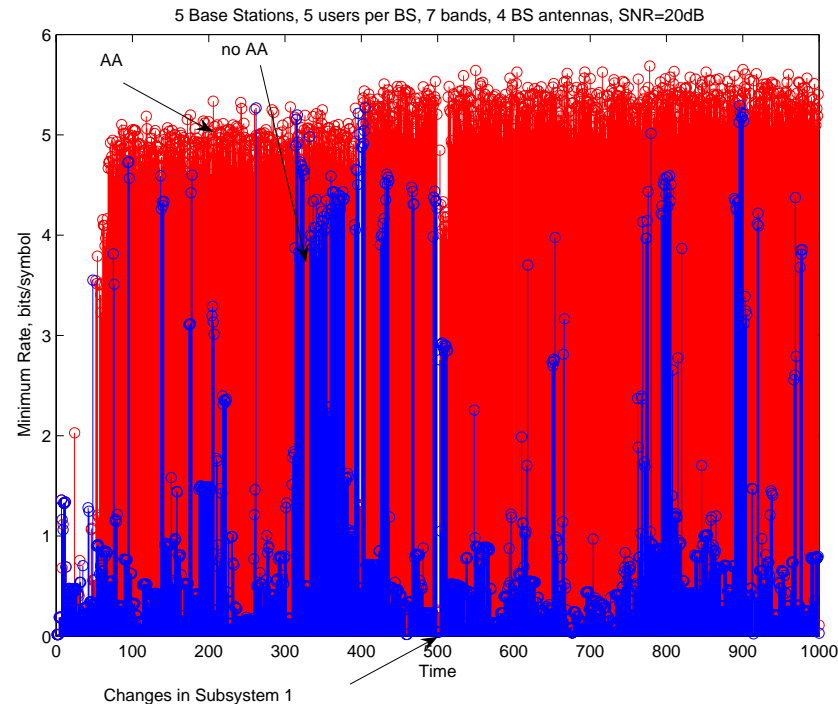


Figure 8.12. Comparison of the AA and non AA results in non-stationary environment for $T = 6$

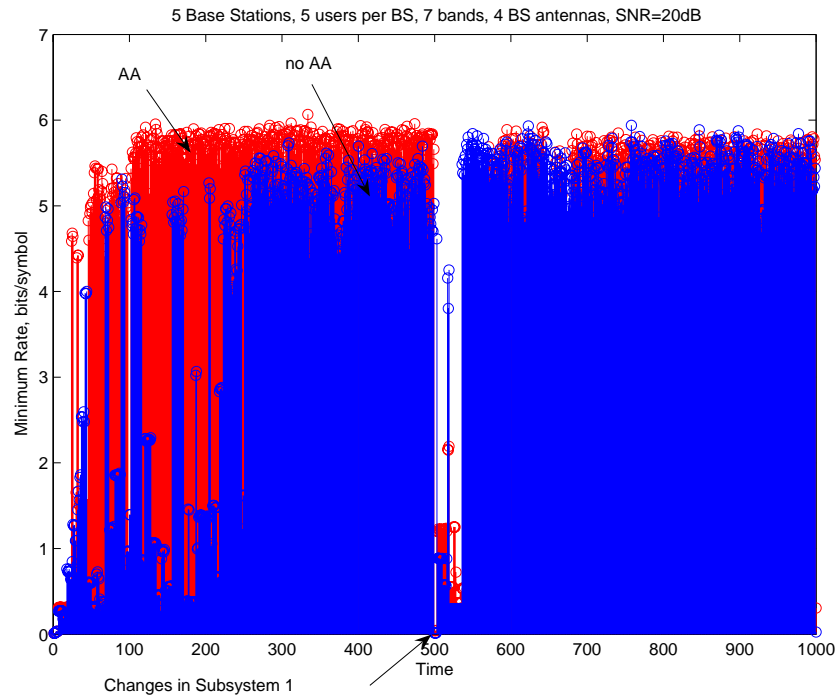


Figure 8.13. Comparison of the AA and non AA results in non-stationary environment for $T = 12$

The simulation results in Figs. 8.11 – 8.13 show the following:

- The AA performance in the stationary environment is practically the same for $T = 6$ and $T = 12$, which allows significant reduction in the overhead leading to better spectral efficiency of considered DSA network. At the same time, sensing with $T = 6$ pilots practically fails for the basic algorithm without AA.
- In the non-stationary conditions, spectrum sensing with AA demonstrates fast convergence to new band allocations as illustrated in Figs. 8.12 and 8.13.

8.7 Conclusions

In this chapter we have focused on the issues associated with finite training sample support, involved in estimation of the propagation channels and interference covariance matrices in uncoordinated spectrum sharing networks based on the FBMC PHY. The main results are as follows:

- The modified GN algorithms with locally estimated second-order statistics and corresponding spectrum sensing protocol have been proposed.
- Simplified Markov chain modelling of the IM-based DSA networks taking into account the finite amount of data spectrum sensing effects have been introduced. It allows qualitative analysis of long-term behaviour of low-dimension networks. Particularly, an average time before reaching states with the given low probability to leave can be found for any initial states of the network.
- The spectrum sensing algorithm for the GN IM-based DSA has been proposed and studied that allows significant reduction of the required number of pilot symbols leading to better spectrum sensing efficiency. Particularly, adaptive averaging with variable threshold for the

stationarity test has been introduced. Efficiency of the advanced sensing algorithm has been demonstrated in stationary and non-stationary environments.

9 Summary

The deliverable continues investigation of the FBMC PHY as a potential physical layer for CR spectrum sharing networks started in [D8109]. Spectrum sensing algorithms have been developed, analyzed and compared with the OFDM case taking into account the increased FBMC frequency selectivity leading to better spectral efficiency of CR networks.

The main results are as follows.

Sections 2-4 (TUT):

- Section 2 presented a new continuous spectrum monitoring scheme for FBMC based secondary transmission. The scheme is based on quiet sensing subcarriers which are placed in-between active subcarriers used in secondary transmission. Improved analytical models were developed for energy sensing using sensing subcarriers. They take into account the effect of the spectrum sensing filter response and spectral regrowth effects due to nonlinear transmitter power amplifier. The proposed scheme provides comparable spectrum sensing performance with an alternative scheme based on time-domain quiet periods, but it was argued to be a much better match for opportunistic secondary spectrum usage scenarios.
 - Sequential detection was discussed Section 3 and a novel variant of the sequential detection method for spectrum monitoring was developed. This method employs multiple parallel sequential detection processes, with different start times, for rapidly detecting reappearing PU signals. Regarding the analysis of the spectrum sensing performance with frequency selective fading channels, it was proposed that the problem can be partitioned into separate analysis of the effects of frequency selectivity and effects of fading. It was shown that a simple analytic model for the effects of frequency selectivity matches quite well with simulations, and for sensing wideband PUs, a simple criterion for adjusting the sensing parameters was stated. For analyzing the fading effects, flat fading models widely available in the literature are expected to be sufficient when they are complemented with the frequency selectivity model.
 - Based on the literature, CP autocorrelation was found to be quite interesting alternative for OFDM PU's. In Section 4, FBMC-based frequency-domain implementation for this method was developed and tested. This method is a promising approach in the spectrum monitoring context because it has low additional complexity in an FBMC-based SU receiver, it overcomes the noise uncertainty problem of energy detection, and it can operate when strong interferences are covering parts of the PU signal band. Further, this approach can be combined with the sequential detection ideas for rapid detection of primary users.
 - Based on the set of tools developed in Sections 2-4, an overall spectrum monitoring concept was formulated in Section 4.2. This scheme is designed for rapid detection of reappearing primary users, and it is consistent with the PHYDYAS dynamic spectrum access scheme.
-

Section 5 (CNAM):

- In this section, we have investigated the PFB based spectrum analyzer to show its applicability for multiband sensing in cognitive radio context. Our study includes theoretical and experimental analysis for three kinds of spectrum analyzers: conventional PSE, PHYDYAS based PFB and PSW based PFB with non-overlapping filters. The simulation results reveal that PSE based spectrum analyzer is sensitive to the spectral leakage. Conversely, PFB demonstrates more efficient and reliable detection performance by taking advantage of its low spectral leakage property, which further enhances the multiband sensing application of PFB in cognitive radio networks. Furthermore, we have shown that due to the ISI at the output of the PSW filter bank, the false alarm detection and detection probability of PHYDYAS based PFB are better compared to PSW. From the view of computational complexity, the performance gain obtained by PFB doesn't come with the penalty of increased complexity due to the inherent parallel structure of PFB.

Section 6 (CTTC):

- This section presented a new spectrum sensing approach named Candidate detector, based on generalized spectral subtraction, and applied this approach to FBMC signals with Phydyas prototype filter bank [D5109]. The FBMC signal, considered as the primary user signature in a cognitive radio scenario, is successfully detected in the presence of narrowband interferers, which may correspond to secondary users, in SNR regimes ranging from -15 up to -9 dB that correspond to realistic scenarios. Requiring only the spectral shape of the primary user, the Candidate Spectrum estimation detector (CASE) stays always with superior quality compared with traditional energy detectors. The candidate detector provides accurate power level estimates and center frequency location, even in the presence of severe narrow band interferences. The method presents very good performance for FBMC primaries, and seems robust even in presence of narrow interference.
- The developed implementation in Section 6 complements in a certain way the set of tools developed in Section 4.1, where the autocorrelation based sensing property is used to detect OFDM primary user. The work in Section 6 assumes a FBMC system as PU and uses, besides the autocorrelation properties to detect the signature of desired PUs, a process to detect its power level.
- In general, based on the weakness of the energy detection methods (see section 6.2), due to noise uncertainty, the studies in both Section 6 and Section 4.1 constitute alternative sensing techniques. In this sense, the methods of Sections 4.1 and 6 are complementary to those of Sections 2 and 5.

Section 7 (AGI):

- In this work, we have reviewed both the classical windowed DFT approach and a filterbank based approach. We have seen that the windowed DFT analysis is limited by the rectangular window length (window length = FFT length). While more advanced windowing (Gaussian, Hann...) will improve the dynamic range (reduced spectral leakage), it will on the other hand reduce the resolution. Overlapping / Averaging (Welch method) improves the variance but not the resolution. To improve the latter, an increased FFT size is required.
 - Conversely, we have seen that filterbanks have a higher complexity than the windowed DFT approach.
-

- Both schemes are of interest, the choice between the two should be conducted accordingly to the application targeted.

Section 8 (ALUK):

- The modified GN algorithms with locally estimated second-order statistics and corresponding spectrum sensing protocol have been proposed.
 - Simplified Markov chain modelling of the IM-based DSA networks taking into account the finite amount of data spectrum sensing effects have been introduced. It allows qualitative analysis of long-term behaviour of low-dimension networks. Particularly, an average time before reaching states with the given low probability to leave can be found for any initial states of the network.
 - The spectrum sensing algorithm for the GN IM-based DSA has been proposed and studied that allows significant reduction of the required number of pilot symbols leading to better spectrum sensing efficiency. Particularly, adaptive averaging with variable threshold for the stationarity test has been introduced. Efficiency of the advanced sensing algorithm has been demonstrated in stationary and non-stationary environments.
-

References

- [Abr09] Y. I. Abramovich, A. M. Kuzminskiy, "Performance bounds for dynamic spectrum allocation based on adaptive antenna array interference mitigation diversity," in Proc. SSP, Sept. 2008.
- [Abr92] Y. I. Abramovich, V. Mikhaylyukov, I. Malyavin, "Test of interference stationarity in adaptive filtering systems", Soviet Journal on Communications Technologies and Electronics, vol.37, no.3, pp.1-10, 1992.
- [Aky06] I. F. Akyldiz, et al. "Next Generation/Dynamic Spectrum Access/Cognitive radio wireless networks: A survey," Computer Networks, Vol. 101, 109 v1.2.1, 2006
- [Bel08] M. Bellanger, "Filter banks and OFDM/OQAM for high throughput wireless LAN", 3rd International Symposium on Communications, Control and Signal Processing. ISCCSP 2008, pp 758-761, Malta, Mar 2008.
- [Bel09] M. Bellanger, T. Ihalainen, and M. Renfors, "Filter bank based cognitive radio physical layer," in Proc. of the ICT-MobileSummit, Santander, Spain, June 2008.
- [Cab04] D. Cabric, S. M. Mishra, and R. W. Brodersen, "Implementation Issues in Spectrum Sensing for Cognitive Radios" in Proc. of the Thirty-Eighth Asilomar Conference on Signals, Systems, and Computers, Vol. 1, November 2004, pp. 772-776.
- [Cha08] S. Chaudhari, V. Koivunen, and H. V. Poor, "Distributed autocorrelation-based sequential detection of OFDM signals in cognitive radio," in Proc. IEEE Int. Conf. Cognitive Radio Oriented Wireless Networks and Communications, Singapore, May 2008, pp. 1-6.
- [Cha09] S. Chaudhari, V. Koivunen, and H. V. Poor, "Autocorrelation-based decentralized sequential detection of OFDM signals in cognitive radio," IEEE Trans. Signal Processing, vol. 57, pp. 2690-2700, July 2008.
- [Che08] H.-S. Chen, W. Gao, D. G. Daut, "Spectrum sensing for OFDM systems employing pilot tones and application to DVB-T OFDM," in Proc. IEEE Int. Conf. on Communications, Beijing, China, May 2008, pp. 3421-3426.
- [Che09] B. Chen, T. Liu, F. Shu, J. Wang, "On Performance Comparison of Wideband Multiple Primary User Detection Methods in Cognitive Radios," WiCOM'09, 2008.
- [Coa59] R. H. Coase, "The federal communications commission," The Journal of Law and Economics, vol. 2, pp. 1-40, Oct. 1958.
- [Cog09] "Cognitive radio part 1: practical perspective," S. Haykin, J. H. Reed, G. Y. Li, and M. Shafi, Ed., Proc. of the IEEE, vol. 97, no. 4, Apr. 2008.
-

- [D5109] INFISO-ICT-211887 Project PHYDYAS, Deliverable 5.1: Prototype filter and structure optimization, Jan. 2009. [Online]. Available: <http://www.ict-phydyas.org/userfiles/file/PHYDYAS-D5-1.pdf>
- [D8109] INFISO-ICT-211887 Project PHYDYAS, Deliverable 8.1: Application of the FBMC physical layer in a cognitive radio scenario, July 2009.
- [Dig03] F. F. Digham, M.-S. Alouini, M. K. Simon, "On the energy detection of unknown signals over fading channels," in Proc. IEEE Int. Conf. on Communications, Anchorage, Alaska, USA, May 2003, pp. 3575-3578.
- [Far08] B. Farhang-Boroujeny, "Filter Bank Spectrum Sensing for Cognitive Radios", Signal Processing, IEEE Transactions, Volume: 56, Issue: 5, On page(s): 1801-1811, May 2008.
- [FCC04] FCC, "FCC spectrum policy task force report 04-113," May 2004.
- [Fel57] W. Feller, "An introduction to probability theory and its applications," John Wiley & Sons, Inc., 1957.
- [Goo04] E. Goodman, "Spectrum rights in the telecoms to come," San Diego Law Review, vol. 41, pp. 269-404, 2004.
- [Gho06] M. Ghoszi, F. Marx, M. Dohler, and J. Palicot, "Cyclostationarity-Based test for Detection of Vacant Frequency Bands," Crowcom Conference, Mykonos, Greece, June 2006.
- [Gra94] L. S. Gradshteyn, I. M. Ryzhik, "Tables of integrals, series, and products," Academic Press, 1994.
- [Han08] N. Han, G. Zheng, S. H. Sohn, J. M. Kim, "Cyclic autocorrelation based blind OFDM detection and identification for cognitive radio," in Proc. 4th Int. Conf. Wireless Communications, Networking and Mobile Computing, Dalian, China, Oct. 2008, pp. 1-5.
- [Har78] F. J. Harris, "On the use of windows for harmonic analysis with the discrete Fourier transform," Proceedings of the IEEE, Vol. 66, NO. 1, Jan. 1978.
- [Hay05] S. Haykin, "Cognitive radio: Brain-empowered wireless communications," IEEE J. Select. Areas Commun., vol. 23, no. 2, pp.201-220, Feb. 2005.
- [Hon98] HongbinLi, Petre Stoica and Jian Li, Capon estimation of covariance sequences, [Circuits, Systems, and Signal Processing](#) pp. 29-48.1998.
- [Hur06] Y. Hur, J. Park, W. Woo, K. Lim, C.-H. Lee, H.S. Kim, J. Laskar, "A wideband analog multi-resolution spectrum sensing (MRSS) technique for cognitive radio (CR) systems," IEEE Int. Symp. on Circuits and Syst'06, pp. 4090-4093, May 2006.
- [IEE06] Sensing scheme for DVB-T, IEEE Std.802.22-06/0127r1, Huawei Technologies and UESTC, Jul. 2006.
-

- [Kem66] J. G. Kemeny, G. L. Thompson, Introduction to finite mathematics, Prentice-Hall, N. J., 1966.
- [Kim09-1] S.-J. Kim and G. B. Giannakis, "Rate-optimal and reduced-complexity sequential sensing algorithms for cognitive OFDM radios," EURASIP J. Advances in Signal Processing, vol. 2009, Article ID 421540, 11 pages, 2008.
- [Kim09-2] M. Kim, J. Naganawa, J. Takada, "Multichannel Spectrum Sensing using Polyphase DFT Filter Bank for Opportunistic Cognitive Radios," The Institute of Electronics, Information and Communication Engineers (IEICE), vol. 109, pp. 121-127, May 2008.
- [Kun07] N. Kundargi and A. Tewfik, "Hierarchical sequential detection in the context of dynamic spectrum access for cognitive radios," in Proc. IEEE Int. Conf. Electronics, Circuits, and Systems, Marrakech, Morocco, Dec. 2007, pp. 514-517.
- [Kuz06] A. M. Kuzminskiy, Y. I. Abramovich, "Second-Order Asynchronous Interference Cancellation: Regularized Semi-Blind Technique and Non-Asymptotic Maximum Likelihood Benchmark," Signal Processing, vol. 86, no. 12, pp. 3849-3863, Dec. 2006.
- [Kuz08] A.M.Kuzminskiy, "Self-optimized (cognitive) multi-band multi-user uncoordinated networks in licensed exempt spectrum," European patent application 08360017.1, 17/10/2008.
- [Kuz09-1] A. M. Kuzminskiy, Y. I. Abramovich, "Decentralized dynamic spectrum allocation based on adaptive antenna array interference mitigation diversity: Algorithms and Markov chain analysis," in Proc. ICASSP, Apr. 2008.
- [Kuz09-2] A. M. Kuzminskiy, Y. I. Abramovich, "Adaptive antenna array interference mitigation diversity for decentralized dynamic spectrum allocation in license-exempt spectrum," in Proc. ICC, June 2008.
- [Kuz10-1] A. M. Kuzminskiy, Y. I. Abramovich, "Decentralized dynamic spectrum allocation based on adaptive antenna array interference mitigation diversity," to appear in IEEE Trans. Signal Processing, 2010.
- [Kuz10-2] A.Kuzminskiy, Y.Abramovich, "Randomized decentralized "good neighbor" DSA based on adaptive antenna array interference mitigation diversity," to appear in Proc. ICASSP, Dallas, March 2010.
- [Kuz10-3] A.Kuzminskiy, Y.Abramovich, "Rule-breaks effect on decentralized rule-regulated "good neighbour" DSA based on adaptive antenna array interference mitigation diversity," to appear in Proc. DySpan, Singapore, April 2010.
- [Lag08] Miguel A. Lagunas Hernandez, Miguel A. Rojas, Petre Stoica, "New Spectral Estimation Based on Filter Bank for Spectrum Sensing" in Proc. IEEE ICASSP 2008, pp 3509-3512. Las Vegas, Nevada-USA. April 2008.
- [Lag08-1] Miguel A. Lagunas Hernandez, Petre Stoica, , Miguel A. Rojas," ARMA Parameter Estimation: Revisiting a Cepstrum-Based Method," in Proc. of the IEEE ICASSP 2008, pp. 3685-3688. Las Vegas, Nevada-USA. April 2008.
-

- [Lai08] L. Lai, Y. Fan, and H. V. Poor, "Quickest detection in cognitive radio: A sequential change detection framework," in Proc. IEEE Global Communications Conference, New Orleans, USA, Nov.-Dec. 2008, pp. 1-5.
- [Lar02] E Larsson, P Stoica and J. Li, Spectral estimation via adaptive filterbank methods: a unified analysis and a new algorithm. Signal Processing, vol 82, 1991-2001, 2002.
- [Li08] H. Li, C. Li, and H. Dai, "Quickest spectrum sensing in cognitive radio," in Proc. Conf. Information Science and Systems, Princeton, USA, Mar. 2008, pp. 203-208.
- [Mah08] R. Mahesh, A. P. Vinod, C. Moy, J. Palicot, "A Low Complexity Reconfigurable Filter Bank Architecture for Spectrum Sensing in Cognitive Radios," CrownCom 2008. 3rd International Conference on, pp.1-6, May 2008.
- [Mit00] Joseph Mitola, Cognitive Radio: an integrated agent architecture for software defined radio, Ph.d. thesis, KTH Royal Inst. of Tech., Stockholm, Sweden, 2000.
- [Mon80] R. A. Monzingo and T. W. Miller, "Introduction to Adaptive Arrays," Wiley, 1980.
- [Qua09] Z. Quan, S. Cui, A. H. Sayed, H. V. Poor, "Optimal Multiband Joint Detection for Spectrum Sensing in Cognitive Radio Networks," Signal Processing, IEEE Transactions on, vol. 57, On pp: 1128-1140, March 2008.
- [Ree74] I. S. Reed, J. D. Mallett, L. E. Brennan, "Rapid convergence rate in adaptive arrays," IEEE Trans. Aerospace and Electronic Systems, vol. AES-10, no. 6, pp. 853-863, Nov. 1974.
- [Roj08] Miguel A. Rojas, Miguel A. Lagunas, Ana I. Pérez-Neira, Petre Stoica, "Spectrum Labeling for Cognitive Radio Systems: Candidate Spectral Estimation," in Proc. 1st IARP in Cognitive Radio and Networks (CiP), Santoniri, Greece, June 2008.
- [Roj09] Miguel A. Rojas, Ana I. Pérez-Neira, Miguel A. Lagunas, "DVB-T Candidate Power Detector for Cognitive Radio," in Proc of 17th European Signal Processing Conference (EUSIPCO'2009). Glasgow, Scotland. August 2008.
- [She08] Y. Shei and Y. T. Su, "A sequential test based cooperative spectrum sensing scheme for cognitive radio," in Proc. IEEE Int. Symp. Personal, Indoor, and Mobile Radio Communications, Cannes, France, Sep. 2008, pp. 1-5.
- [She09] F. Sheikh, S. Masud, B. Bing, "Harmonic power detection in wideband cognitive radios," Signal Processing, IET, vol. 3, pp. 40-50, January 2008.
- [Sio02] P. Siohan, C. Siclet and N. Lacaille, "Analysis and design of OFDM/OQAM systems based on filterbank theory", IEEE Trans. Signal Processing, Vol. 50, May 2002, pp. 1170-1183.
- [Ste05] C. R. Stevenson, C. Cordeiro, E. Sofer, and G. Chouinard, "Functional requirements for the 802.22 WRAN standard," <https://mentor.ieee.org/802.22/file/05/22-05-0007-48-0000-draft-wran-rqmts-doc.doc>
-

- [Sto05] P. Stoica and Moses, "Spectral Analysis of Signals," Pearson Prentice Hall, 2005.
- [Tan04] Rahul Tandra, Shridhar Mubaraq Mishra, and Anant Sahai, "What is a spectrum hole and what does it take to recognize one?" Proc. of the IEEE, special issue on Cognitive Radio, 2008.
- [Tan08] R. Tandra and A. Sahai, "SNR walls for signal detection," IEEE J. Select. Topics Signal Processing, vol. 2, pp. 4-17, Feb. 2008.
- [Tas09] S. Tascioglu, O. Üreten, "Bayesian Wideband Spectrum Segmentation for Cognitive Radios," Proceedings of 18th International Conference on Computer Communications and Networks, pp.1-6, 2008.
- [Tia06] Z. Tian, and G. Giannakis, "A Wavelet approach to wideband spectrum sensing for cognitive radios," in Proc. of 1st international Conference on Cognitive radio Oriented Wireless Networks and Communications (CrownCom), June 2006.
- [Val06] M. Valkama, A. Shahed Hagh Ghadam, L. Anttila, M. Renfors, "Advanced digital signal processing techniques for compensation of nonlinear distortion in wideband multicarrier radio receivers," IEEE Trans. Microwave Theory and Techniques, vol. 54, pp. 2356-2366, June 2006.
- [Van69] A. De Vany, R. D. Eckert, C. T. Meyers, D.J. O'Hara, and R. C. Scott, "A property system for market allocation of the electromagnetic spectrum: A legal-economic-engineering study," Stanford Law Review, vol. 3, pp. 145-162, 1968.
- [Vih09] A. Viholainen, T. Ihalainen, Tobias Hidalgo Stitz, M. Renfors, and M. Bellanger, "Prototype filter design for filter bank based multicarrier transmission," in Proc. of the 17th European Signal Processing Conference, Glasgow, Scotland, Aug. 2009, pp. 1359-1363.
- [Wal45] A. Wald, "Sequential tests of statistical hypothesis," Annals of Mathematical Statistics, vol. 16, pp. 117-186, June 1945.
- [Wei03] T. Weiss, J. Hillenbrand, A. Krohn, F. K. Jondral, "Efficient signaling of spectral resources in spectrum pooling systems," in Proc. 10th Symp. Communications and Vehicular Technology, Eindhoven, Netherlands, Nov. 2003.
- [Xin09] Y. Xin and H. Zhang, "A simple sequential spectrum sensing scheme for cognitive radio," submitted to IEEE Trans. Signal Processing, 2008.
- [Yan98] Yang, C.; Wu, B. & Ko, C. A ray-tracing method for modeling indoor wave propagation and penetration Antennas and Propagation, IEEE Transactions on, 1998, 46, 907-918.
-